AWARD NUMBER: **W81XWH-16-1-0106**

TITLE: **Fragment-Based Approaches to Enhance GTP Competitive KRAS G12C Inhibitors**

PRINCIPAL INVESTIGATOR: **Kenneth Westover**

CONTRACTING ORGANIZATION: **University of Texas Southwestern Medical Center**
Dallas,TX 75390

REPORT DATE: **October 2017**

TYPE OF REPORT: **Annual**

PREPARED FOR: U.S. Army Medical Research and Materiel Command
Fort Detrick, Maryland 21702-5012

DISTRIBUTION STATEMENT: Approved for Public Release; Distribution Unlimited

The views, opinions and/or findings contained in this report are those of the author(s) and should not be construed as an official Department of the Army position, policy or decision unless so designated by other documentation.

REPORT DOCUMENTATION PAGE

Form Approved
OMB No. 0704-0188

Public reporting burden for this collection of information is estimated to average 1 hour per response, including the time for reviewing instructions, searching existing data sources, gathering and maintaining the data needed, and completing and reviewing this collection of information. Send comments regarding this burden estimate or any other aspect of this collection of information, including suggestions for reducing this burden to Department of Defense, Washington Headquarters Services, Directorate for Information Operations and Reports (0704-0188), 1215 Jefferson Davis Highway, Suite 1204, Arlington, VA 22202-4302. Respondents should be aware that notwithstanding any other provision of law, no person shall be subject to any penalty for failing to comply with a collection of information if it does not display a currently valid OMB control number. **PLEASE DO NOT RETURN YOUR FORM TO THE ABOVE ADDRESS.**

1. REPORT DATE
October 2017

2. REPORT TYPE
Annual

3. DATES COVERED
30 Sep 2016 - 29 Sep 2017

4. TITLE AND SUBTITLE
Fragment-Based Approaches to Enhance GTP Competitive KRAS G12C Inhibitors

5a. CONTRACT NUMBER

5b. GRANT NUMBER
W81XWH-16-1-0106

5c. PROGRAM ELEMENT NUMBER

6. AUTHOR(S)
Kenneth Westover, M.D. Ph.D.

E-Mail: Kenneth.Westover@UTSouthwestern.edu

5d. PROJECT NUMBER

5e. TASK NUMBER

5f. WORK UNIT NUMBER

7. PERFORMING ORGANIZATION NAME(S) AND ADDRESS(ES)
University of Texas Southwestern Medical Center
5323 Harry Hines Blvd
Dallas TX, 75390

8. PERFORMING ORGANIZATION REPORT NUMBER

9. SPONSORING / MONITORING AGENCY NAME(S) AND ADDRESS(ES)

U.S. Army Medical Research and Materiel Command
Fort Detrick, Maryland 21702-5012

10. SPONSOR/MONITOR'S ACRONYM(S)

11. SPONSOR/MONITOR'S REPORT NUMBER(S)

12. DISTRIBUTION / AVAILABILITY STATEMENT

Approved for Public Release; Distribution Unlimited

13. SUPPLEMENTARY NOTES

14. ABSTRACT

During the current period we completed work on a series of guanine nucleotide mimetics and published results. As part of this we developed and reported a novel method of measuring small molecule binding to KRAS G12C active site. We also published 2 additional manuscripts about KRAS G12C directed compounds that bind to the switch 2 pocket. Reports of 2 novel assays were also included in these reports. These compounds showed improved potency compared to previously reported compounds. Structural analysis of KRAS using x-ray crystallography was provided in all papers.

15. SUBJECT TERMS
KRAS, small molecule inhibitors, lung cancer, smoking

16. SECURITY CLASSIFICATION OF:			17. LIMITATION OF ABSTRACT	18. NUMBER OF PAGES	19a. NAME OF RESPONSIBLE PERSON
a. REPORT	b. ABSTRACT	c. THIS PAGE			USAMRMC
Unclassified	Unclassified	Unclassified	Unclassified	62	19b. TELEPHONE NUMBER *(include area code)*

Standard Form 298 (Rev. 8-98)
Prescribed by ANSI Std. Z39.18

TABLE OF CONTENTS

	Page
1. Introduction	4
2. Keywords	4
3. Accomplishments	4
4. Impact	22
5. Changes/Problems	23
6. Products	25
7. Participants & Other Collaborating Organizations	27
8. Special Reporting Requirements	29
9. Appendices	29

1. **INTRODUCTION:** Narrative that briefly (one paragraph) describes the subject, purpose and scope of the research.

This research seeks to discover tool compounds that target a leading genetic driver of lung cancer, KRAS G12C. Such compounds will be considered for advancement to preclinical testing as possible therapeutic agents.

2. **KEYWORDS:** Provide a brief list of keywords (limit to 20 words).

KRAS, small molecule inhibitor, lung cancer, smoking

3. **ACCOMPLISHMENTS:** The PI is reminded that the recipient organization is required to obtain prior written approval from the awarding agency grants official whenever there are significant changes in the project or its direction.

What were the major goals of the project?
List the major goals of the project as stated in the approved SOW. If the application listed milestones/target dates for important activities or phases of the project, identify these dates and show actual completion dates or the percentage of completion.

Specific Aim 1: Solve x-ray crystal structures of KRAS G12C in complex with covalent fragments
Major Task 1: Solve x-ray crystal structures
Planned: Months 1-18
Completion (%): 75%
Projected completion date: Month 18
Milestones: Solve 3 x-ray crystal structures

Specific Aim 2: Use 3D structures to design hybrid compounds containing elements of guanosine and fragments
Major Task 2: Design hybrid guanosine-covalent fragment compounds
Planned time: Months 6-24
Completion (%): 75%
Projected completion date: Month 24
Milestone: Synthesis of 40 analogues

Major Task 3: Progress promising compounds through a flowchart of assays
Planned time: Months 9-24
Completion (%): 75%
Projected completion date: Month 24
Milestone: Development of cell permeable inhibitors of KRAS G12C; publication of 1-2 peer reviewed papers

What was accomplished under these goals?
For this reporting period describe: 1) major activities; 2) specific objectives; 3) significant results or key outcomes, including major findings, developments, or conclusions (both positive and negative); and/or 4) other achievements. Include a discussion of stated goals not met. Description shall include pertinent data and graphs in sufficient detail to explain any significant results achieved. A succinct

description of the methodology used shall be provided. As the project progresses to completion, the emphasis in reporting in this section should shift from reporting activities to reporting accomplishments.

Specific Aim 1: Solve x-ray crystal structures of KRAS G12C in complex with covalent fragments
Major Task 1: Solve x-ray crystal structures
Subtask 1: Express and purify KRAS G12C in large scale for x-ray crystallography
Construct and cell lines: p-His-TEV-KRASG12C
Subtask 2: Label purified KRAS G12C with covalent fragments and verify labeling by mass spectrometry
Subtask 3: Screen for crystallization conditions for labeled KRAS G12C and once found produce crystals and freeze for diffraction.
Subtask 4: X-ray diffraction and structure solution by molecular replacement
Planned time: Months 3-18

GDP-mimetics.

X-Ray structure of KRAS G12C with XY-02-075 (compound 47). New GDP analogs did not achieve the comparable labeling efficiency or potency observed for SML-8-73-1 (see Aim 2 below). To gain insight into why our analogs were inferior to SML-8-73-1 we determined the X-ray crystal structure of XY-02-075 bound to KRAS G12C. Complete labeling of KRAS G12C with XY-02-075 was confirmed prior to crystallization using mass spectrometry. Crystals were in the monoclinic space group C_2 with a unit cell similar to other KRAS structures obtained previously(1). Molecular replacement using WT KRAS GDP-bound structure as a search model (PDBID 4OBE) was used to obtain phase information and the final model was refined to a resolution of 2.70 Å with R-work of 28.0%, R-free of 33.5% and average B-factor of 89.0 $Å^2$.

The structure of the G domain is similar to previously solved RAS family protein structures including the previously reported SML-8-73-1-bound structure (PDB 4NMM) (RMSD=0.43Å, 166 atoms aligned). Continuous positive density connecting the terminal carbon atom of XY-02-075 to Cys12 confirmed a covalent link between the compound and protein. The conformation of residues surrounding the guanosine binding site, including P-loop (residue 10-17), ^{57}DXXG, ^{116}NKXD and ^{146}SAK motifs, were similar to the SML-8-73-1-bound structure with several differences. Importantly there is a lack of density where a magnesium ion and coordinated water molecules have been observed in nearly all previous structures of HRAS and KRAS (Figure 1B, C). Also, in the XY-02-075-bound structure we observed a hydrogen bond between the amide carbonyl oxygen atom and the backbone nitrogen atom of Gly13, whereas the linker amide group formed a hydrogen bond with the ε-nitrogen group of Lys16 in the SML-8-73-1 structure (Figure 1B, C). We also noted an outward displacement of Switch I residues Try32 and Asp33 (Figure 1A). Finally, due to poor electron density and a high B-factor, Switch II residues 63 and 64 could not be unambiguously assigned in our model.

Replacement of β-phosphate with sulfonamide apparently leads to dissociation of the magnesium ion and its coordinated water network. Compared to the SML-8-73-1 structure, the magnesium-bridged interaction between the β-phosphate and Tyr 32 and Asp 33 is lost when bound to XY-02-075. Additionally, an intramolecular hydrogen bond forms within XY-02-075 between the amide hydrogen of

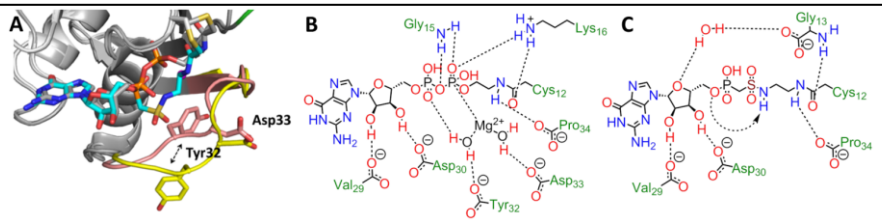

Figure 1. Comparison between G12C in complex with XY-02-075 (cyan/blue) and SML 8-73-1 (gray/orange). (A) Structural superposition of nucleotide binding pocket: Switch I is highlighted in XY-02-075-bound structure in yellow and in SML-8-73-1 in salmon. Tyr32 and Asp33 are in sticks as labeled. (B, C) Schematic representation comparing interactions between SML-8-73-1 (B) or XY-02-075 (C) and Kras G12C. Dashed lines represent the hydrogen bonding interactions.

the sulfonamide and the oxygen atom of the α-phosphonate resulting in a kink in the inhibitor conformation relative to SML-8-73-1 (Figure 1B, C). This kink contributes to displacement of switch I residues Try32 and Asp33 by 3.3 Å relative to the position observed in the SML-8-73-1-bound structure. The folded conformation of XY-02-075 also does not allow the sulfonamide oxygens to form hydrogen bonds with the backbone nitrogen atoms of P-loop residues Gly15 and Lys16 as observed with SML-8-73-1. Consequently, the orientation of the linker amide group of XY-02-075 is shifted in comparison to SML-8-73-1.

To confirm that our compounds do not coordinate efficiently with Mg^{2+} we performed a ^{31}PNMR $MgCl_2$ titration study(2) against fixed concentrations of GDP, GTP and several of our compounds including XY-02-075. These showed a Mg^{2+}-dependent shift in the ^{31}PNMR signal with the half-maximal effect at ~0.5 equivalents for GDP and GTP and a plateau by 2 equivalents. However, with the same concentration of our phosphonate compounds, up to 20 equivalents Mg^{2+} were required before the shift in signal began to plateau demonstrating our phosphonate analogs bind Mg^{2+} with much lower affinity than phosphate-containing analogs.

Switch 2 pocket compounds:

Exploration of direct RAS-targeting strategies has seen a stunning renaissance, reversing the long chill on RAS drug development that followed disappointing clinical trials results for farnesyl transferase inhibitors almost 15 years ago (3). Approaches have included targeting SOS-mediated nucleotide exchange activity (4, 5), targeting intracellular RAS transport mechanisms that are mediated by PDEδ (6) and targeting binding pockets on RAS (7-9). Others discovered a novel allosteric regulatory site beneath the Switch II pocket (SIIP) that was successfully utilized to covalently target KRAS G12C (10) (11-13). We hypothesized that it might be possible to overcome the limits of current GDP mimetic compounds by designing compounds that incorporate elements of both SIIP and the guanosine pharmacophores or by developing bivalent compounds that could recruit ligases to affect the ubiquitin-mediated degradation of RAS (14, 15). As a first step in that direction we characterized and elaborated a series of quinazoline SIIP binders whose chemical structures were first reported in the patent literature (16). Using x-ray crystallography and novel SIIP-directed biochemical assays we identified design principles that contribute to the potency of this class of inhibitor and inform the development of bivalent inhibitors. Notably we find that introduction of an amino amide substituent to the quinazoline scaffold allows further interactions with

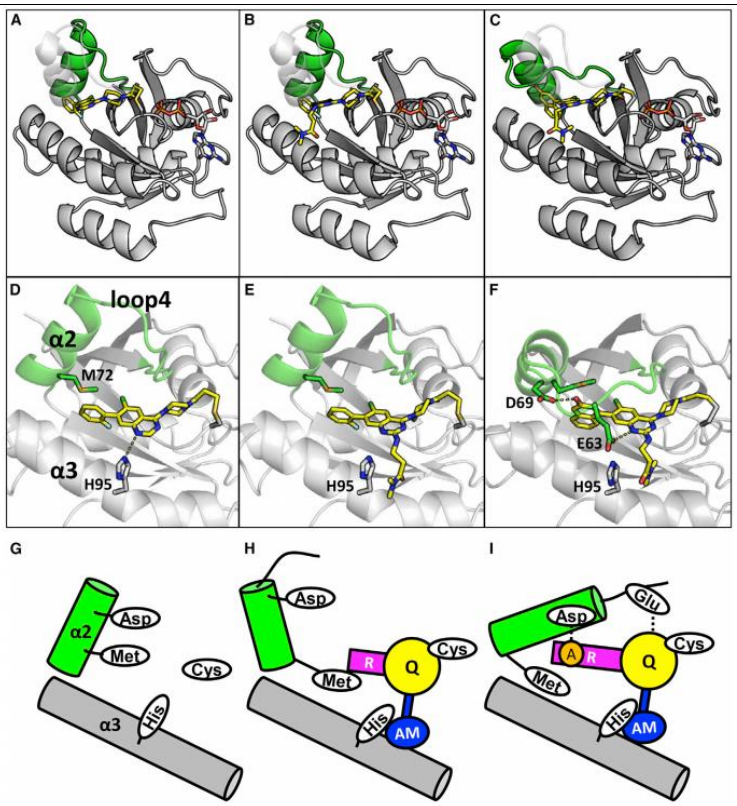

Figure 2. Ligand-Dependent Conformational Changes of SIIP (A–C) Crystal structures of KRAS mutant G12C in bound to compound 1 (A), 1_AM (B), and 3_AM (C) show new alterations in conformation of SWII (green) relative to that seen in for ''apo'' GDP-KRAS (transparent gray). Inhibitors and GDP in sticks and colored by an element with carbon yellow (inhibitor) or white (GDP). (D–F) Detailed view of interactions in SIIP corresponding to (A–C). Dashed lines represent hydrogen bond interactions. (G–I) Schematic diagram of interactions and structural changes in SWII for ''apo'' GDP-KRAS (G), 1/1_AM (H), and 3_AM (I). Dashed lines represent hydrogen bond interactions. Blue circle (AM), amide substituent; yellow circle (Q), quinazoline core; cyan stick (R), steric ring; and orange circle (A), H-bond acceptor.

KRAS G12C, and remarkably increases the labeling efficiency and rates, potency, and selectivity of KRAS G12C inhibitors. In addition, we demonstrate that these compounds are capable of selectively inhibiting KRAS G12C dependent signaling and cellular proliferation at sub-micromolar concentrations.

X-ray crystallography reveals two configurations of SWII for quinazoline SIIP compounds

A series of SIIP compounds were developed as described below (Aim 2). To understand the structural basis of the SAR findings, we solved x-ray crystal structures of KRAS G12C bound to **1_AM** and **3_AM**. Additional electron density within the SIIP confirmed **1_AM** or **3_AM** bound between helix α2 and helix α3 similar to previously reported SIIP binders such as compounds 12 and ARS-853 (10, 12). The structures were notable for substantial differences in the position of SWII with **1_AM** showing an extended conformation compared to **3_AM** (Figure 2). In the **1_AM** complex, protein residue Met72 is rotated away from helix α3 to accommodate **1_AM's** phenyl ring, resulting in the outward rotation of the helix α2 (Figure 2B). The piperazine ring of **1_AM** also displaces loop 4 (part of SW II) away from the binding pocket. As a result, the entirety of SW II is shifted away from the protein main body. This conformation is similar to the conformation seen previously with **1** (Figure 2A, PDB 5V71). The main exception is that the amide substituent of **1_AM** interacts with His95 through π-π stacking while in **1** a hydrogen bond is observed (Figures 2D-2F).

In contrast to **1** and **1_AM**, SWII is considerably altered by **3_AM** binding (Figure 2C). As in **1_AM**, Met72 moves to accommodate the naphthalene ring of **3_AM**. However, the hydrogen bond between Asp69 and hydroxynaphthyl group of **3_AM** causes Met72 to shift towards helix α3 thereby pinning the SW II helix against the binding pocket. This conformation is reinforced by hydrogen bonds between Glu63 and **3_AM**. The sum of these interactions gives a closed SW II conformation (Figures 2C and 2F). The addition of these new interactions seen with the compounds bearing hydroxynaphthyl and/or the amide substituent are consistent with enhancements in thermal stability seen for DSF, improved rankings seen in the Alpha assay and enhancement of potencies of compounds tested for electrophoretic mobility shift or pERK activity (see results in Aim 2).

Specific Aim 2: Use 3D structures to design hybrid compounds containing elements of guanosine and fragments

Major Task 2: Design hybrid guanosine-covalent fragment compounds

Subtask 1: Molecular docking and computer-aided modeling

Subtask 2: Synthesis of SML analogues

Major Task 3: Progress promising compounds through a flowchart of assays

Subtask 1: Test for covalent labeling of purified KRAS G12C by MS

Subtask 2: Prioritize compounds for further development using biochemical assays (RAS:RBD, Kinetic GDP displacement, Kinact/KI)

<u>GDP-mimetics</u>:

We developed a GDP mimetic inhibitor SML-8-73-1, which contains an alpha-chloroacetamide electrophile and reacts with Cys12 upon inhibitor binding to KRAS G12C. SML-8-73-1 is also able to compete *in vitro* with high concentration of GDP and GTP and decreases the affinity of KRAS G12C for the RAS binding domain (RBD) of BRAF(8). Furthermore, unbiased proteomics based profiling showed that SML-8-73-1 is highly selective for KRAS G12C amongst other GTP binding proteins(1). Nevertheless, SML-8-73-1 contains multiple charged phosphate groups and cannot pass through the cell membrane. Caging strategies to shield the charged phosphates were hampered by compound instability(8).

To enable caging strategies and to explore the possibility of other chemical moieties that might improve properties of the diphosphate pharmacophore for covalent targeting of KRAS G12C we investigated structure-activity relationship (SAR) on a series of analogs of SML-8-73-1 that varied the diphosphate group as well as the linker moiety. Here we report biochemical characterization of these compounds including an illustrative x-ray crystal structure demonstrating key difficulties inherent to this approach.

A diphosphate compound, SML-8-73-1 suffers from chemical and enzymatic instability, given that the phosphate anhydride bond is prone to hydrolysis.(17, 18) This is problematic from two perspectives: first, unstable compounds are inherently disadvantageous from a pharmacokinetic perspective; and second, a caging strategy will likely be required to shield charged atoms in the phosphate pharmacophore to enhance cell permeability and the resulting steric bulk from caging groups may further destabilize the phosphate anhydride bond. To address these potential issues, the central oxygen was substituted with a methylene group, and corresponding bisphosphonate is considered to be resistant to acidic and enzymatic hydrolysis at the P-C-P bond(19, 20), and has been broadly used as an isostere of the diphosphate.

Synthesis of the bisphosphonates utilizes a one-pot reaction sequence, starting with nucleophilic addition-elimination reaction between methylenebis(phosphonic dichloride) and acetonide-protected guanosine **3** affording phosphonic chloride **5**, which was subsequently reacted with ethanolamine **6** to give phosphoric ester **7** after aqueous quench. Deprotection of the Boc and acetonide groups under acidic conditions followed by selective acylation using activated NHS-ester **9** gave rise to desired bisphosphonate diester **10** (XY-01-103) (Scheme 1). This synthetic sequence allows facile and quick access to bisphosphonate analogs **10** to **20** with various linkers and different guanine analogs, by utilizing different alcohol reaction partners.

Scheme 1. synthesis of bisphosphonate analogs.[a]

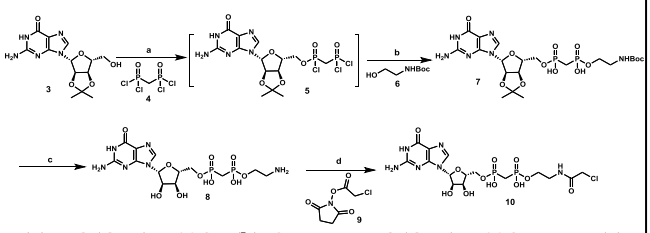

[a] **(a) $PO(OEt)_3$, 0°C; (b) 6, NEt_3, $PO(OEt)_3$, 0°C to rt; (c) TFA/DCM, rt; (d) 9, DIEA, DMF, 0°C.**

Different routes were employed to synthesize various bisphosphonate isosteres, such as compounds with carboxylate ester or sulfonamide as replacements for the phosphate group. Synthesis of phosphonate intermediate **25** commenced with DCC coupling of diethylphosphonoacetic acid **21** and ethanolamine **22**, and the resulting phosphoryl acetate **23** was deprotected and further coupled to guanosine **3** to yield phosphoryl acetate **25**. Similarly, reverse phosphoryl acetate **29** was obtained by using an altered coupling sequence. Deprotection of intermediates **25** and **29**, followed by selective acylation with activated NHS ester **9** gave rise to phosphoryl acetate compounds **30** and **31**, respectively.

The synthesis of compound **47** started from sulfonylation of ethylene diamine **32**. The resulting sulfonamide **34** was deprotonated and reacted with diethyl chlorophosphate **35**. Following deprotection, the collidine salt of sulfamoyl phosphoric acid **37** was obtained. DCC coupling with guanosine **3** gave sulfamoyl phosphonate **44**, which was deprotected and acylated to provide compound **47** (XY-02-075). For compound **48**, sequential addition of ethanolamine **22** and guanosine **3** to chlorosulfonyl isocyanate **38** gave rise to sulfamate **45**, which after deprotection was acylated to yield compound **48**. Alternatively, the synthesis of compound **49** started from reaction of ethylene diamine **40** with chlorosulfonyl acetate **41**. Subsequent saponification and DCC coupling with guanosine **3** yielded the requisite sulfamoylacetate **46**, which was deprotected and acylated to give compound **49**.

We developed a series of biochemical assays to measure various aspects of compound interactions with recombinant G12C KRAS protein. In particular we were concerned with the ability of our compounds to displace guanine nucleotides from the KRAS G12C active site and with establishing a method for measuring relative compound binding affinities to KRAS G12C. As these assays are not routinely used to measure covalent KRAS inhibitors we describe them in detail below.

Chemosensor Assay. To measure GDP displacement we utilized a competitive 'chemosensor assay', wherein purified recombinant GDP-loaded KRAS G12C is incubated with compound, then probed at various time points with a compound that detects the presence of free (unreacted) G12C thiol. This assay provides a composite measurement of kinetic displacement of GDP and covalent inactivation of KRAS G12C. The assay was reported previously(1) and is shown schematically in Figure 3A. An example dataset for XY-01-103 and XY-02-075 is shown in Figure 3B.

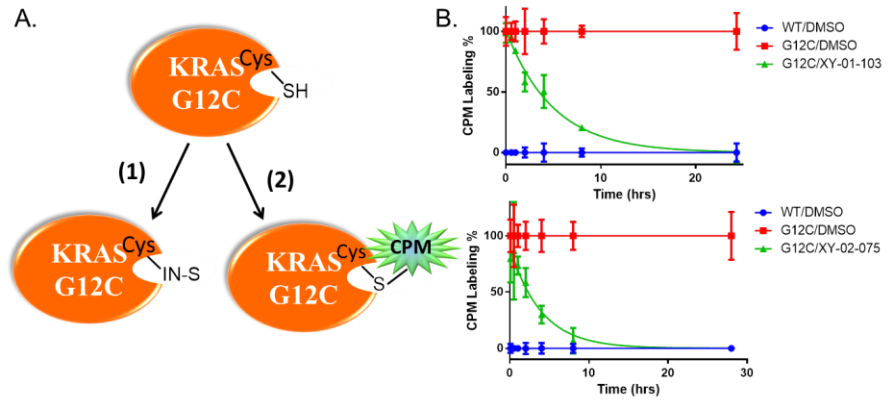

Figure 3. Chemosensor Assay. (A) Assay principle. CPM probe is used to detect free cysteine 12 at indicated time points. (B) GDP-loaded KRas G12C was incubated with a 10X excess of inhibitor XY-01-103 (compound 10) or XY-02-075 (compound 47) and the rate of CPM labeling determined (green). DMSO treated WT (blue) and G12C (red) KRAS were used as negative and positive labeling controls, respectively..

ActivAlpha assay. To determine the relative affinities of compounds we measured k_{inact}/K_I using GMP-stabilized KRAS G12C (Figure 4). For covalent compounds k_{inact}/K_I is a preferred enzymological parameter for assessing covalent probes (also known as inactivators) because it incorporates measures of both passive affinity (K_I) and the irreversible inactivation (k_{inact}) rates(21). To obtain these values we used the strategy advocated by Copeland(21) wherein reaction rates are plotted vs. compound concentrations and fit to the curve described by equation 2:

$$k_{obs} = \frac{k_{inact}[I]}{K_I + [I]}$$

Using the fit, estimates for k_{inact} and K_I can be extracted (Figure 4C, D).

For this assay purified nucleotide free KRAS G12C was prepared and stabilized with an excess of GMP, which has a low affinity of 3.5×10^4 M^{-1} for RAS(22). GMP-stabilized RAS is incubated with compound then probed with a GTP-desthiobiotin probe which, similar to widely used GTP-biotin (ActivX) probes(23, 24), contains a reactive acyl phosphate anhydride that reacts with lysine 16 of KRAS. Desthiobiotinylated protein is detected using AlphaScreen (PerkinElmer) reagents. A schematic

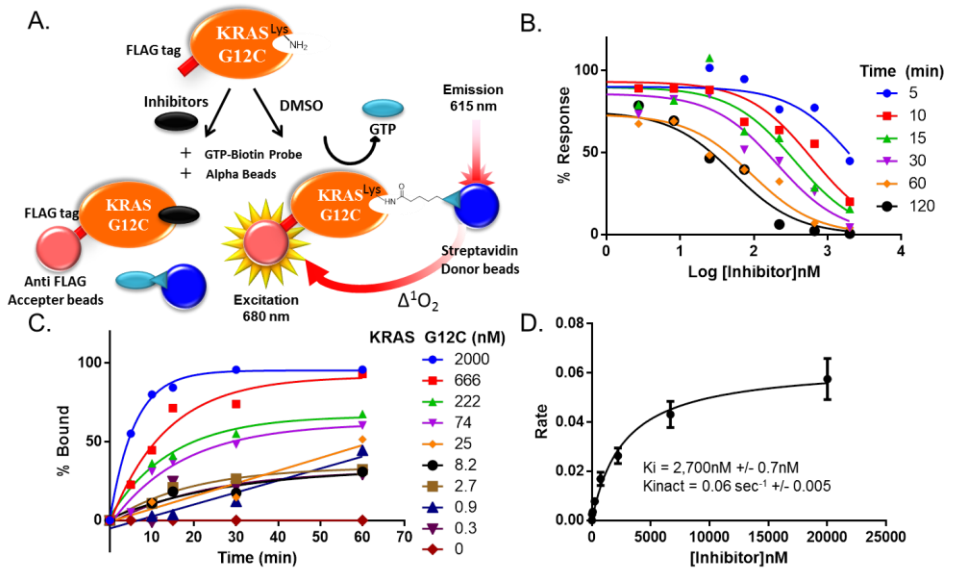

Figure 4. ActivAlpha kinact/KI assay. (A) Assay principle: a GTP-competitive probe is used to detect occupancy of the GTP binding site of KRAS G12C by small molecules. The probe covalently reacts with a lysine in the active site of KRAS. AlphaScreen (PerkinElmer) beads are directed against a KRAS affinity tag and streptavidin. (B, C) Time dependent IC50 curves can be transformed for calculation of the first order rate constants for each concentration shown in subpanel C. (D) kinact/KI can be obtained by plotting rate vs. inhibitor concentration and fitting to equation 2

representation is shown in Figure 4A. Because the ActivX and AlphaScreen reagents are used in combination we call this assay ActivAlpha. Example data for XY-01-103 is shown in Figure 4D including time dependent changes in IC_{50} (panel B), the transform to a time dependent plot from which rates can be calculated (panel C) and the curve fit (panel D).

Mass Spectrometry. A third assay consists of incubating recombinant G12C KRAS with new inhibitors and then performing electrospray ionization mass spectrometry as reported previously(8). The percent labeling of the protein can be detected as shown in Figure 5.

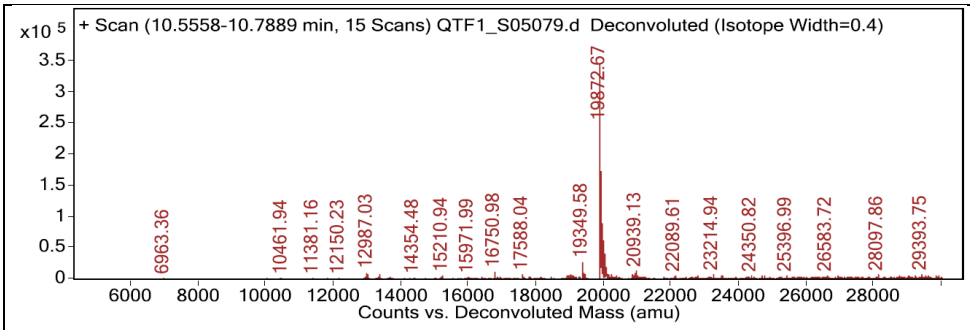

Figure 5. MS labeling of KRAS G12C with XY-02-075 (compound 47).

SAR Analysis. To meet our overarching goal of developing GTP-competitive inhibitors that have anti-cancer effects in cells, compounds will likely need to achieve adequate RAS inhibition well within the typical timescale of the RAS protein turn over; the half-life has been estimated at 12-24 hours(25, 26). We previously performed rudimentary kinetics simulations(27) showing that G12C KRAS inactivators with a k_{inact} of 0.6 min^{-1} and K_I of 10 nM will yield 50% inhibition of KRAS G12C in 5 hours. We therefore adopt these as preliminary standards for inhibitor development. Nevertheless it should be noted that the ActivAlpha assay reported here utilizes an excess of GMP to stabilize the KRAS protein, and unlike the *in vivo* situation does not require displacement of GDP or GTP.

In the ActivAlpha assay diphosphate compound **1** (SML-8-73-1) shows an excellent K_I of 9 nM and a relatively fast k_{inact} of 0.86 min^{-1} which is consistent with the reactive chloroacetamide electrophile of SML-8-73-1. However the corresponding methylenebisphosphonate analog **10** loses 300-fold in binding affinity (K_I), and labels KRAS at a rate that is 11 fold slower (Table 1). This highlights the importance of interactions between the oxygen atom of the diphosphate and the various residues in the P-loop of KRAS. By substituting the central oxygen in SML-8-73-1 with a methylene group in compound **10**, both the pK_a of resulting phosphoric acid, as well as bond lengths and bond angles of the P-X-P linkage (X = O, CH_2) are altered, which may result in lower affinity.(28) To regain the electronic and conformational properties as in SML-8-73-1, difluoromethylene and monofluoromethylene groups were incorporated in compounds **11** and **12**, respectively. Fluorinated phosphonates are widely used in pharmaceutical industry as phosphate isosteres, and are found to be better mimetics than phosphonates(29, 30). In this case, difluoromethylene-bisphosphonate analog **11** improved the affinity for KRAS by 7 fold, compared to bisphosphonate analog **10**, while the monofluoromethylene bisphosphonate analog **12** showed a lower affinity and slower labeling rate.(31)

The acrylamide analog of SML-8-73-1 (compound **2**) exhibits a higher rate constant k_{inact} than α-chloroacetamide-containing SML-8-73-1, although it is generally believed that the α-chloroacetamide warhead is more reactive towards cysteine group than acrylamide(32). We postulated that longer length between the β-phosphate and the reactive site of the acryl amide in compound **2** may be optimal for the requisite covalent bond formation. Analogs with a propyl linker (compound **13**, **14**) improved the affinity to KRAS G12C, possibly due to a combinatory effect of optimal spacing, and better trajectory of the electrophile warhead towards nucleophilic substitution of Cys12. On the contrary, analog **20**, with an internal electrophile and shorter distance between the β-phosphate and the reactive site for Cys12, showed complete loss of activity.

We hypothesized that a rigid linker with a preferred trajectory may further improve labeling efficiency, and a series of analogs with cyclic linkers were synthesized. In the case of compound **16** with a pyrrolidine linker, a larger k_{inact} of 2.2 min^{-1} was observed, along with fast labeling of G12C KRAS in the chemosensor assay ($t_{1/2}$ of 1.1h). Cyclopentane-containing analogs **18** and **19** which place the nitrogen in the exocyclic position also showed larger k_{inact}, however the affinities for these two compounds are significantly lower. A piperidine linker in compound **17** did not improve affinity or labeling efficiency.

We also examined substitution of one or both phosphates with carbonyl or sulfonyl groups. The results showed that both phosphates are crucial in achieving high binding affinity to KRAS; substituting one or both phosphates significantly lowered affinity and resulted in longer labeling time. Among these, phosphonyl sulfonamide analog **47** (XY-02-075) had the lowest K_I of 1.6 μM and a $t_{1/2}$ of 2.3 h. A co-crystal structure of compound XY-02-075 with KRAS G12C showed an intramolecular hydrogen bonding between the sulfonamide hydrogen and the phosphonate oxygen (see below for further discussion). Phosphoryl acetate analog **31**, in which the β-phosphate was replaced with an acetate group, showed a 7-fold lower K_I than the corresponding reversed phosphoryl acetate **30**. This observation is in line with previous reports that interactions between the β-phosphate in GDP and Ras or magnesium are stronger than that of the α-phosphate(22). Further replacement of the remaining phosphonate with sulfonamide moiety in compounds **48** and **49** didn't significantly improve affinity. Incorporation of a squaryldiamide group, a common isostere for diphosphates and bisphosphonates(33), in compound **50** only resulted in poor affinity.

Table 1. SAR of bisphosphonate analogs and diphosphate isosteres.

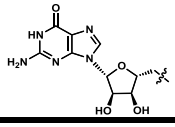

Cmpds	substitution	chemo-sensor $t_{1/2}$ (h)	K_I (μM)	k_{inact} (min^{-1})	k_{inact}/K_I (min^{-1} •μM^{-1})
1	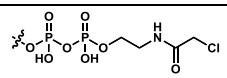	0.68	0.009	0.86	95
2	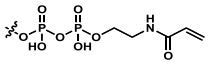	0.6	0.28	2.124	7.6
10	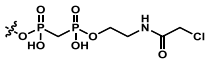	2.1	2.7	0.06	0.02
11	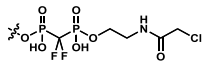	4.2	0.38	0.365	0.9
12	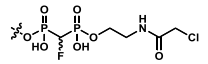	6.6	8	0.21	0.03
13	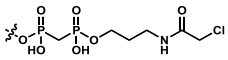	2.5	0.374	0.07	0.2
14	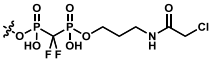	1.06	0.382	0.3	0.8
15	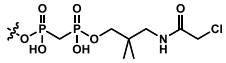	20	5	0.14	0.028
16	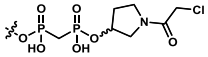	1.1	0.92	2.2	2.4
17	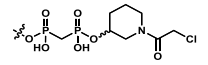	12	3.5	0.55	0.16
18	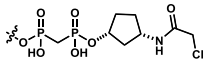	>36 (42)	50	1	0.02
19	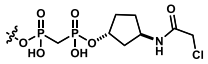	>36 (64)	36	2.3	0.06
20	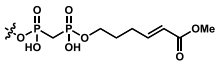	>36 (120)	>20	--	--
30	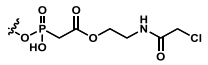	>36 (84)	15.2	0.055	0.003
31	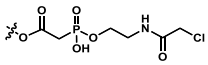	>36 (47)	2.2	0.053	0.02
47	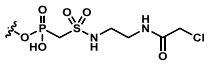	2.3	1.6	0.33	0.2
48	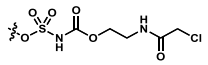	9.5	5	0.24	0.05
49	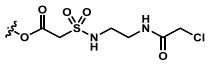	24	>10	--	--
50	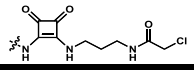	13	>25	--	--

Switch 2 pocket compounds:

A novel readout for the labeling efficiency of KRAS inhibitors. To explore the possibility of designing compounds that occupy both the SWII pocket (SIIP) and guanine binding site, we considered previously reported SIIP compounds including the well-characterized chloro hydroxy aniline core (ARS-853) compounds (11-13) and a class of relatively uncharacterized quinazoline-containing compounds that appeared in the patent literature (16). The quinazoline compounds offered significant advantages to present chemical diversity to sub-regions of the SIIP. To better understand the potential properties of the quinazoline compounds we evaluated the ability of these compounds to inhibit the function of KRAS G12C.

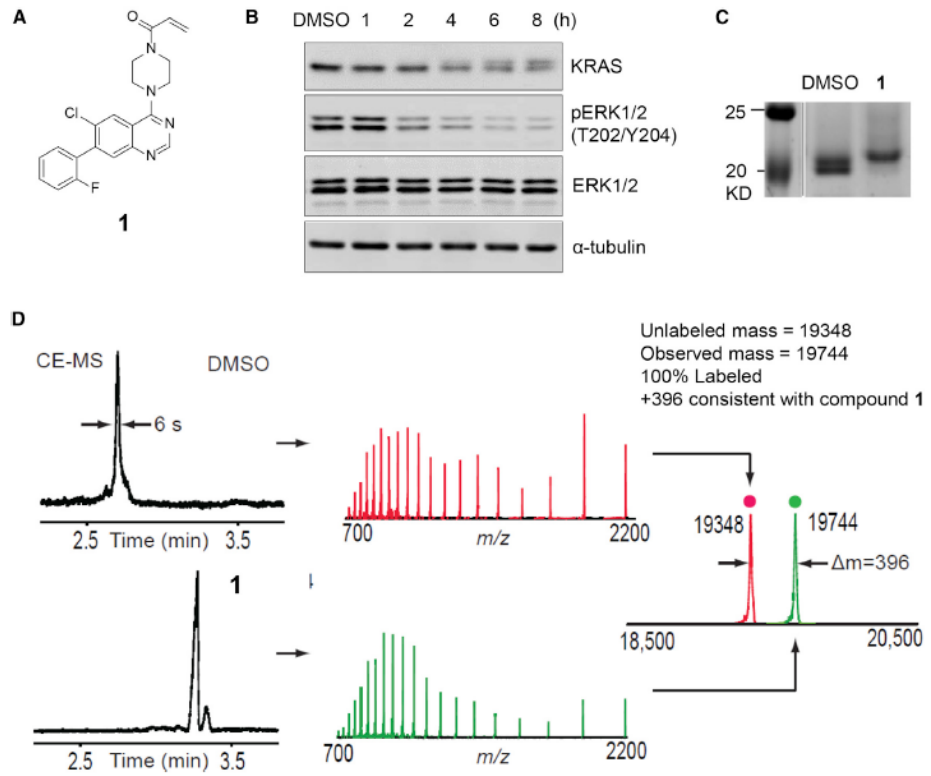

Figure 6. Electrophoretic Mobility of KRAS as a Readout for the Labeling Efficiency of KRAS Inhibitors (A) Chemical structure of 1 (Araxes patent WO2015054572). (B) KRAS-G12C mutant cells (H358) were treated with compound 1 in a time-dependent manner at 10 mM. Electrophoretic mobility of KRAS-G12C and MAPK phosphorylation were determined by immunoblotting with the indicated antibodies. (C) Purified recombinant KRAS-G12C protein was incubated with 1 for 2 hr at 10 mM, and the protein-1 mixture was resolved on a 12% SDS-PAGE. (D) Capillary electrophoresis-mass spectrometry (CE-MS analysis) confirms covalent labeling of KRAS-G12C. After incubation of protein with DMSO or compound 1, as in Figure 1C, reactions were resolved by CE and introduced to the mass spectrometer by electrospray ionization directly from the chip. Zero-charge mass spectra reveal a shift in protein mass corresponding to 1.

We prepared several examples of quinazoline reported to effectively label G12C KRAS by MS, including compound **1** decorated with fluorophenyl and piperazinyl substituents and an electrophilic acrylamide warhead attached to the piperazine (Figure 6A) (16) (Araxes patent WO2015054572). As an initial test of cellular efficacy, we utilized the cancer cell line H358, a KRAS addicted non-small cell lung cancer cell line harboring the KRAS G12C allele (34). Interestingly, when protein extracts from H358 cells exposed to **1** were subjected to western blot analysis, we noted an upward shift in the KRAS G12C band in a time-dependent manner (Figures 6B). A similar phenomenon was also observed in 293T cells transiently transfected with Flag-tagged KRAS G12C. We verified that this shift is a consequence of covalent attachment of compounds to KRAS G12C by incubating the inhibitors with purified recombinant KRAS G12C and observing a similar electrophoretic mobility shift and by observing the expected mass gain using mass spectrometry (Figures 6C and 1D). This electrophoretic mobility shift provided us with a convenient and direct means of assessing target engagement of KRAS for subsequent iterations of compounds in this series.

Attaching an amide substituent to KRAS G12C inhibitor enhances its labeling efficiency and potency

We profiled a set of analogs of **1** in order to explore the structure activity relationship. We initially fixed the quinazoline 4- and 7-positions with piperazinyl-acrylamide and 2-fluorophenyl substituents and

introduced a variety of amine substituents at the C2-position (Figure 7A). To evaluate their relative potency, we treated H358 cells and assessed the electrophoretic mobility of KRAS G12C and the impact on downstream MAPK signaling by monitoring the phosphorylation status of ERK by immunoblotting. Of the compounds prepared, **1_AM** with an amino amide substituent showed the most complete labeling of KRAS at 10 µM. FRF-01-167, the only example with a tertiary amine at the quinazoline 2-position, showed no labeling of KRAS, while other examples showed labeling to varying extents (Figure 7B). As expected, the degree of KRAS G12C mobility shift tightly correlated with the inhibition of ERK phosphorylation (Figure 7B). Furthermore, we found that **1_AM** induced the electrophoretic mobility shift of KRAS G12C at a faster rate than compound **1** (Figure 7C), indicating improved labeling kinetics. We also compared **1_AM** to **1** for the ability to decrease active KRAS G12C levels. Consistent with prior observations on ARS-853 series compounds which show a propensity for binding to GDP-bound KRAS preferentially (11, 12), treating H358 cells with **1_AM** decreased levels of GTP-bound KRAS by ~80% compared to **1** (Figure 7D) with corresponding decreases in phosphorylation of ERK and MEK.

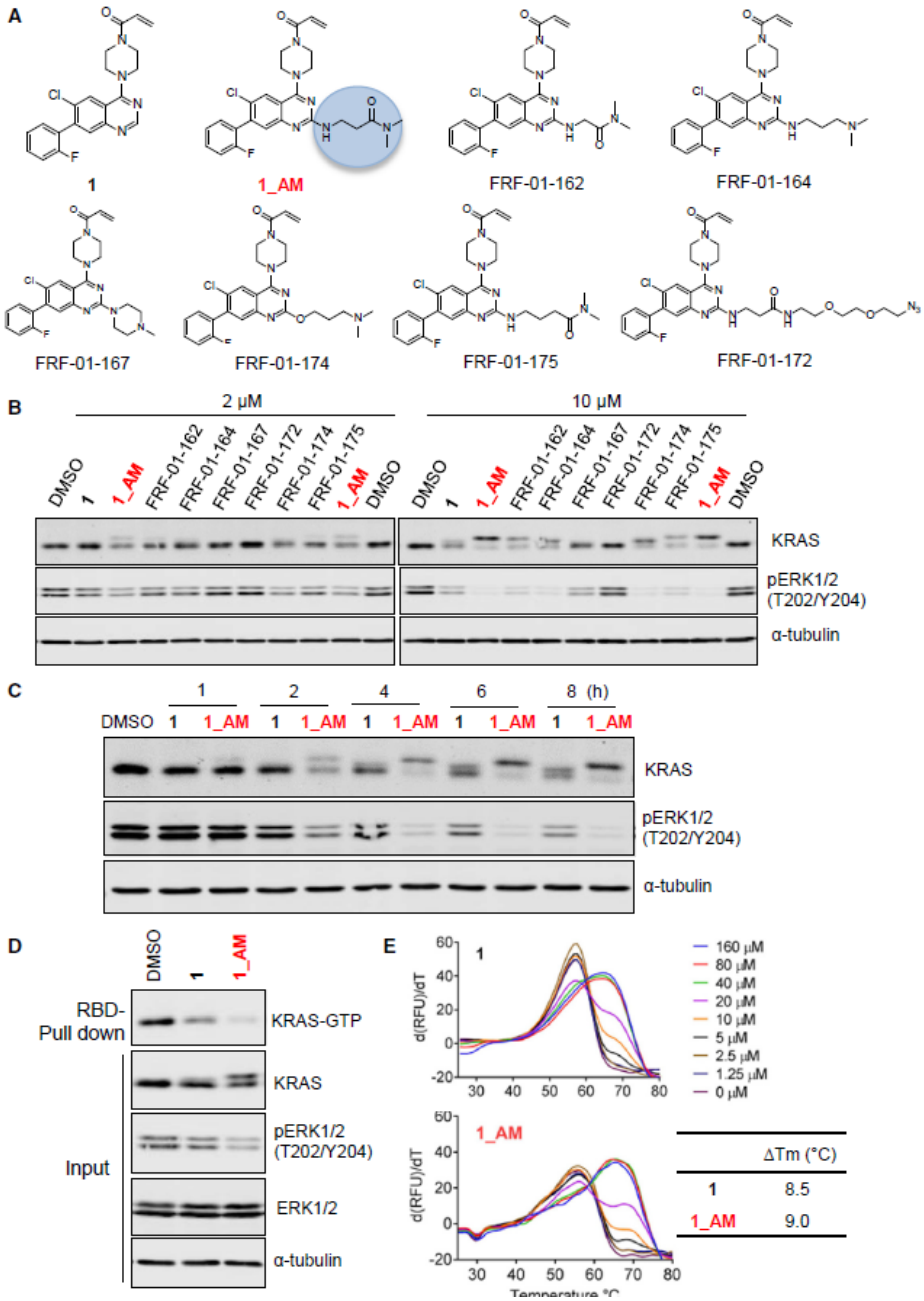

Figure 7. Figure 2. Amide Substituent Enhances the Covalent Labeling Efficiency and the Potency of KRAS-G12C Inhibitors (A) Chemical structures of the synthetic molecules for studying the structure-activity relationship of the amino amide substituent (the amino amide substituent in 1_AM is highlighted in the gray circle).

As an additional measure of how substitutions at the 2-position alter interactions between KRAS G12C and the compounds, we performed differential scanning fluorimetry (DSF), which measures ligand-induced changes in protein thermal stability (35). Compound **1_AM** demonstrated a small enhancement in the thermal stability relative to **1** of fully labeled KRAS G12C when compared to unlabeled GDP-bound protein, with a small but reproducible change in the melting temperature (ΔTm) of 9 °C vs. 8.5 °C for **1_AM** and **1** respectively (Figure 7E). This increase suggests that an N-linked amide substituent

at the 2-position may increase labeling efficiency with KRAS G12C relative to compounds lacking such moieties.

Development of potent KRAS-G12C inhibitors with the amide substituent. With the new finding that the amide substituent confers potency advantages, we next evaluated a series of quinazoline matched pairs, with and without the 2-amino amide substituent (Figure 8A). Addition of a fluorine at position 8 (pairs 2 and 4) modestly improved the potency of compounds relative to those without, while addition of a hydroxynaphthyl at the 7-position (pairs 3 and 4) substantially further enhanced potency as measured by inhibition of ERK phosphorylation and DSF (Figures 8B and 8C). In all pairs the presence of amide improved the potency of compounds for engagement of KRAS and inhibition of ERK phosphorylation, when tested in H358 (KRAS G12C) cells (Figures 8B). Similar findings were readily apparent in five additional KRAS G12C cancer cell lines (H23, H1792, Calu-1, H2122, Mia Paca-2), as well as in 293T cells with ectopic expression of KRAS G12C.

We further evaluated these compounds for changes in levels of GTP-bound KRAS and for shifts in thermal stability by DSF. Consistent with its effect on KRAS G12C mobility shift and on ERK phosphorylation, adding the amide

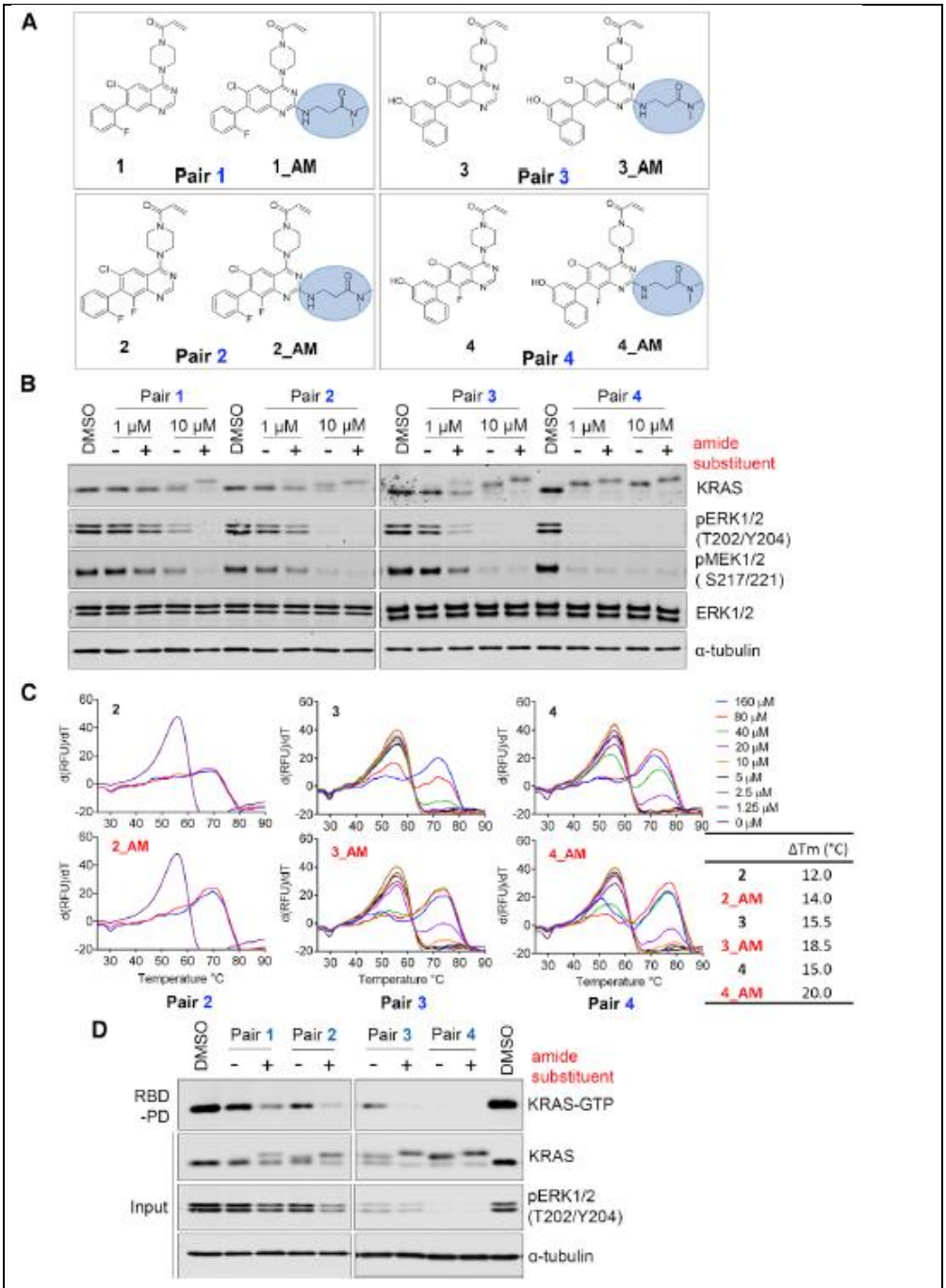

Figure 8. Development of Potent KRASG12C Inhibitors with the Amide Substituent
(A) Chemical structures of the four pairs of SIIP binders, organized by presence or absence of the amino amide substituent (light blue highlights). (B) Pairwise comparison of compound set in H358 cells by immunoblot for electrophoretic mobility of KRAS-G12C, and MAPK and MEK phosphorylation show a comparative improvement in compound potency by adding the amino amide substituent. Pairs 3 and 4, which include the hydroxynaphthyl, are substantially more potent than 1 and 2 that lack this group. (C) Differential scanning fluorimetry (DSF) comparison of compound pairs 2, 3, and 4. DSF shows increases in thermal stability for compounds containing the amino amide substituent in a dosedependent manner. First derivatives of temperature- dependent signals are shown. (D) Immunoblot analysis after RBD pull-down of GTP-KRAS from H358 cells exposed to compound pair shows decreases in recovery of GTP-KRAS for compounds including the amino amide substituent and for pairs including the hydroxynaphthyl (1 and 2 versus 3 and 4).

substituent to **2**, **3,** and **4** decreased GTP-bound KRAS (Figures 8D), and increased the thermal stability of KRAS G12C (Tm: 14.0°C vs. 12.0°C for pair 2; 18.5°C vs. 15.5°C for pair 3; 20°C vs. 15°C for pair 4) (Figures 8C). Interestingly, larger shifts in Tm are seen when comparing compound pairs with and without the hydroxynaphthyl group (9°C vs. 18.5°C for **1_AM** vs. **3_AM**). Both compound **4** and **4_AM** labeled and inhibited KRAS G12C at sub-micromolar concentrations (Figure 8B).

Measuring target labeling via a novel SIIP Alpha assay. As one of the primary challenges to the development of new SIIP compounds, all screening assays have relied upon covalent interactions between the protein and compounds which have been monitored using either mass spectrometry (10, 12) or the electrophoretic gel shift assay described earlier. We reasoned that it might be possible to develop a competition binding assay using a probe based on **4_AM** to detect binding. We previously developed a competition binding assay to evaluate for small molecule binding in the guanosine nucleotide pocket using a covalent GTP-biotin probe, tagged KRAS and AlphaScreen beads (9). We developed a similar binding assay for the SIIP using a biotinylated version of **4_AM** with the biotin extending from the amide linker, **5**. The assay was performed in competition fashion by co-incubating with test compounds in escalating doses with fixed concentrations of Flag-tagged KRAS G12C and **5**, then developing the assay using AlphaScreen beads. Optimization for 384 well format resulted in a sufficient Alpha signal to produce an assay window that could be used for robust dose

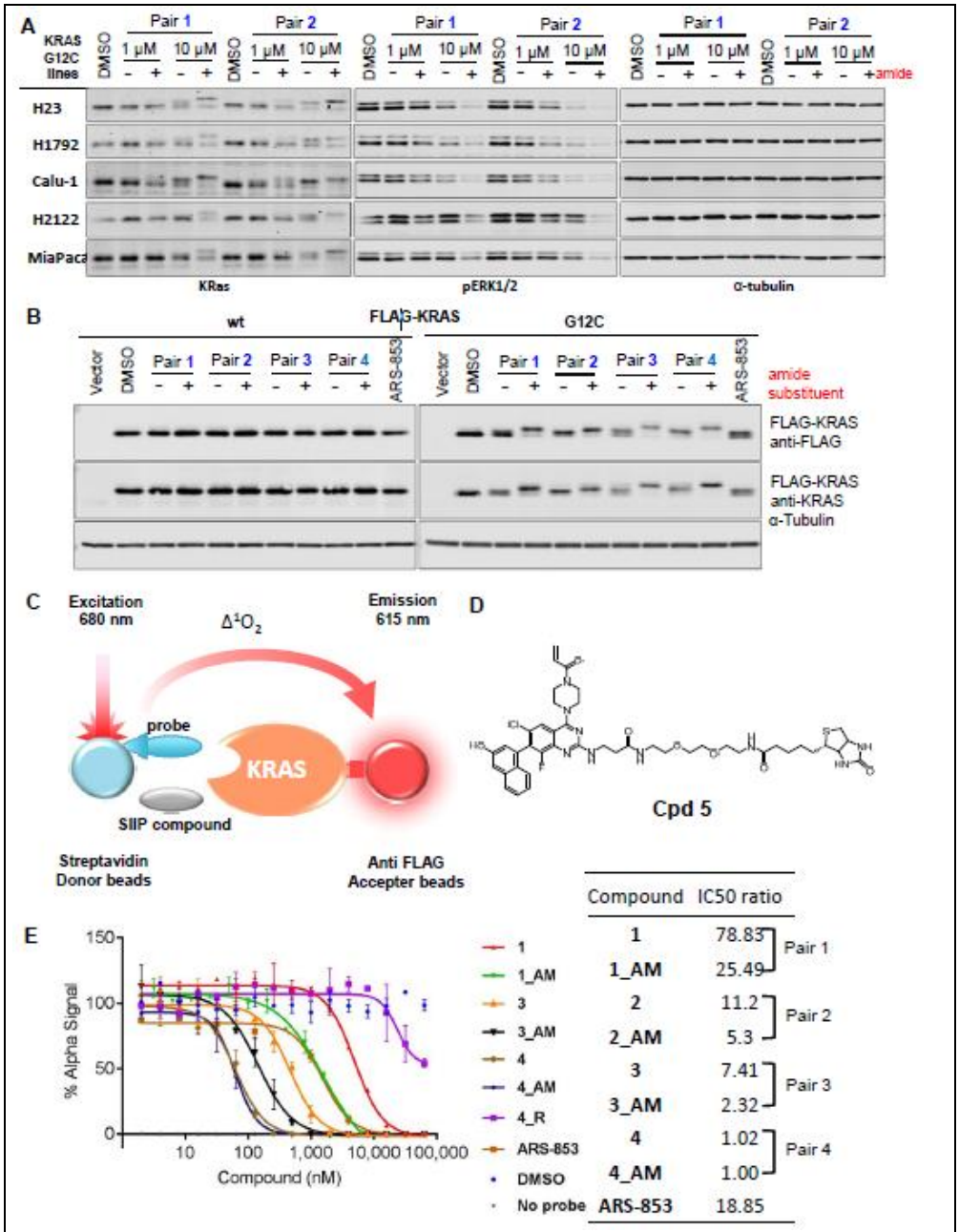

Figure 9.. Characterization of SIIP inhibitors containing the amide substituent. (Related to Figure 3) A. Assessment of SIIP inhibitors in a panel of KRAS-G12C cell lines. Efficacy of pairs 1, 2 for labeling KRAS G12C and decreasing pERK in a panel of KRAS-G12C lung cancer /pancreatic cancer cell lines (H23, H1792, Calu-1, H2122, and Mia Paca-2). B. SIIP inhibitors induce electrophoretic mobility of exogenous KRAS-G12C. HEK293T cells were transfected with GFP, or FLAGtagged-KRAS wild type, or KRAS-G12C constructs for 24 hours, followed by treatment KRAS was determined by immunoblotting. C. Biochemical competition binding assay concept. KRAS-G12C protein is incubated with test compounds and probe together for 2 hours, followed by development with AlphaScreen beads. D. Chemical structures of assay probe (Cpd 5). Cpd 5 is based on 4_AM and incorporates a biotin substituent. E. Biochemical competition binding assay. The dose response analysis of quinazoline compound sets measured using AlphaScreen assay. Data are represented as mean +/- SD (n=3).

response measurements. Dose response experiments showed good discrimination between covalent quinazoline compounds in a pattern similar to that observed previously using DSF and the western blot assays. Specifically, when comparing substitutions at the quinazoline 2-positions, both compound **1_AM** and **3_AM** showed 3-fold increases in potency compared to their counterparts **1** and **3** (Figure 9). Also, substitutions of 2-fluorophenyl (pair **1**) for 3-hydroxynaphthyl (pair **3**) showed a 10-fold improvement in IC50. Finally, addition of a fluorine at position 8 (compare pair **4** to pair **3**; pair **2** to pair **1**) substantially improves potency. Of note, consistent with their cellular activities, both **4** and **4_AM** exhibit lower IC50 compared to pairs 1, 2, and 3, and no significant difference was observed between **4** and **4_AM**. It should be noted that because this assay is not performed under equilibrium conditions and relies on a covalent probe, the resulting IC50 values are batch-dependent and are not accurate estimates of compound Kd's. Nevertheless when calibrated on a per-batch basis to a control (**4_AM** IC50), the results are highly reproducible between assay runs for rank ordering compounds.

Subtask 3: Test high priority compounds for cell permeability
Planned time: Months 18-24
Subtask 4. Test high priority compounds for antiproliferative activity

Enhanced anti-proliferative potency and induction of apoptotic cell death by attachment of the amide substituent. Given that compounds with the amide substituent increased labeling efficiency to KRAS G12C as well as potency in inhibiting ERK phosphorylation, we proceeded to investigate if these characteristics would translate into an impact on KRAS G12C-dependent cell proliferation. To this end, we treated KRAS-G12C cancer cells lines for five days with all the four pairs of compounds at the final concentrations of 5 µM. Compared to their parental analogs, compounds with the amide substituent demonstrated enhanced cell growth inhibition (Figure 10A). To understand if an induction

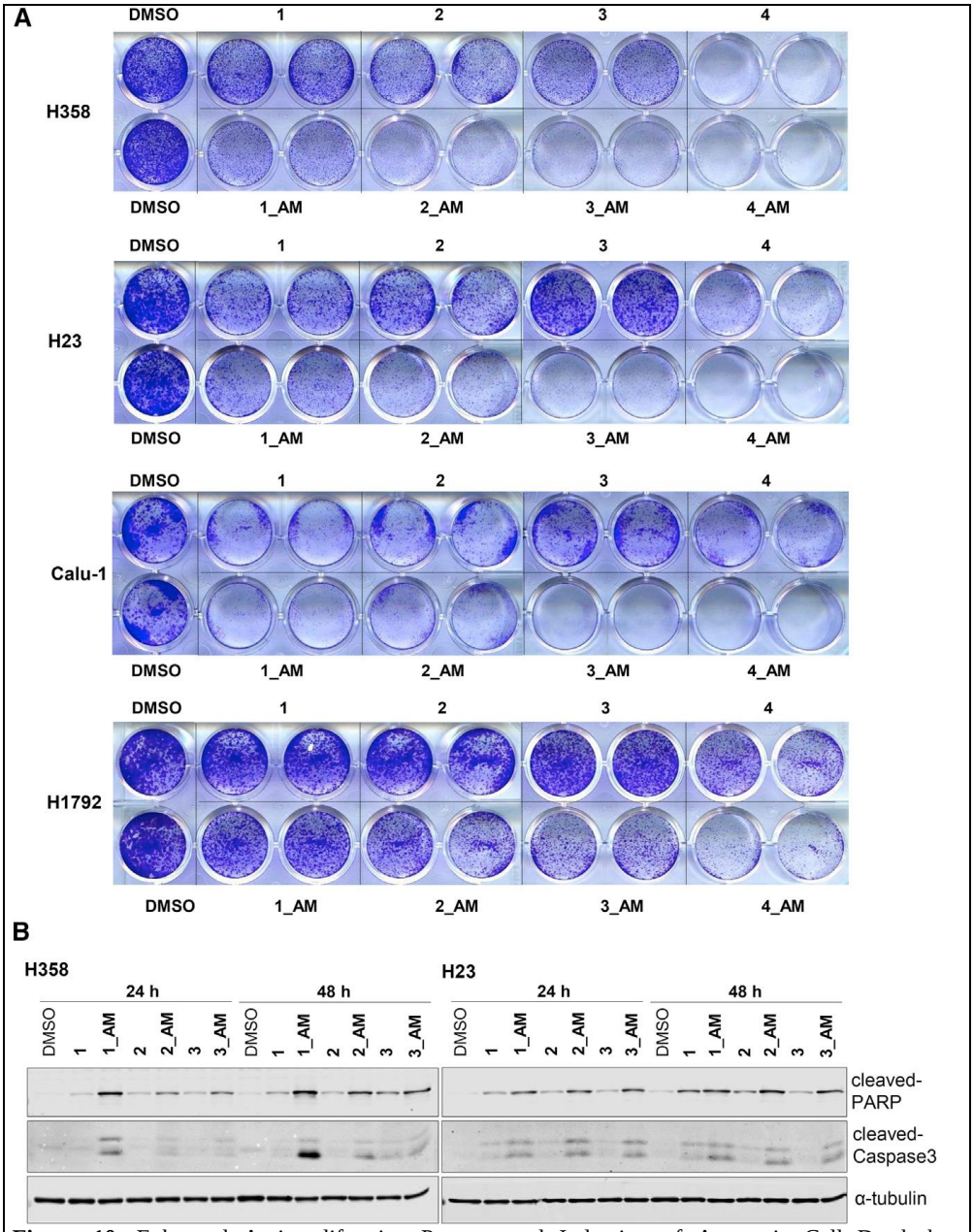

Figure 10. Enhanced Anti-proliferative Potency and Induction of Apoptotic Cell Death by Attachment of the Amide Substituent (A) Exposure of KRAS-G12C lung cancer cell lines, H358, H23, Calu-1, and H1792, to four pairs of compounds at 5 mM for 5 days shows consistent improvements in anti-proliferative properties of compounds including the amino amide substituent(each compound treatment in duplicate wells). (B) Appearance of apoptosis markers, cleaved PARP, and cleaved Caspase-3, in two KRASG12C lung cancer cell lines, H358 and H23, is enhanced in compounds including the amide substituent.

of cell death may be responsible for cell growth inhibition upon KRAS G12C inhibitor treatment, we used the cleaved form of PARP and Caspase 3 as the readout of apoptotic cell death, and found that attachment of the amide substituent significantly increased apoptosis (Figure 10B). Therefore we concluded that the amide substituent enhances the anti-proliferative and cell killing potency of KRAS G12C inhibitors.

Sub-micromolar inhibition of KRAS G12C cell lines Prior SIIP compounds such as ARS-853 showed anti-proliferative activity in the high micromolar range in cell proliferation assays (11, 12). As a direct comparison between ARS-853 and our panel of compounds we measured cell proliferation and MAPK phosphorylation in the KRAS G12C cancer cell lines, Calu-1 and H358. ARS-853 showed a 50% decrease in pERK at ~ 5 μM, while **1_AM**, **3_AM**, and **4_AM** all showed enhanced pERK inhibition with **4_AM** showing ~50% inhibition at around 100 nM (Figure 11A). Similarly, **1_AM** and **4_AM** showed substantial improvements in IC50's for anti-proliferative activity for cell lines, H358 and Calu-1 (Figure 11B).

We further compared the amide substituent-modified compounds, **1_AM**, **3_AM**, and **4_AM** with ARS-853 in terms of the kinetics of target labeling. To this end, we treated cells with inhibitors for different time points and harvested cell lysates for assaying the electrophoretic mobility of KRAS G12C. Consistent with the improved anti-pERK and anti-proliferative potency, all the compounds with amide substituent caused a faster alteration of electrophoretic mobility of KRAS G12C, with alterations observed as early as 1 h post treatment (Figure 11C). These data suggest that addition of the amide substituent improved potency.

Subtask 5: Test high priority compounds selectivity using MS selectivity profiling
Planned time: Months 18-24
Completion (%): 50%
Projected completion date: Month 24
Milestone(s): Development of cell permeable inhibitors of KRAS G12C; publication of 1-2 peer reviewed papers

The amide substituent increased the selectivity of KRAS G12C inhibitors

All data to this point suggest that the covalent portion of SIIP compounds contributes significantly to the potency of SIIP compounds. We therefore expected our current panel of compounds to have

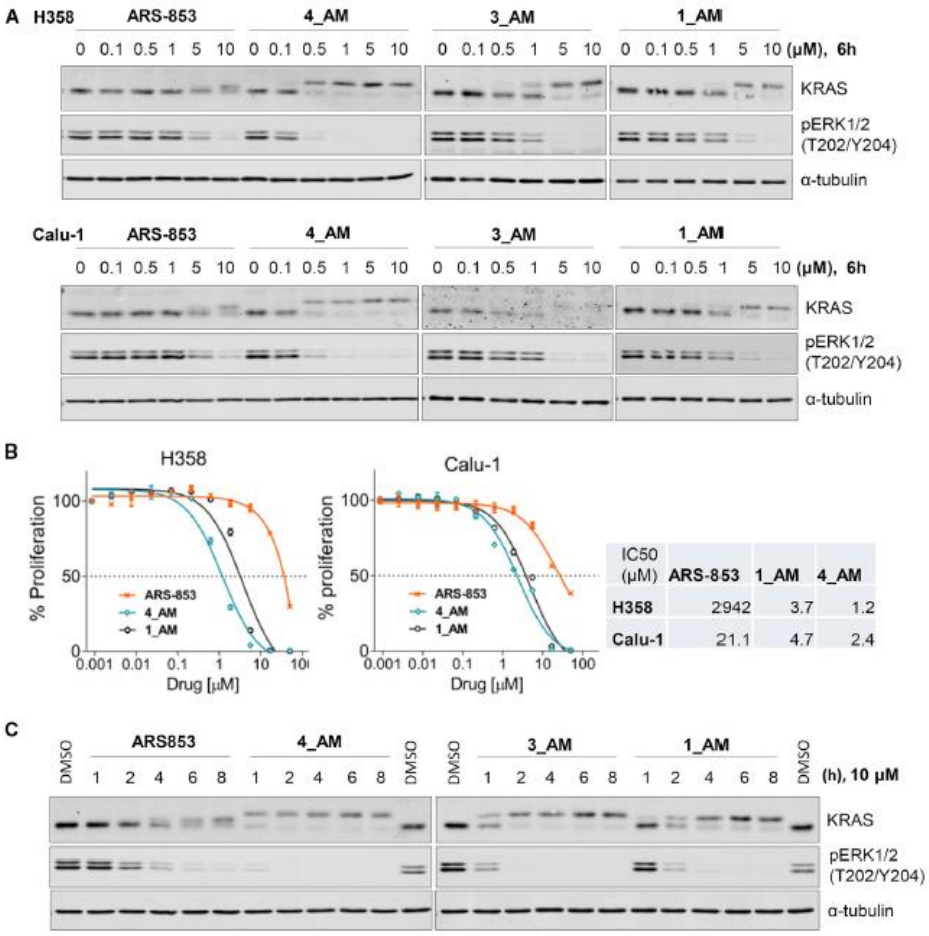

Figure 11. SIIP Inhibitors for KRAS-G12C with Sub-micromolar Potency (A) Dose response of KRAS and pERK levels in KRAS-G12C cell lines, H358 and Calu-1, after 6 hr exposure of 1_AM, 3_AM, 4_AM, and ARS-853. (B) Dose response of cell viability for H358 and Calu-1 cells treated for 5 days with indicated inhibitors. Data are represented as mean ± SD (n = 3). (C) Time courses of KRAS and pERK levels in H358 cells treated with 1_AM, 3_AM, 4_AM, and ARS-853 at 10 mM show enhanced labeling kinetics for 4_AM..

activity only against cells bearing the KRAS G12C mutation. We could not use previously developed As expected, MAPK signaling was not affected in multiple RAS cancer cell lines bearing non-G12C mutations. In A549 (G12S), H441 (G12V), and HCT116 (G13D) cells, inhibitors failed to suppress ERK phosphorylation (Figures 12A and 11B). To further evaluate the specificity of our compounds towards the KRAS G12C isoform, we developed an isogenic *Ras-less* MEFs model system expressing different human KRAS mutants. In this system endogenous HRas/NRas/KRas were knocked out resulting in a non-proliferative phenotype. Re-introduction of human KRAS mutant and wild type isoforms restore proliferation in this system (36). We found that compounds 1, 2, 3, 4, as well as their derivatives with amide substituents, showed increased anti-proliferative potency in $KRAS^{G12C}$ *Ras-less* cells relative to $KRAS^{G12V}$ *Ras-less* cells $KRAS^{G12V}$ *Ras-less* cells. All these data suggest that the compounds selectively target G12C, not the other mutated forms of KRAS.

Interestingly, for cell lines harboring wildtype KRAS (HCC827, PC9), ERK phosphorylation was suppressed when cells were exposed to the compounds 1, 2, 3 and 4 at 10 µM (Figure 12B, dashed black arrow). Notably, the amide side chain containing compounds dramatically reversed this effect (Figure 12B, bold black arrow), suggesting that the amide substituent appears sufficient to improve the selectivity profile of the quinazoline compounds. However, perhaps more importantly, these results also suggest that the reversible component of quinazoline compounds have the capacity to bind to a SIIP in wild type KRAS. To explore this possibility further, we performed Active RAS pull down experiments to determine the level of GTP-bound KRAS in cells exposed to our panel of SIIP binders. Remarkably, we observed decreased levels of KRAS-GTP for cells exposed to compounds lacking the amide substituent compared to those where it was maintained (Figure 12C). These

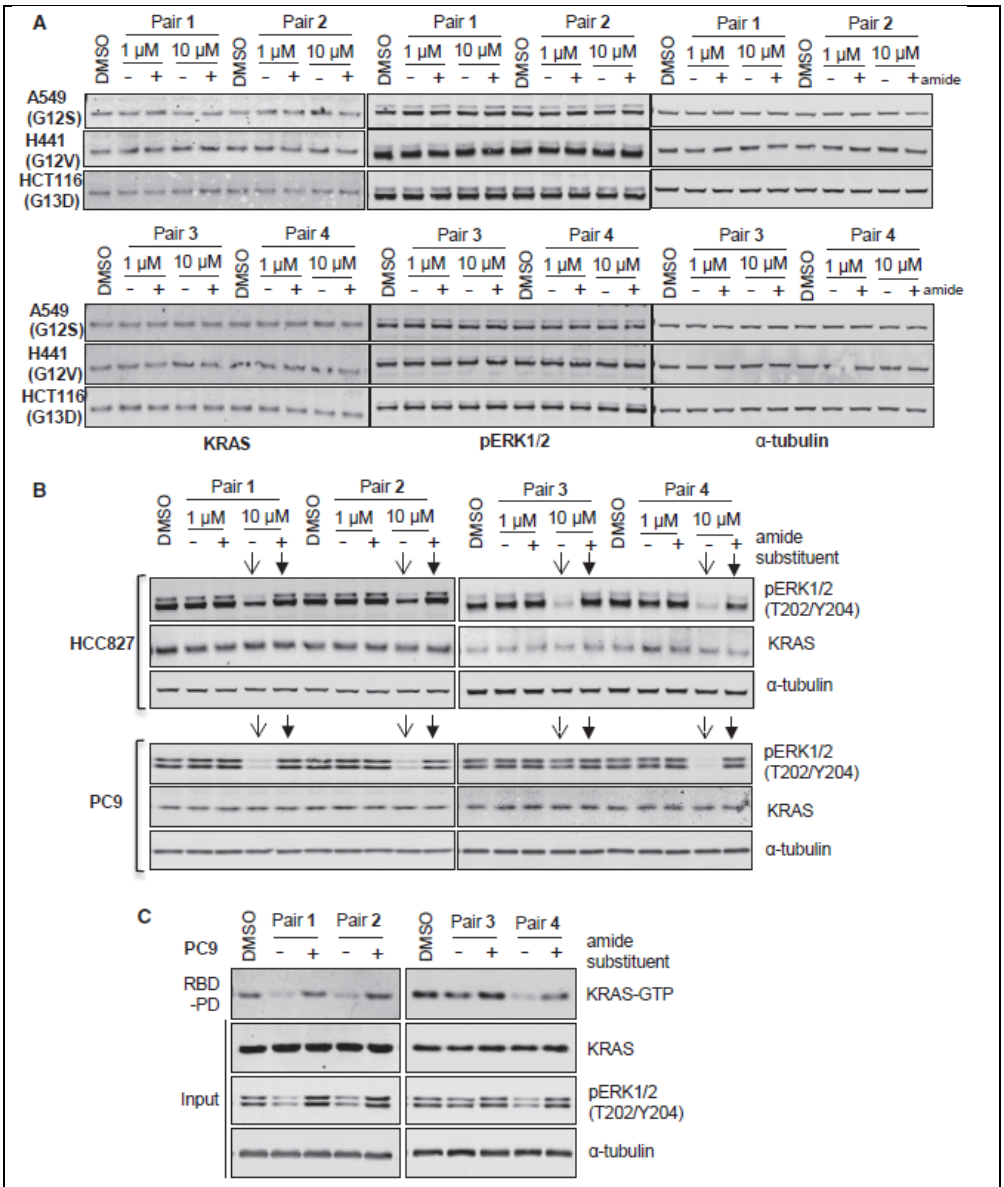

Figure 12. (A) Exposure of non-G12C KRAS cell lines, A549 (G12S), H441 (G12V), and HCT116 (G13D) treated to compounds for 6 hr at 1 and 10 mM shows no effect on KRAS protein and pERK levels as determined by immunoblotting. (B) Exposure of KRAS wild-type/EGFR mutant cell lines, HCC827, and PC9 cells, show inhibition of pERK for selected compounds lacking amino amide substituent (dashed black arrow), but show restored pERK level for compounds including the amino amide substituent (bold black arrow). (C) PC9 cells were treated with the indicated compounds for 6 hr at 10 mM. The effect on the level of active/GTP-bound KRAS was determined by a RAS-binding domain pull-down assay and immunoblotting with KRAS-specific antibody.

results support the hypothesis that compounds lacking the amide substituent are able to bind to wildtype KRAS-GDP, enriching the cellular pools of GDP-KRAS and thereby depleting the ratio of GTP-KRAS to GDP-KRAS. These results also demonstrate that the amide substituent functions to improve the selectivity of covalent G12C targeted quinazoline compounds.

REFERENCES:

1. Hunter JC, Gurbani D, Ficarro SB, Carrasco MA, Lim SM, Choi HG, et al. In situ selectivity profiling and crystal structure of SML-8-73-1, an active site inhibitor of oncogenic K-Ras G12C. Proc Natl Acad Sci U S A. 2014;111(24):8895-900. doi: 10.1073/pnas.1404639111. PubMed PMID: 24889603; PubMed Central PMCID: PMC4066474.
2. Pecoraro VL, Hermes JD, Cleland WW. Stability constants of Mg2+ and Cd2+ complexes of adenine nucleotides and thionucleotides and rate constants for formation and dissociation of MgATP and MgADP. Biochemistry. 1984;23(22):5262-71. PubMed PMID: 6334536.
3. Adjei AA, Mauer A, Bruzek L, Marks RS, Hillman S, Geyer S, et al. Phase II study of the farnesyl transferase inhibitor R115777 in patients with advanced non–small-cell lung cancer. Journal of clinical oncology. 2003;21(9):1760-6.
4. Maurer T, Garrenton LS, Oh A, Pitts K, Anderson DJ, Skelton NJ, et al. Small-molecule ligands bind to a distinct pocket in Ras and inhibit SOS-mediated nucleotide exchange activity. Proc Natl Acad Sci U S A. 2012;109(14):5299-304. doi: 10.1073/pnas.1116510109. PubMed PMID: 22431598; PubMed Central PMCID: PMC3325706.
5. Sun Q, Burke JP, Phan J, Burns MC, Olejniczak ET, Waterson AG, et al. Discovery of small molecules that bind to K-Ras and inhibit Sos-mediated activation. Angew Chem Int Ed Engl. 2012;51(25):6140-3. doi: 10.1002/anie.201201358. PubMed PMID: 22566140; PubMed Central PMCID: PMC3620661.
6. Zimmermann G, Papke B, Ismail S, Vartak N, Chandra A, Hoffmann M, et al. Small molecule inhibition of the KRAS-PDE [delta] interaction impairs oncogenic KRAS signalling. Nature. 2013;497(7451):638.
7. Welsch ME, Kaplan A, Chambers JM, Stokes ME, Bos PH, Zask A, et al. Multivalent Small-Molecule Pan-RAS Inhibitors. Cell. 2017;168(5):878-89 e29. doi: 10.1016/j.cell.2017.02.006. PubMed PMID: 28235199.
8. Lim SM, Westover KD, Ficarro SB, Harrison RA, Choi HG, Pacold ME, et al. Therapeutic targeting of oncogenic K-Ras by a covalent catalytic site inhibitor. Angew Chem Int Ed Engl. 2014;53(1):199-204. doi: 10.1002/anie.201307387. PubMed PMID: 24259466; PubMed Central PMCID: PMC3914205.
9. Xiong Y, Lu J, Hunter J, Li L, Scott D, Choi HG, et al. Covalent Guanosine Mimetic Inhibitors of G12C KRAS. ACS Med Chem Lett. 2017;8(1):61-6. doi: 10.1021/acsmedchemlett.6b00373. PubMed PMID: 28105276; PubMed Central PMCID: PMC5238463.
10. Ostrem JM, Peters U, Sos ML, Wells JA, Shokat KM. K-Ras(G12C) inhibitors allosterically control GTP affinity and effector interactions. Nature. 2013;503(7477):548-51. doi: 10.1038/nature12796. PubMed PMID: 24256730; PubMed Central PMCID: PMC4274051.
11. Lito P, Solomon M, Li LS, Hansen R, Rosen N. Allele-specific inhibitors inactivate mutant KRAS G12C by a trapping mechanism. Science. 2016;351(6273):604-8. doi: 10.1126/science.aad6204. PubMed PMID: 26841430; PubMed Central PMCID: PMC4955282.
12. Patricelli MP, Janes MR, Li LS, Hansen R, Peters U, Kessler LV, et al. Selective Inhibition of Oncogenic KRAS Output with Small Molecules Targeting the Inactive State. Cancer discovery. 2016;6(3):316-29. doi: 10.1158/2159-8290.CD-15-1105. PubMed PMID: 26739882.
13. Westover KD, Janne PA, Gray NS. Progress on Covalent Inhibition of KRAS(G12C). Cancer discovery. 2016;6(3):233-4. doi: 10.1158/2159-8290.CD-16-0092. PubMed PMID: 26951837.
14. Winter GE, Buckley DL, Paulk J, Roberts JM, Souza A, Dhe-Paganon S, et al. Phthalimide conjugation as a strategy for in vivo target protein degradation. Science. 2015;348(6241):1376-81.

15. Toure M, Crews CM. Small-Molecule PROTACS: New Approaches to Protein Degradation. Angewandte Chemie International Edition. 2016;55(6):1966-73.
16. Ren P, Liu Y, Li L, Feng J. Irreversible covalent inhibitors of the gtpase k-ras g12c. Google Patents; 2014.
17. Budovskii EI, Shibaev VN. Kinetics of the acid hydrolysis of uridine diphosphate glucose and 3-N-methyluridine diphosphate glucose. Chem Nat Compd. 1968;4(4):199-201. doi: 10.1007/bf00571136.
18. Stockbridge RB, Wolfenden R. Enhancement of the rate of pyrophosphate hydrolysis by nonenzymatic catalysts and by inorganic pyrophosphatase. J Biol Chem. 2011;286(21):18538-46. doi: 10.1074/jbc.M110.214510. PubMed PMID: 21460215; PubMed Central PMCID: PMC3099670.
19. Harris MR, Usher DA, Albrecht HP, Jones GH, Moffatt JG. The hydrolysis of uridine cyclic phosphonate catalyzed by ribonuclease-A: implications for the mechanism of action of the enzyme. Proc Natl Acad Sci U S A. 1969;63(2):246-52. PubMed PMID: 5257121; PubMed Central PMCID: PMC223554.
20. Widler L, Jahnke W, Green JR. The chemistry of bisphosphonates: from antiscaling agents to clinical therapeutics. Anticancer Agents Med Chem. 2012;12(2):95-101. PubMed PMID: 21864230.
21. Copeland RA. Evaluation of enzyme inhibitors in drug discovery a guide for medicinal chemists and pharmacologists Hoboken, N.J.: J. Wiley; 2005. Available from: http://search.ebscohost.com/login.aspx?direct=true&scope=site&db=nlebk&db=nlabk&AN=129367.
22. John J, Sohmen R, Feuerstein J, Linke R, Wittinghofer A, Goody RS. Kinetics of interaction of nucleotides with nucleotide-free H-ras p21. Biochemistry. 1990;29(25):6058-65. PubMed PMID: 2200519.
23. Patricelli MP, Szardenings AK, Liyanage M, Nomanbhoy TK, Wu M, Weissig H, et al. Functional interrogation of the kinome using nucleotide acyl phosphates. Biochemistry. 2007;46(2):350-8. doi: 10.1021/bi062142x. PubMed PMID: 17209545.
24. Xiao YS, Guo L, Jiang XN, Wang YS. Proteome-Wide Discovery and Characterizations of Nucleotide-Binding Proteins with Affinity-Labeled Chemical Probes. Anal Chem. 2013;85(6):3198-206. doi: 10.1021/ac303383c. PubMed PMID: WOS:000316520500023.
25. Ulsh LS, Shih TY. Metabolic turnover of human c-rasH p21 protein of EJ bladder carcinoma and its normal cellular and viral homologs. Molecular and cellular biology. 1984;4(8):1647-52.
26. Shukla S, Allam US, Ahsan A, Chen G, Krishnamurthy PM, Marsh K, et al. KRAS protein stability is regulated through SMURF2: UBCH5 complex-mediated β-TrCP1 degradation. Neoplasia. 2014;16(2):115-W5.
27. Westover KD. Enzymology of GTP-competitive RAS inhibitors: National Cancer Institute Ras Initiative; 2015. Available from: http://www.cancer.gov/research/key-initiatives/ras/ras-central/blog/Enzymology-of-GTP-competitive-RAS-inhibitors.
28. For a table of pKa, bond lengths, and bond angles for different diphosphate isosteres, see supporting information.
29. Romanenko VD, Kukhar VP. Fluorinated phosphonates: synthesis and biomedical application. Chem Rev. 2006;106(9):3868-935. doi: 10.1021/cr051000q. PubMed PMID: 16967924.
30. Elliott TS, Slowey A, Ye Y, Conway SJ. The use of phosphate bioisosteres in medicinal chemistry and chemical biology. MedChemComm. 2012;3(7):735-51. doi: 10.1039/C2MD20079A.
31. Imidobisphosphate (P-NH-P linkage) is also a common isostere for diphosphate. Due to difficulties in the synthesis of the corresponding diester, this analog was not obtained.
32. Flanagan ME, Abramite JA, Anderson DP, Aulabaugh A, Dahal UP, Gilbert AM, et al. Chemical and Computational Methods for the Characterization of Covalent Reactive Groups for the Prospective Design of Irreversible Inhibitors. J Med Chem. 2014;57(23):10072-9. doi: 10.1021/jm501412a.
33. Niewiadomski S, Beebeejaun Z, Denton H, Smith TK, Morris RJ, Wagner GK. Rationally designed squaryldiamides - a novel class of sugar-nucleotide mimics? Org Biomol Chem. 2010;8(15):3488-99. doi: 10.1039/c004165c. PubMed PMID: 20532300.

34. Singh A, Greninger P, Rhodes D, Koopman L, Violette S, Bardeesy N, et al. A gene expression signature associated with "K-Ras addiction" reveals regulators of EMT and tumor cell survival. Cancer cell. 2009;15(6):489-500. doi: 10.1016/j.ccr.2009.03.022. PubMed PMID: 19477428; PubMed Central PMCID: PMC2743093.
35. Niesen FH, Berglund H, Vedadi M. The use of differential scanning fluorimetry to detect ligand interactions that promote protein stability. Nature protocols. 2007;2(9):2212-21.
36. Drosten M, Dhawahir A, Sum EY, Urosevic J, Lechuga CG, Esteban LM, et al. Genetic analysis of Ras signalling pathways in cell proliferation, migration and survival. The EMBO journal. 2010;29(6):1091-104.

What opportunities for training and professional development has the project provided?
If the project was not intended to provide training and professional development opportunities or there is nothing significant to report during this reporting period, state "Nothing to Report."

Describe opportunities for training and professional development provided to anyone who worked on the project or anyone who was involved in the activities supported by the project. "Training" activities are those in which individuals with advanced professional skills and experience assist others in attaining greater proficiency. Training activities may include, for example, courses or one-on-one work with a mentor. "Professional development" activities result in increased knowledge or skill in one's area of expertise and may include workshops, conferences, seminars, study groups, and individual study. Include participation in conferences, workshops, and seminars not listed under major activities.

Dr. Westover was invited to speak at the 2017 Forbec Forum as one of 15 RAS investigators representing the "cream of oncology expertise from around the world".

How were the results disseminated to communities of interest?
If there is nothing significant to report during this reporting period, state "Nothing to Report."

Describe how the results were disseminated to communities of interest. Include any outreach activities that were undertaken to reach members of communities who are not usually aware of these project activities, for the purpose of enhancing public understanding and increasing interest in learning and careers in science, technology, and the humanities.

We published 3 manuscripts during the reporting period.

What do you plan to do during the next reporting period to accomplish the goals?
If this is the final report, state "Nothing to Report."

Describe briefly what you plan to do during the next reporting period to accomplish the goals and objectives.

Our focus will shift to evaluating additional KRAS binding compounds using our established methods and publishing results. In particular we will focus on the GTP-binding pocket. We also wish to study the impact of these compounds on RAS dimers.

4. **IMPACT:** Describe distinctive contributions, major accomplishments, innovations, successes, or any change in practice or behavior that has come about as a result of the project relative to:

What was the impact on the development of the principal discipline(s) of the project?
If there is nothing significant to report during this reporting period, state "Nothing to Report."

Describe how findings, results, techniques that were developed or extended, or other products from the project made an impact or are likely to make an impact on the base of knowledge, theory, and research in the principal disciplinary field(s) of the project. Summarize using language that an intelligent lay audience can understand (Scientific American style).

1. Developed 2 new classes of KRAS binding compounds.
2. Developed new methods to evaluate new RAS-binding compounds.
3. Solved 4 x-ray crystal structures that were deposited in the protein databank.
4. Published 3 manuscripts reporting these activities.

What was the impact on other disciplines?
If there is nothing significant to report during this reporting period, state "Nothing to Report."

Describe how the findings, results, or techniques that were developed or improved, or other products from the project made an impact or are likely to make an impact on other disciplines.

Assay methods we developed could have implications for other drug development projects.

What was the impact on technology transfer?
If there is nothing significant to report during this reporting period, state "Nothing to Report."

Describe ways in which the project made an impact, or is likely to make an impact, on commercial technology or public use, including:

- *transfer of results to entities in government or industry;*
- *instances where the research has led to the initiation of a start-up company; or*
- *adoption of new practices.*

Assay methods we reported are likely to be adopted within pharmaceutical companies

What was the impact on society beyond science and technology?
If there is nothing significant to report during this reporting period, state "Nothing to Report."

Describe how results from the project made an impact, or are likely to make an impact, beyond the bounds of science, engineering, and the academic world on areas such as:

- *improving public knowledge, attitudes, skills, and abilities;*
- *changing behavior, practices, decision making, policies (including regulatory policies), or social actions; or*
- *improving social, economic, civic, or environmental conditions.*

Nothing to Report.

5. **CHANGES/PROBLEMS:** The PD/PI is reminded that the recipient organization is required to obtain prior written approval from the awarding agency grants official whenever there are significant changes in the project or its direction. If not previously reported in writing, provide the following additional information or state, "Nothing to Report," if applicable:

In addition to exploring fragments discussed in the original proposal, we also examined quinazoline compounds. We also recently began studying the biological importance of RAS dimerization and request permission to use DOD funding to understand the effect of these compounds on RAS dimerization. Essentially developed a cell-based FRET system that allows us to detect RAS dimers. We plan to test if RAS compounds disrupt the RAS dimer in this system.

Actual or anticipated problems or delays and actions or plans to resolve them
Describe problems or delays encountered during the reporting period and actions or plans to resolve them.

Sourcing certain compounds of interest has been slow in some cases. We are continuously re-evaluating compound sourcing options.

Changes that had a significant impact on expenditures

Describe changes during the reporting period that may have had a significant impact on expenditures, for example, delays in hiring staff or favorable developments that enable meeting objectives at less cost than anticipated.

Delays in hiring staff delayed expenditures in the first year.

Significant changes in use or care of human subjects, vertebrate animals, biohazards, and/or select agents

Describe significant deviations, unexpected outcomes, or changes in approved protocols for the use or care of human subjects, vertebrate animals, biohazards, and/or select agents during the reporting period. If required, were these changes approved by the applicable institution committee (or equivalent) and reported to the agency? Also specify the applicable Institutional Review Board/Institutional Animal Care and Use Committee approval dates.

Significant changes in use or care of human subjects

Nothing to Report

Significant changes in use or care of vertebrate animals

Nothing to Report

Significant changes in use of biohazards and/or select agents

Nothing to Report

6. **PRODUCTS:** List any products resulting from the project during the reporting period. If there is nothing to report under a particular item, state "Nothing to Report."

Publications, conference papers, and presentations
Report only the major publication(s) resulting from the work under this award.

Journal publications. *List peer-reviewed articles or papers appearing in scientific, technical, or professional journals. Identify for each publication: Author(s); title; journal; volume: year; page numbers; status of publication (published; accepted, awaiting publication; submitted, under review; other); acknowledgement of federal support (yes/no).*

- Lu J, Harrison RA, Li L, Zeng M, Gondi S, Scott D, Gray NS, Engen JR, Westover KD. KRAS G12C Drug Development: Discrimination between Switch II Pocket Configurations Using Hydrogen/Deuterium-Exchange Mass Spectrometry. Structure. 2017 Sep 5;25(9):1442-1448, published, acknowledged – yes
- Xiong, Y, Lu J, Hunter J, Li L, Scott D, Choi HG, Lim SM, Manandhar A, Gondi S, Sim T, **Westover KD***, Gray NS*. Development of covalent guanosine mimetic inhibitors of G12C KRAS. ACS Med Chem Lett. 2016 Nov 30;8(1):61-66. Published, acknowledged – yes
- Zeng M, Lu J, Li L, Feru F, Quan C, Gero TW, Ficarro SB, Xiong Y, Ambrogio C, Paranal RM, Catalano M, Shao J, Wong KK, Marto JA, Fischer ES, Jänne PA, Scott DA, **Westover KD***, Gray NS*. Potent and Selective Covalent Quinazoline Inhibitors of KRAS G12C. Cell Chem Biol. 2017 Aug 17;24(8):1005-1016. Published, acknowledged – yes

Books or other non-periodical, one-time publications. *Report any book, monograph, dissertation, abstract, or the like published as or in a separate publication, rather than a periodical or series. Include any significant publication in the proceedings of a one-time conference or in the report of a one-time study, commission, or the like. Identify for each one-time publication: author(s); title; editor; title of collection, if applicable; bibliographic information; year; type of publication (e.g., book, thesis or dissertation); status of publication (published; accepted, awaiting publication; submitted, under review; other); acknowledgement of federal support (yes/no).*

None

Other publications, conference papers and presentations. *Identify any other publications, conference papers and/or presentations not reported above. Specify the status of the publication as noted above. List presentations made during the last year (international, national, local societies, military meetings, etc.). Use an asterisk (*) if presentation produced a manuscript.*

None

- **Website(s) or other Internet site(s)**
  List the URL for any Internet site(s) that disseminates the results of the research activities. A short description of each site should be provided. It is not necessary to include the publications already specified above in this section.

None

- **Technologies or techniques**
  Identify technologies or techniques that resulted from the research activities. Describe the technologies or techniques were shared.

Assay to detect binding of compounds to switch 2 pocket of KRAS G12C Assay to detect protein dynamics of switch 2 of KRAS Assay to detect shifts in thermal stability of KRAS G12C upon binding to small molecule inhibitors

- **Inventions, patent applications, and/or licenses**
  Identify inventions, patent applications with date, and/or licenses that have resulted from the research. Submission of this information as part of an interim research performance progress report is not a substitute for any other invention reporting required under the terms and conditions of an award.

None.

- **Other Products**
  Identify any other reportable outcomes that were developed under this project. Reportable outcomes are defined as a research result that is or relates to a product, scientific advance, or research tool that makes a meaningful contribution toward the understanding, prevention, diagnosis, prognosis, treatment and /or rehabilitation of a disease, injury or condition, or to improve the quality of life. Examples include:
  - *data or databases;*

- *physical collections;*
- *audio or video products;*
- *software;*
- *models;*
- *educational aids or curricula;*
- *instruments or equipment;*
- *research material (e.g., Germplasm; cell lines, DNA probes, animal models);*
- *clinical interventions;*
- *new business creation; and*
- *other.*

None

7. PARTICIPANTS & OTHER COLLABORATING ORGANIZATIONS

What individuals have worked on the project?
Provide the following information for: (1) PDs/PIs; and (2) each person who has worked at least one person month per year on the project during the reporting period, regardless of the source of compensation (a person month equals approximately 160 hours of effort). If information is unchanged from a previous submission, provide the name only and indicate "no change".

Example:

Name:	*Mary Smith*
Project Role:	*Graduate Student*
Researcher Identifier (e.g. ORCID ID):	*1234567*
Nearest person month worked:	*5*
Contribution to Project:	*Ms. Smith has performed work in the area of combined error-control and constrained coding.*
Funding Support:	*The Ford Foundation (Complete only if the funding support is provided from other than this award.)*

No change.

Has there been a change in the active other support of the PD/PI(s) or senior/key personnel since the last reporting period?
If there is nothing significant to report during this reporting period, state "Nothing to Report."

If the active support has changed for the PD/PI(s) or senior/key personnel, then describe what the change has been. Changes may occur, for example, if a previously active grant has closed and/or if a previously pending grant is now active. Annotate this information so it is clear what has changed from the previous submission. Submission of other support information is not necessary for pending changes or for changes in the level of effort for active support reported previously. The awarding agency may require prior written approval if a change in active other support significantly impacts the effort on the project that is the subject of the project report.

Nothing to Report.

What other organizations were involved as partners?
If there is nothing significant to report during this reporting period, state "Nothing to Report."

Describe partner organizations – academic institutions, other nonprofits, industrial or commercial firms, state or local governments, schools or school systems, or other organizations (foreign or domestic) – that were involved with the project. Partner organizations may have provided financial or in-kind support, supplied facilities or equipment, collaborated in the research, exchanged personnel, or otherwise contributed.

Provide the following information for each partnership:
Organization Name:
Location of Organization: (if foreign location list country)
Partner's contribution to the project (identify one or more)

- *Financial support;*
- *In-kind support (e.g., partner makes software, computers, equipment, etc., available to project staff);*
- *Facilities (e.g., project staff use the partner's facilities for project activities);*
- *Collaboration (e.g., partner's staff work with project staff on the project);*
- *Personnel exchanges (e.g., project staff and/or partner's staff use each other's facilities, work at each other's site); and*

Dana Farber Cancer Institute, Boston, MA, Collaboration
Northeastern University, Boston, MA, Collaboration

8. SPECIAL REPORTING REQUIREMENTS

COLLABORATIVE AWARDS: For collaborative awards, independent reports are required from BOTH the Initiating Principal Investigator (PI) and the Collaborating/Partnering PI. A duplicative report is acceptable; however, tasks shall be clearly marked with the responsible PI and research site. A report shall be submitted to **https://ers.amedd.army.mil** for each unique award.

QUAD CHARTS: If applicable, the Quad Chart (available on https://www.usamraa.army.mil) should be updated and submitted with attachments.

9. APPENDICES:

Attach all appendices that contain information that supplements, clarifies or supports the text. Examples include original copies of journal articles, reprints of manuscripts and abstracts, a curriculum vitae, patent applications, study questionnaires, and surveys, etc.

Published manuscripts.

ACS Medicinal Chemistry Letters

Letter

pubs.acs.org/acsmedchemlett

Covalent Guanosine Mimetic Inhibitors of G12C KRAS

Yuan Xiong,[†,‡] Jia Lu,[§] John Hunter,[§] Lianbo Li,[§] David Scott,[†,‡] Hwan Geun Choi,[∥] Sang Min Lim,[⊥] Anuj Manandhar,[§] Sudershan Gondi,[§] Taebo Sim,[#,¶] Kenneth D. Westover,[*,§] and Nathanael S. Gray[*,†,‡]

[†]Department of Cancer Biology, Dana Farber Cancer Institute, 450 Brookline Avenue, Boston, Massachusetts 02115, United States

[‡]Department of Biological Chemistry and Molecular Pharmacology, Harvard Medical School, Boston, Massachusetts 02215, United States

[§]Departments of Biochemistry and Radiation Oncology, The University of Texas, Southwestern Medical Center, 5323 Harry Hines Boulevard, Dallas, Texas 75390, United States

[∥]New Drug Development Center, Daegu-Gyeongbuk Medical Innovation Foundation, Daegu 41061, Republic of Korea

[⊥]Center for Neuro-Medicine, Korea Institute of Science and Technology, Seoul 02792, Republic of Korea

[#]Chemical Kinomics Research Center, Korea Institute of Science and Technology, Seoul 02792, Republic of Korea

[¶]KU-KIST Graduate School of Converging Science and Technology, Korea University, Seoul 02841, Republic of Korea

Supporting Information

ABSTRACT: Ras proteins are members of a large family of GTPase enzymes that are commonly mutated in cancer where they act as dominant oncogenes. We previously developed an irreversible guanosine-derived inhibitor, SML-8-73-1, of mutant G12C RAS that forms a covalent bond with cysteine 12. Here we report exploration of the structure−activity relationships (SAR) of hydrolytically stable analogues of SML-8-73-1 as covalent G12C KRAS inhibitors. We report the discovery of difluoromethylene bisphosphonate analogues such as compound **11**, which, despite exhibiting reduced efficiency as covalent G12C KRAS inhibitors, remove the liability of the hydrolytic instability of the diphosphate moiety present in SML-8-73-1 and provide the foundation for development of prodrugs to facilitate cellular uptake. The SAR and crystallographic results reaffirm the exquisite molecular recognition that exists in the diphosphate region of RAS for guanosine nucleotides which must be considered in the design of nucleotide-competitive inhibitors.

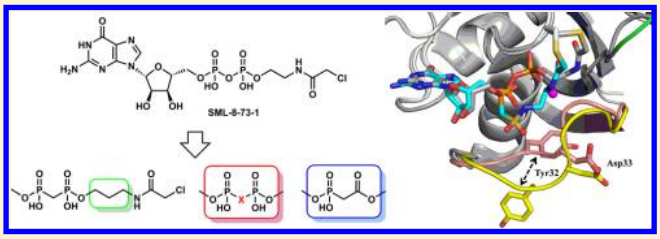

KEYWORDS: *KRAS G12C, drug design, covalent inhibitor, GDP mimetic, bisphosphonate, bioisostere, CPM, ActivX*

RAS mutations are frequently observed in malignant tumors and support diverse hallmarks of cancer including genomic instability,[1,2] cell proliferation,[3] suppression of apoptosis,[4] reprogramming of metabolism,[5,6] alteration of the microenvironment,[7,8] evasion of immune responses,[9,10] and promotion of metastases.[11,12] Consistent with its pervasive influence on cancer cell function, extinction of oncogenic KRAS in many established tumor models results in tumor regression.[6,13,14] Targeting RAS as a therapeutic measure is therefore a high priority.[15]

RAS mutations appear to fall into functional categories and will likely require tailored strategies to target each functional class.[16−18] KRAS G12C is the most commonly found RAS mutation in non-small cell lung cancer, the leading cause of cancer death in the United States.[19] Previously we hypothesized that the activating cysteine mutation in KRAS G12C might allow development of covalent GTP-competitive inhibitors. We reasoned that targeting the active site of KRAS would likely perturb KRAS G12C-mediated signaling based on the observation that RAS signaling is predicated on the identity of its bound ligand.[20,21]

We developed a GDP mimetic inhibitor SML-8-73-1, which contains an alpha-chloroacetamide electrophile and reacts with Cys12 upon inhibitor binding to KRAS G12C (Scheme 1). SML-8-73-1 is also able to compete *in vitro* with high concentration of GDP and GTP and decreases the affinity of KRAS G12C for the

Scheme 1. Analogue Design Based on Diphosphate Bioisosteres

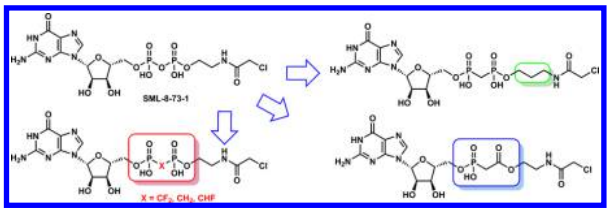

Received: September 22, 2016
Accepted: November 30, 2016
Published: November 30, 2016

ACS Publications © 2016 American Chemical Society

DOI: 10.1021/acsmedchemlett.6b00373
ACS Med. Chem. Lett. 2017, 8, 61−66

RAS binding domain (RBD) of BRAF.[22] Furthermore, unbiased proteomics based profiling showed that SML-8-73-1 is highly selective for KRAS G12C among other GTP binding proteins.[23] Nevertheless, SML-8-73-1 contains multiple charged phosphate groups and cannot pass through the cell membrane. Caging strategies to shield the charged phosphates were hampered by compound instability.[22]

To enable caging strategies and to explore the possibility of other chemical moieties that might improve properties of the diphosphate pharmacophore for covalent targeting of KRAS G12C, we investigated structure−activity relationships (SAR) on a series of analogues of SML-8-73-1 that varied the diphosphate group as well as the linker moiety. Here we report biochemical characterization of these compounds including an illustrative X-ray crystal structure demonstrating key difficulties inherent to this approach.

A diphosphate compound, SML-8-73-1 suffers from chemical and enzymatic instability, given that the phosphate anhydride bond is prone to hydrolysis.[24] This is problematic from two perspectives: first, unstable compounds are inherently disadvantageous from a pharmacokinetic perspective; and second, a caging strategy will likely be required to shield charged atoms in the phosphate pharmacophore to enhance cell permeability, and the resulting steric bulk may further destabilize the phosphate anhydride bond. To address these potential issues, the central oxygen was substituted with a methylene group. The corresponding bisphosphonate is considered to be resistant to acidic and enzymatic hydrolysis at the P−C−P bond,[25,26] and has been broadly used as an isostere of the diphosphate.

Synthesis of the bisphosphonates utilizes a one-pot reaction sequence, starting with nucleophilic addition−elimination reaction between methylenebis(phosphonic dichloride) and acetonide-protected guanosine **3** affording phosphonic chloride **5**, which was subsequently reacted with ethanolamine **6** to give phosphoric ester **7** after aqueous quench (Scheme 2).

Scheme 2. Synthesis of Bisphosphonate Analogues[a]

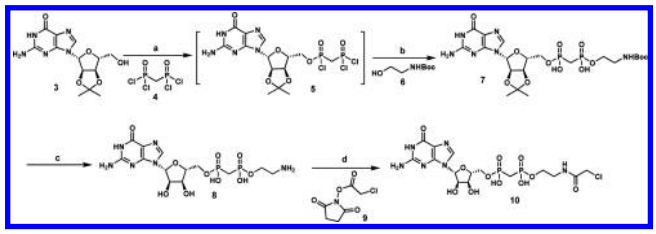

[a](a) $PO(OEt)_3$, 0 °C; (b) **6**, NEt_3, $PO(OEt)_3$, 0 °C to rt; (c) TFA/DCM, rt; (d) **9**, DIEA, DMF, 0 °C.

Deprotection under acidic conditions followed by selective acylation using activated NHS-ester **9** gave rise to desired bisphosphonate diester **10** (XY-01-103). This synthetic sequence allows facile and quick access to bisphosphonate analogues **10** to **20** with various linkers and different guanine analogues, by utilizing different alcohol reaction partners.

Different routes were employed to synthesize various bisphosphonate isosteres. Synthesis of phosphonate intermediate **25** commenced with DCC coupling of diethylphosphonoacetic acid **21** and ethanolamine **22**, and the resulting phosphoryl acetate **23** was deprotected and coupled to guanosine **3** to yield phosphoryl acetate **25** (Scheme 3). Similarly, phosphoryl acetate **29** was obtained by an altered sequence. Deprotection and selective acylation of intermediates **25** and **29** gave rise to

Scheme 3. Synthesis of Bisphosphonate Isosteres[a]

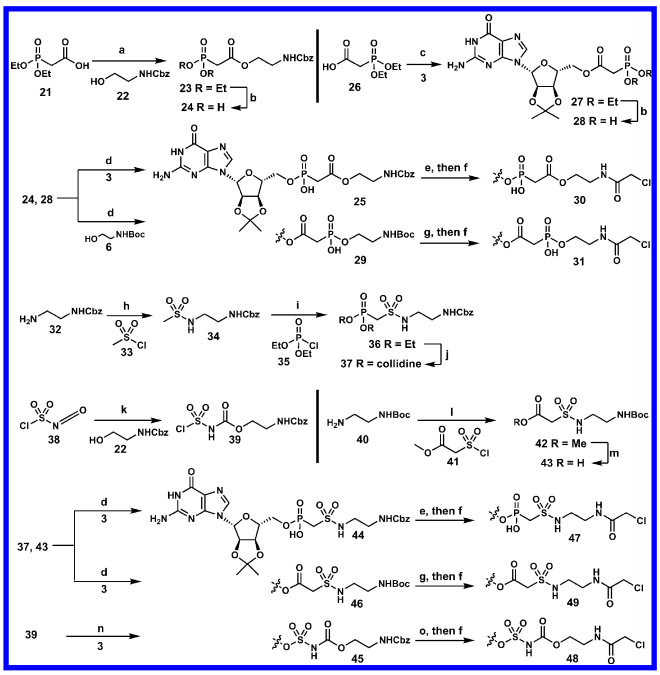

[a](a) **22**, DCC, cat. DMAP, DCM, rt; (b) TMSBr, MeCN, 0 °C to rt; (c) **3**, DCC, cat. DMAP, DMF, 60 °C; (d) **3** or **6**, DCC, cat. DMAP, DMF, rt; (e) H_2, Pd/C, MeOH, rt; then PTSA, DCM, rt; (f) **9**, DIEA, DMF, 0 °C; (g) TFA/DCM, rt; (h) **33**, NEt_3, DCM, 0 °C; (i) **35**, *n*BuLi, THF, −78 °C; (j) TMSBr, collidine, MeCN, rt; (k) **22**, NEt_3, DCM, 0 °C; (l) **41**, NEt_3, DCM, 0 °C to rt; (m) NaOH aq, EtOH, rt; (n) **3**, MeCN/pyridine, rt; (o) H_2, Pd/C, MeOH, rt; then 4 N HCl in dioxane, DCM, rt.

phosphoryl acetate compounds **30** and **31**, respectively. The synthesis of **47** started from sulfonylation of ethylenediamine **32**. The resulting sulfonamide **34** was deprotonated and reacted with diethyl chlorophosphate **35**. Following deprotection, the collidine salt **37** was coupled with guanosine **3** to give sulfamoyl phosphonate **44**, which was deprotected and acylated to provide **47** (XY-02-075). For **48**, sequential addition of ethanolamine **22** and guanosine **3** to chlorosulfonyl isocyanate **38** gave rise to sulfamate **45**, which after deprotection was acylated to yield **48**. Alternatively, the synthesis of **49** started from reaction of ethylenediamine **40** with chlorosulfonyl acetate **41**. Subsequent saponification and DCC coupling with guanosine **3** yielded the requisite sulfamoylacetate **46**, which was deprotected and acylated to give **49**.

To measure GDP displacement we utilized a competitive "chemosensor assay", wherein purified recombinant GDP-loaded KRAS G12C is incubated with compound, then probed at various time points with a probe compound that detects the presence of free (unreacted) G12C thiol. This assay provides a composite measurement of kinetic displacement of GDP and covalent inactivation of KRAS G12C (Figure S1).[23]

To determine the relative affinities of compounds we measured k_{inact}/K_i using GMP-stabilized KRAS G12C (Figure S2). To obtain these values we used the strategy advocated by Copeland[27] wherein reaction rates are plotted vs compound concentrations and fit to the curve described by the equation $k_{obs} = k_{inact}[I]/(K_i + [I])$. Using the fit, estimates for k_{inact} and K_i can be extracted (Figure S2C,D). For this assay purified nucleotide free KRAS G12C was prepared and stabilized with an excess of GMP, which has a low affinity of $3.5 \times 10^4\ M^{-1}$ for RAS.[28] GMP-stabilized RAS

DOI: 10.1021/acsmedchemlett.6b00373
ACS Med. Chem. Lett. 2017, 8, 61−66

is incubated with compound then probed with a GTP-desthiobiotin probe which, similarly to widely used ATP-biotin (ActivX) probes,[29,30] contains a reactive acyl phosphate anhydride that reacts with lysine 16 of KRAS. Desthiobiotinylated protein is detected using AlphaScreen (PerkinElmer) reagents (Figure S2A). Because the ActivX and AlphaScreen reagents are used in combination, we call this assay ActivAlpha (Figure S2D).

A third assay consists of incubating recombinant G12C KRAS with new inhibitors and then performing electrospray ionization mass spectrometry as reported previously.[22] The percent labeling of the protein can be detected as shown in Figure S3.

To meet our overarching goal of developing GTP-competitive inhibitors that have anticancer effects in cells, compounds will likely need to achieve adequate RAS inhibition well within the typical time scale of the RAS protein turnover; the half-life has been estimated at 12−24 h.[31,32] We previously performed rudimentary kinetics simulations[33] showing that G12C KRAS inactivators with a k_{inact} of 0.6 min^{-1} and K_i of 10 nM will yield 50% inhibition of KRAS G12C in 5 h. We therefore adopt these as preliminary standards for inhibitor development. Nevertheless it should be noted that the ActivAlpha assay utilizes an excess of GMP to stabilize the KRAS protein and, unlike the *in vivo* situation, does not require displacement of GDP or GTP.

In the ActivAlpha assay diphosphate **1** (SML-8-73-1) shows an excellent K_i of 9 nM and a relatively fast k_{inact} of 0.86 min^{-1}, which is consistent with the reactive chloroacetamide electrophile of SML-8-73-1. However, the corresponding methylenebisphosphonate analogue **10** loses 300-fold in binding affinity (K_i), and labels KRAS at a rate that is 11-fold slower (Table 1). This highlights the importance of interactions between the oxygen atom of the diphosphate and the various residues in the P-loop of KRAS. By substituting the central oxygen with a methylene group in **10**, both the pK_a of the resulting phosphoric acid and bond lengths and bond angles of the P−X−P linkage (X = O, CH_2) are altered, which may result in lower affinity.[34] To regain the electronic and conformational properties as in SML-8-73-1, difluoromethylene and monofluoromethylene groups were incorporated in compounds **11** and **12**, respectively. Fluorinated phosphonates are widely used in the pharmaceutical industry as phosphate isosteres and are found to be better phosphate mimetics than phosphonates.[35,36] In this case, difluoromethylene bisphosphonate analogue **11** improved the affinity for KRAS by 7-fold, compared to bisphosphonate analogue **10**, while the monofluoromethylene bisphosphonate analogue **12** showed a lower affinity and slower labeling rate.[37]

The acrylamide analogue of SML-8-73-1 (**2**) exhibits a higher rate constant k_{inact} than α-chloroacetamide-containing SML-8-73-1, although it is generally believed that the α-chloroacetamide warhead is more reactive toward cysteine group than acrylamide.[38] We postulated that longer length between the β-phosphate and the reactive site of the acrylamide in **2** may be optimal for the requisite covalent bond formation. Analogues with a propyl linker (**13**, **14**) improved the affinity to KRAS G12C, possibly due to a combinatory effect of optimal spacing, and better trajectory of the electrophile warhead toward nucleophilic substitution of Cys12. On the contrary, analogue **20**, with an internal electrophile and shorter distance between the β-phosphate and the reactive site for Cys12, showed complete loss of activity.

We hypothesized that a rigid linker with a preferred trajectory may further improve labeling efficiency, and a series of analogues with cyclic linkers were synthesized. In the case of **16** with a pyrrolidine linker, a larger k_{inact} of 2.2 min^{-1} was observed, along with fast labeling of G12C KRAS in the chemosensor assay ($t_{1/2}$ of 1.1h). Cyclopentane-containing analogues **18** and **19** which place the nitrogen in the exocyclic position also showed larger k_{inact}, however the affinities for these two compounds are significantly lower. A piperidine linker in **17** did not improve affinity or labeling efficiency.

We also examined substitution of one or both phosphates with carbonyl or sulfonyl groups. The results showed that both phosphates are crucial in achieving high binding affinity to KRAS; substituting one or both phosphates significantly lowered affinity

Table 1. SAR of Bisphosphonate Analogues and Diphosphate Isosteres

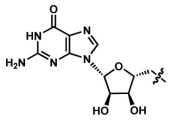

Cmpds	substitution	chemo-sensor $t_{1/2}$ (h)	K_I (μM)	k_{inact} (min^{-1})	k_{inact}/K_I (min^{-1} •μM^{-1})
1	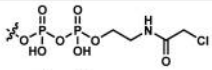	0.68	0.009	0.86	95
2	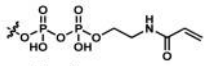	0.6	0.28	2.124	7.6
10	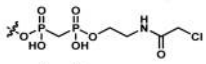	2.1	2.7	0.06	0.02
11	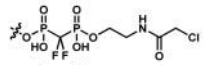	4.2	0.38	0.365	0.9
12	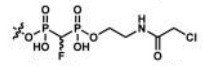	6.6	8	0.21	0.03
13	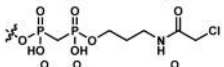	2.5	0.374	0.07	0.2
14	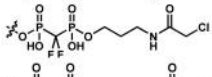	1.06	0.382	0.3	0.8
15	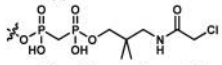	20	5	0.14	0.028
16	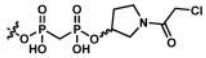	1.1	0.92	2.2	2.4
17	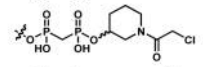	12	3.5	0.55	0.16
18	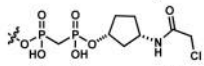	>36 (42)	50	1	0.02
19	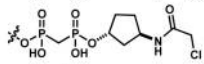	>36 (64)	36	2.3	0.06
20	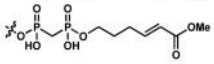	>36 (120)	>20	--	--
30	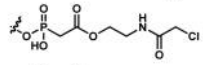	>36 (84)	15.2	0.055	0.003
31	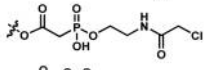	>36 (47)	2.2	0.053	0.02
47	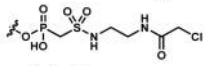	2.3	1.6	0.33	0.2
48	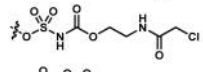	9.5	5	0.24	0.05
49	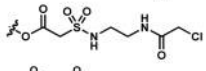	24	>10	--	--
50	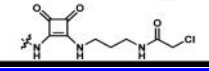	13	>25	--	--

DOI: 10.1021/acsmedchemlett.6b00373
ACS Med. Chem. Lett. 2017, 8, 61−66

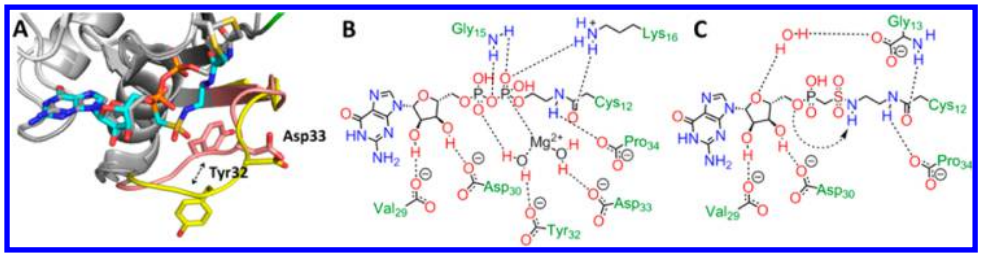

Figure 1. Comparison between G12C in complex with XY-02-075 (cyan/blue) and SML 8-73-1 (gray/orange). (A) Structural superposition of nucleotide binding pocket: switch I is highlighted in XY-02-075-bound structure in yellow and in SML-8-73-1 in salmon. Tyr32 and Asp33 are in sticks as labeled. (B, C) Schematic representation comparing interactions between SML-8-73-1 (B) or XY-02-075 (C) and Kras G12C. Dashed lines represent the hydrogen bonding interactions.

and resulted in longer labeling time. Among these, phosphonyl sulfonamide analogue **47** (XY-02-075) had the lowest K_i of 1.6 μM and a $t_{1/2}$ of 2.3 h. A cocrystal structure of XY-02-075 with KRAS G12C showed an intramolecular hydrogen bonding between the sulfonamide hydrogen and the phosphonate oxygen (see below). Phosphoryl acetate analogue **31**, in which the α-phosphate was replaced with an acetate group, showed a 7-fold lower K_i than the corresponding reversed phosphoryl acetate **30**. This observation is in line with previous reports that interactions between the β-phosphate in GDP and Ras or magnesium are stronger than that of the α-phosphate.[28] Further replacement of the remaining phosphonate with sulfonamide in compounds **48** and **49** did not significantly improve affinity. Incorporation of a squaryldiamide group, a common isostere for diphosphates and bisphosphonates,[39] in **50** resulted in poor affinity.

New GDP analogues did not achieve the comparable labeling efficiency observed for SML-8-73-1. To gain insight into why our analogues were inferior to SML-8-73-1, we determined the X-ray crystal structure of XY-02-075 bound to KRAS G12C. Complete labeling of KRAS G12C with XY-02-075 was confirmed prior to crystallization using mass spectrometry (Figure S3). Crystals were in the monoclinic space group C_2 with a unit cell similar to other KRAS structures obtained previously.[23] Molecular replacement using WT KRAS GDP-bound structure as a search model (PDB 4OBE) was used to obtain phase information, and the final model was refined to a resolution of 2.70 Å with *R*-work of 28.0%, *R*-free of 33.5%, and average *B*-factor of 89.0 Å^2 (Table S2).

The structure of the G domain is similar to previously solved RAS family protein structures including the previously reported SML-8-73-1-bound structure (PDB 4NMM) (RMSD = 0.43 Å, 166 atoms aligned). Continuous positive density connecting the terminal carbon atom of XY-02-075 to Cys12 confirmed a covalent link between the compound and protein (Figure S4). The conformation of residues surrounding the guanosine binding site, including P-loop (residue 10−17), ^{57}DXXG, ^{116}NKXD, and ^{146}SAK motifs, were similar to the SML-8-73-1-bound structure with several differences. Importantly there is a lack of density where a magnesium ion and coordinated water molecules have been observed in nearly all previous structures of HRAS and KRAS (Figure 1B,C). Also, in the XY-02-075-bound structure we observed a hydrogen bond between the amide carbonyl oxygen atom and the backbone nitrogen atom of Gly13, whereas the linker amide group formed a hydrogen bond with the ε-nitrogen group of Lys16 in the SML-8-73-1 structure. We also noted an outward displacement of switch I residues Tyr32 and Asp33 (Figure 1A). Finally, due to poor electron density and a high *B*-factor, switch II residues 63 and 64 could not be unambiguously assigned in our model.

Replacement of β-phosphate with sulfonamide apparently leads to dissociation of the magnesium ion and its coordinated water network. Compared to the SML-8-73-1 structure, the magnesium-bridged interaction between the β-phosphate and Tyr 32 and Asp 33 is lost when bound to XY-02-075. Additionally, an intramolecular hydrogen bond forms within XY-02-075 between the amide hydrogen of the sulfonamide and the oxygen atom of the α-phosphonate resulting in a kink in the inhibitor conformation relative to SML-8-73-1 (Figure 1B,C). This kink contributes to displacement of switch I residues Tyr32 and Asp33 by 3.3 Å relative to the position observed in the SML-8-73-1-bound structure. The folded conformation of XY-02-075 also does not allow the sulfonamide oxygens to form hydrogen bonds with the backbone nitrogen atoms of P-loop residues Gly15 and Lys16 as observed with SML-8-73-1. Consequently, the orientation of the linker amide group of XY-02-075 is shifted in comparison to SML-8-73-1.

To confirm that our compounds do not coordinate efficiently with Mg^{2+}, we performed a ^{31}P NMR $MgCl_2$ titration study[40] against fixed concentrations of GDP, GTP, and several of our compounds. These showed a Mg^{2+}-dependent shift in the ^{31}PNMR signal with the half-maximal effect at ∼0.5 equiv for GDP and GTP and a plateau by 2 equiv. However, with the same concentration of our phosphonate compounds, up to 20 equiv of Mg^{2+} was required before the shift in signal began to plateau, demonstrating that our phosphonate analogues bind Mg^{2+} with much lower affinity (Figures S5, S6).

Mono-, di-, and triphosphate esters are ubiquitously found in biological molecules including small molecules such as nucleotides, acetyl CoA, inositides, and phospholipids and as post-translational modifications to serine, threonine, and tyrosine on many proteins. Therefore, it is not surprising that a host of protein catalytic and binding pockets have evolved to use these molecules as substrates, cofactors, and recognition motifs. While phosphates are powerful binding elements and vastly improve the water solubility of compounds to which they are attached, they typically impair passive diffusion across a lipid bilayer and therefore are typically not found in small molecule drugs. Medicinal chemists have found a number of phosphate bioisosteres that are recognized by these pockets, but typically there is a considerable loss of binding affinity.[36] An alternative approach is to create phosphate prodrugs in which the phosphate is unveiled following intracellular metabolism by a suitable enzyme.

In stark contrast to the relative success in finding mono-phosphate mimetics, there has been much more limited effort and success in developing diphosphate mimetics. For example, squaryldiamides have been studied as diphosphate surrogates in mannosyltransferase targeting sugar-nucleotide mimics;[39] phos-

DOI: 10.1021/acsmedchemlett.6b00373
ACS Med. Chem. Lett. 2017, 8, 61−66

phinylformate has been used as diphosphate isostere in squalene synthetase inhibitors;[41] furthermore, sulfonylbenzoyl-nitrostyrenes were explored as bisubstrate type inhibitors of EGFR, in which the sulfonylbenzoyl moiety served as a diphosphate mimic.[42] However, these bioisosteres suffer from lowered bioactivity when compared with their diphosphate counterparts. We faced this challenge when considering how to generate a cell penetrant version of our prototype G12C KRAS labeling compound SML-8-73-1. We envisioned two possible approaches: to find noncharged phosphate mimetics or to create diphosphate prodrugs. Here we described the synthesis and biological characterization of 18 analogues where we explored phosphate replacements and "linker" variation. We discovered that relatively subtle changes to the diphosphate group resulted in dramatic reduction in affinity and labeling efficiency.

Based on our structural analysis the loss of affinity appears to be, at least in some cases, driven by disruption of the coordination between our compounds and magnesium resulting in loss of numerous interactions seen in native ligand-bound structures. Future efforts to optimize the phosphate pharmacophore will likely benefit from analysis of coordination between compounds and Mg^{2+}. This structure also adds evidence to the already extensive data supporting the highly dynamic nature of the RAS switches and their dependence on bound ligand for sampling certain conformations. In the structure reported here, switch I (especially residues 32 and 33) is shifted outward to accommodate the folded XY-02-075, which does not coordinate magnesium and water molecules. This suggests that even small alterations to a ligand bound to KRAS will result in conformational changes that will likely disrupt interactions with RAS effectors that use the switch I or switch II interfaces. The list of such proteins includes important proteins that transduce major signaling cascades from RAS including PI3K and B-RAF. This suggests that development of GTP-competitive inhibitors, if possible, will be highly likely to perturb RAS-dependent cellular processes such as oncogenesis in the case of activated RAS.

A promising compound obtained in this study, **11**, possesses a difluoromethylene bisphosphonate moiety and exhibits a 40-fold reduced affinity relative to SML-8-73-1 but has the potential advantage of more facile prodrug creation due to not having the chemical instability that results from the phosphate anhydride bond. Current efforts focus on development of prodrugs of difluoromethylene bisphosphonate analogues as well as replacement of the guanine heterocycle with moieties that possess better binding affinity in order to regain affinity lost in the phosphate binding pocket.

■ ASSOCIATED CONTENT

Supporting Information

The Supporting Information is available free of charge on the ACS Publications website at DOI: 10.1021/acsmedchemlett.6b00373.

Experimental methods, X-ray data, and Figures S1−S6 (PDF)

■ AUTHOR INFORMATION

Corresponding Authors

*E-mail: Kenneth.Westover@UTSouthwestern.edu.
*E-mail: Nathanael_Gray@dfci.harvard.edu.

ORCID

Nathanael S. Gray: 0000-0001-5354-7403

Funding

Y.X., N.S.G., and K.D.W. were supported by Astellas Pharma Inc. K.D.W. was also supported by the Welch Foundation I1829, the V Foundation for Cancer Research, and DOD W81XWH-16-1-0106.

Notes

The authors declare no competing financial interest.

■ ACKNOWLEDGMENTS

Results shown in this article are derived from work performed at Argonne National Laboratory, Structural Biology Center at the Advanced Photon Source. Argonne is operated by U Chicago Argonne, LLC, for the U.S. Department of Energy, Office of Biological and Environmental Research, under Contract DEAC02-06CH11357. Mass spectrometry work shown in this article was performed at the UT Southwestern proteomics core facility.

■ ABBREVIATIONS

DMAP, 4-dimethylaminopyridine; DCC, *N*,*N*′-dicyclohexylcarbodiimide; PTSA, *p*-toluenesulfonic acid; DCM, dichloromethane; TFA, trifluoroacetic acid; DIEA, *N*,*N*-diisopropylethylamine; TMSBr, bromotrimethylsilane

■ REFERENCES

(1) Denko, N. C.; Giaccia, A. J.; Stringer, J. R.; Stambrook, P. J. The human Ha-ras oncogene induces genomic instability in murine fibroblasts within one cell cycle. *Proc. Natl. Acad. Sci. U. S. A.* **1994**, *91*, 5124.

(2) Saavedra, H. I.; Knauf, J. A.; Shirokawa, J. M.; Wang, J.; Ouyang, B.; Elisei, R.; Stambrook, P. J.; Fagin, J. A. The RAS oncogene induces genomic instability in thyroid PCCL3 cells via the MAPK pathway. *Oncogene* **2000**, *19*, 3948.

(3) Pylayeva-Gupta, Y.; Grabocka, E.; Bar-Sagi, D. RAS oncogenes: weaving a tumorigenic web. *Nat. Rev. Cancer* **2011**, *11*, 761.

(4) Cox, A. D.; Der, C. J. The dark side of Ras: regulation of apoptosis. *Oncogene* **2003**, *22*, 8999.

(5) Flier, J. S.; Mueckler, M. M.; Usher, P.; Lodish, H. F. Elevated levels of glucose transport and transporter messenger RNA are induced by ras or src oncogenes. *Science* **1987**, *235*, 1492.

(6) Ying, H.; Kimmelman, A. C.; Lyssiotis, C. A.; Hua, S.; Chu, G. C.; Fletcher-Sananikone, E.; Locasale, J. W.; Son, J.; Zhang, H.; Coloff, J. L. Oncogenic Kras maintains pancreatic tumors through regulation of anabolic glucose metabolism. *Cell* **2012**, *149*, 656.

(7) Rak, J.; Mitsuhashi, Y.; Bayko, L.; Filmus, J.; Shirasawa, S.; Sasazuki, T.; Kerbel, R. S. Mutant ras oncogenes upregulate VEGF/VPF expression: implications for induction and inhibition of tumor angiogenesis. *Cancer Res.* **1995**, *55*, 4575.

(8) Ancrile, B. B.; O'Hayer, K. M.; Counter, C. M. Oncogenic ras-induced expression of cytokines: a new target of anti-cancer therapeutics. *Mol. Interventions* **2008**, *8*, 22.

(9) Weijzen, S.; Velders, M.; Kast, W. Modulation of the immune response and tumor growth by activated Ras. *Leukemia* **1999**, *13*, 502.

(10) Seliger, B.; Harders, C.; Lohmann, S.; Momburg, F.; Urlinger, S.; Tampe, R.; Huber, C. Down-regulation of the MHC class I antigen-processing machinery after oncogenic transformation of murine fibroblasts. *Eur. J. Immunol.* **1998**, *28*, 122.

(11) Lundy, J.; Grimson, R.; Mishriki, Y.; Chao, S.; Oravez, S.; Fromowitz, F.; Viola, M. Elevated ras oncogene expression correlates with lymph node metastases in breast cancer patients. *J. Clin. Oncol.* **1986**, *4*, 1321.

(12) Campbell, P. M.; Der, C. J. Oncogenic Ras and its role in tumor cell invasion and metastasis. *Semin. Cancer Biol.* **2004**, *14*, 105.

(13) Millis, A. J.; Hoyle, M.; McCue, H. M.; Martini, H. Differential expression of metalloproteinase and tissue inhibitor of metalloproteinase genes in aged human fibroblasts. *Exp. Cell Res.* **1992**, *201*, 373.

(14) Fisher, G. H.; Wellen, S. L.; Klimstra, D.; Lenczowski, J. M.; Tichelaar, J. W.; Lizak, M. J.; Whitsett, J. A.; Koretsky, A.; Varmus, H. E. Induction and apoptotic regression of lung adenocarcinomas by regulation of a K-Ras transgene in the presence and absence of tumor suppressor genes. *Genes Dev.* **2001**, *15*, 3249.
(15) Stephen, A. G.; Esposito, D.; Bagni, R. K.; McCormick, F. Dragging ras back in the ring. *Cancer Cell* **2014**, *25*, 272.
(16) Hunter, J. C.; Manandhar, A.; Carrasco, M. A.; Gurbani, D.; Gondi, S.; Westover, K. D. Biochemical and structural analysis of common cancer-associated KRAS mutations. *Mol. Cancer Res.* **2015**, *13*, 1325.
(17) Al-Mulla, F.; Milner-White, E. J.; Going, J. J.; Birnie, G. D. Structural differences between valine-12 and aspartate-12 Ras proteins may modify carcinoma aggression. *J. Pathol.* **1999**, *187*, 433.
(18) De Roock, W.; Jonker, D. J.; Di Nicolantonio, F.; Sartore-Bianchi, A.; Tu, D.; Siena, S.; Lamba, S.; Arena, S.; Frattini, M.; Piessevaux, H. Association of KRAS p. G13D mutation with outcome in patients with chemotherapy-refractory metastatic colorectal cancer treated with cetuximab. *JAMA* **2010**, *304*, 1812.
(19) Siegel, R. L.; Miller, K. D.; Jemal, A. Cancer statistics. *Ca-Cancer J. Clin.* **2015**, *65*, 5.
(20) Milburn, M. V.; Tong, L.; Brunger, A.; Yamaizumi, Z.; Nishimura, S.; Kim, S. Molecular switch for signal transduction: structural differences between active and inactive forms of protooncogenic ras proteins. *Science* **1990**, *247*, 939.
(21) Satoh, T.; Nakafuku, M.; Kaziro, Y. Function of Ras as a molecular switch in signal transduction. *J. Biol. Chem.* **1992**, *267*, 24149.
(22) Lim, S. M.; Westover, K. D.; Ficarro, S. B.; Harrison, R. A.; Choi, H. G.; Pacold, M. E.; Carrasco, M.; Hunter, J.; Kim, N. D.; Xie, T.; Sim, T.; Janne, P. A.; Meyerson, M.; Marto, J. A.; Engen, J. R.; Gray, N. S. Therapeutic targeting of oncogenic K-Ras by a covalent catalytic site inhibitor. *Angew. Chem., Int. Ed.* **2014**, *53*, 199.
(23) Hunter, J. C.; Gurbani, D.; Ficarro, S. B.; Carrasco, M. A.; Lim, S. M.; Choi, H. G.; Xie, T.; Marto, J. A.; Chen, Z.; Gray, N. S.; Westover, K. D. In situ selectivity profiling and crystal structure of SML-8-73-1, an active site inhibitor of oncogenic K-Ras G12C. *Proc. Natl. Acad. Sci. U. S. A.* **2014**, *111*, 8895.
(24) Budovskii, E. I.; Shibaev, V. N. Kinetics of the acid hydrolysis of uridine diphosphate glucose and 3-*N*-methyluridine diphosphate glucose. *Chem. Nat. Compd.* **1968**, *4*, 199.
(25) Harris, M. R.; Usher, D. A.; Albrecht, H. P.; Jones, G. H.; Moffatt, J. G. The hydrolysis of uridine cyclic phosphonate catalyzed by ribonuclease-A: implications for the mechanism of action of the enzyme. *Proc. Natl. Acad. Sci. U. S. A.* **1969**, *63*, 246.
(26) Widler, L.; Jahnke, W.; Green, J. R. The chemistry of bisphosphonates: from antiscaling agents to clinical therapeutics. *Anti-Cancer Agents Med. Chem.* **2012**, *12*, 95.
(27) Copeland, R. A. *Evaluation of enzyme inhibitors in drug discovery a guide for medicinal chemists and pharmacologists*; John Wiley & Sons: 2013.
(28) John, J.; Sohmen, R.; Feuerstein, J.; Linke, R.; Wittinghofer, A.; Goody, R. S. Kinetics of interaction of nucleotides with nucleotide-free H-ras p21. *Biochemistry* **1990**, *29*, 6058.
(29) Patricelli, M. P.; Szardenings, A. K.; Liyanage, M.; Nomanbhoy, T. K.; Wu, M.; Weissig, H.; Aban, A.; Chun, D.; Tanner, S.; Kozarich, J. W. Functional interrogation of the kinome using nucleotide acyl phosphates. *Biochemistry* **2007**, *46*, 350.
(30) Xiao, Y. S.; Guo, L.; Jiang, X. N.; Wang, Y. S. Proteome-wide discovery and characterizations of nucleotide-binding proteins with affinity-labeled chemical probes. *Anal. Chem.* **2013**, *85*, 3198.
(31) Ulsh, L. S.; Shih, T. Y. Metabolic turnover of human c-rasH p21 protein of EJ bladder carcinoma and its normal cellular and viral homologs. *Mol. Cell. Biol.* **1984**, *4*, 1647.
(32) Shukla, S.; Allam, U. S.; Ahsan, A.; Chen, G.; Krishnamurthy, P. M.; Marsh, K.; Rumschlag, M.; Shankar, S.; Whitehead, C.; Schipper, M. KRAS protein stability is regulated through SMURF2: UBCH5 complex-mediated β-TrCP1 degradation. *Neoplasia* **2014**, *16*, 115.
(33) Westover, K. D. Enzymology of GTP-competitive RAS inhibitors. http://www.cancer.gov/research/key-initiatives/ras/ras-central/blog/Enzymology-of-GTP-competitive-RAS-inhibitors.
(34) For a table of pK_a, bond lengths, and bond angles for different diphosphate isosteres, see the Supporting Information.
(35) Romanenko, V. D.; Kukhar, V. P. Fluorinated phosphonates: synthesis and biomedical application. *Chem. Rev.* **2006**, *106*, 3868.
(36) Elliott, T. S.; Slowey, A.; Ye, Y.; Conway, S. J. The use of phosphate bioisosteres in medicinal chemistry and chemical biology. *MedChemComm* **2012**, *3*, 735.
(37) Imidobisphosphate (P-NH-P linkage) is also a common isostere for diphosphate. Due to difficulties in the synthesis of the corresponding diester, this analogue was not obtained.
(38) Flanagan, M. E.; Abramite, J. A.; Anderson, D. P.; Aulabaugh, A.; Dahal, U. P.; Gilbert, A. M.; Li, C.; Montgomery, J.; Oppenheimer, S. R.; Ryder, T.; Schuff, B. P.; Uccello, D. P.; Walker, G. S.; Wu, Y.; Brown, M. F.; Chen, J. M.; Hayward, M. M.; Noe, M. C.; Obach, R. S.; Philippe, L.; Shanmugasundaram, V.; Shapiro, M. J.; Starr, J.; Stroh, J.; Che, Y. Chemical and Computational Methods for the Characterization of Covalent Reactive Groups for the Prospective Design of Irreversible Inhibitors. *J. Med. Chem.* **2014**, *57*, 10072.
(39) Niewiadomski, S.; Beebeejaun, Z.; Denton, H.; Smith, T. K.; Morris, R. J.; Wagner, G. K. Rationally designed squaryldiamides-a novel class of sugar-nucleotide mimics? *Org. Biomol. Chem.* **2010**, *8*, 3488.
(40) Pecoraro, V. L.; Hermes, J. D.; Cleland, W. W. Stability constants of Mg^{2+} and Cd^{2+} complexes of adenine nucleotides and thionucleotides and rate constants for formation and dissociation of MgATP and MgADP. *Biochemistry* **1984**, *23*, 5262.
(41) Biller, S. A.; Forster, C.; Gordon, E. M.; Harrity, T.; Rich, L. C.; Marretta, J.; Ciosek, C. P., Jr. Isoprenyl phosphinylformates: new inhibitors of squalene synthetase. *J. Med. Chem.* **1991**, *34*, 1912.
(42) Traxler, P. M.; Wacker, O.; Bach, H. L.; Geissler, J. F.; Kump, W.; Meyer, T.; Regenass, U.; Roesel, J. L.; Lydon, N. Sulfonylbenzoyl-nitrostyrenes: potential bisubstrate type inhibitors of the EGF-receptor tyrosine protein kinase. *J. Med. Chem.* **1991**, *34*, 2328.

DOI: 10.1021/acsmedchemlett.6b00373
ACS Med. Chem. Lett. 2017, 8, 61−66

Article

Cell Chemical Biology

Potent and Selective Covalent Quinazoline Inhibitors of KRAS G12C

Graphical Abstract

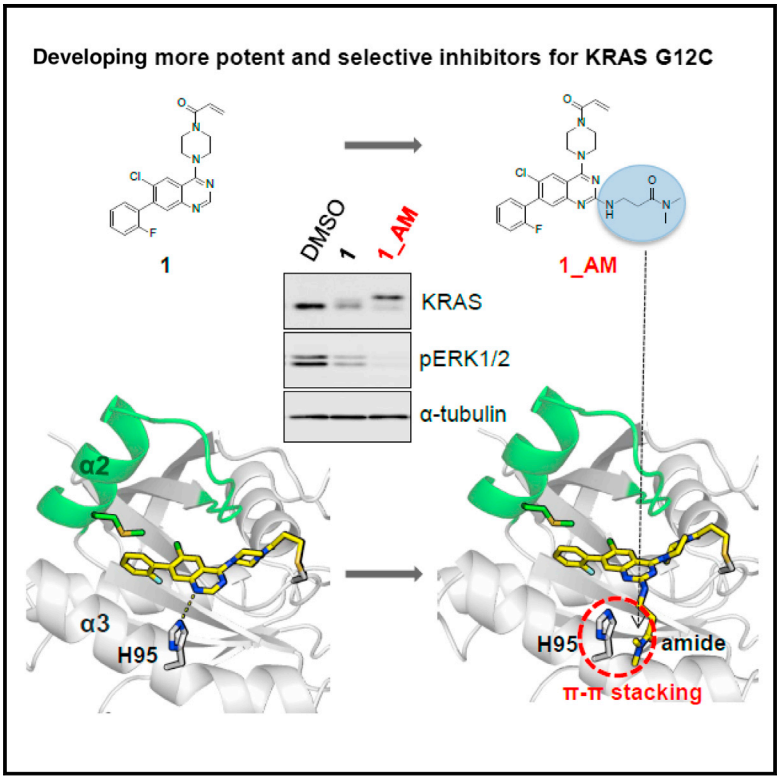

Highlights

- Functional and structural characterization of covalent KRAS G12C inhibitors
- An amino amide substituent enhances the potency and selectivity of inhibitors
- Develop key assays for characterization and discovery of new KRAS inhibitors

Authors

Mei Zeng, Jia Lu, Lianbo Li, ..., David A. Scott, Kenneth D. Westover, Nathanael S. Gray

Correspondence

kenneth.westover@utsouthwestern.edu (K.D.W.), nathanael_gray@dfci.harvard.edu (N.S.G.)

In Brief

Zeng et al. demonstrate that introduction of an amino amide substituent to the quinazoline scaffold remarkably increases the labeling efficiency and rates, potency, and selectivity of KRAS G12C inhibitors. This is supported by structural evidence that amide side chain allows additional interactions with KRAS G12C.

Zeng et al., 2017, Cell Chemical Biology *24*, 1–12
August 17, 2017 © 2017 Elsevier Ltd.
http://dx.doi.org/10.1016/j.chembiol.2017.06.017

CellPress

Please cite this article in press as: Zeng et al., Potent and Selective Covalent Quinazoline Inhibitors of KRAS G12C, Cell Chemical Biology (2017), http://dx.doi.org/10.1016/j.chembiol.2017.06.017

Cell Chemical Biology
Article

Potent and Selective Covalent Quinazoline Inhibitors of KRAS G12C

Mei Zeng,[1,2] Jia Lu,[3] Lianbo Li,[3] Frederic Feru,[1,2] Chunshan Quan,[1,2] Thomas W. Gero,[1,2] Scott B. Ficarro,[1,2,4] Yuan Xiong,[1,2] Chiara Ambrogio,[5] Raymond M. Paranal,[5] Marco Catalano,[5] Jay Shao,[1] Kwok-Kin Wong,[6] Jarrod A. Marto,[1,2,4] Eric S. Fischer,[1,2] Pasi A. Jänne,[5,7] David A. Scott,[1,2] Kenneth D. Westover,[3,*] and Nathanael S. Gray[1,2,8,*]
[1]Department of Cancer Biology, Dana-Farber Cancer Institute, Boston, MA 02115, USA
[2]Department of Biological Chemistry and Molecular Pharmacology, Harvard Medical School, Boston, MA 02115, USA
[3]Departments of Biochemistry and Radiation Oncology, The University of Texas Southwestern Medical Center at Dallas, Dallas, TX 75390, USA
[4]Blais Proteomics Center, Dana-Farber Cancer Institute, Boston, MA 02115, USA
[5]Department of Medical Oncology, Dana-Farber Cancer Institute, Boston, MA 02115, USA
[6]Division of Hematology and Medical Oncology, Department of Medicine, New York University School of Medicine, New York, NY 10016, USA
[7]Belfer Center for Applied Cancer Science, Dana Farber Cancer Institute, Boston, MA 02115, USA
[8]Lead Contact
*Correspondence: kenneth.westover@utsouthwestern.edu (K.D.W.), nathanael_gray@dfci.harvard.edu (N.S.G.)
http://dx.doi.org/10.1016/j.chembiol.2017.06.017

SUMMARY

Targeted covalent small molecules have shown promise for cancers driven by KRAS G12C. Allosteric compounds that access an inducible pocket formed by movement of a dynamic structural element in KRAS, switch II, have been reported, but these compounds require further optimization to enable their advancement into clinical development. We demonstrate that covalent quinazoline-based switch II pocket (SIIP) compounds effectively suppress GTP loading of KRAS G12C, MAPK phosphorylation, and the growth of cancer cells harboring G12C. Notably we find that adding an amide substituent to the quinazoline scaffold allows additional interactions with KRAS G12C, and remarkably increases the labeling efficiency, potency, and selectivity of KRAS G12C inhibitors. Structural studies using X-ray crystallography reveal a new conformation of SIIP and key interactions made by substituents located at the quinazoline 2-, 4-, and 7-positions. Optimized lead compounds in the quinazoline series selectively inhibit KRAS G12C-dependent signaling and cancer cell growth at sub-micromolar concentrations.

INTRODUCTION

RAS GTPases are lynchpins in critical signal transduction pathways that direct cell growth, differentiation, proliferation, and survival. RAS acts as a binary molecular switch that is activated when bound to guanosine triphosphate (GTP) and inactive when bound to guanosine diphosphate (GDP) (Campbell and Der, 2004; Pylayeva-Gupta et al., 2011). State transitions of RAS are brought about by intrinsic or GTPase-activating protein (GAP)-catalyzed GTP hydrolysis activity or guanine nucleotide exchange factor (GEF) facilitated nucleotide exchange (Cox and Der, 2010; Karnoub and Weinberg, 2008). GEFs and GAPs regulate RAS by interacting with two dynamic regions in the effector lobe of RAS consisting of switch I (SWI) and switch II (SWII) (Hall et al., 2002). The conformations of SWI and SWII, which change depending on the nucleotide bound, directly control the interactions between RAS and other protein effectors of RAS.

RAS genes are frequently mutated oncogenes in human cancers, with KRAS the most commonly mutant subtype. Hot spots for single-point mutations at codons G12, G13, and Q61 all surround the guanine nucleotide binding site, consistent with the critical role of the bound ligand in determining the signaling state of RAS. Of particular importance in lung cancer is the KRAS G12C mutation which is the most common RAS mutation seen in non-small-cell lung cancer, found in approximately 25,000 new cases of lung cancer annually and is associated with smoking (Downward, 2003). Although RAS mutations are often considered an early event in promoting carcinogenesis, RAS are also critical for tumor maintenance given that extinction of RAS in laboratory models of RAS-initiated cancers results in tumor regression, suggesting that direct inhibition of RAS would be a viable and valuable therapeutic strategy if achievable (Bardeesy and DePinho, 2002; Fisher et al., 2001; Ying et al., 2012).

Exploration of direct RAS-targeting strategies has seen a stunning renaissance, reversing the long chill on RAS drug development that followed disappointing clinical trials results for farnesyl transferase inhibitors almost 15 years ago (Adjei et al., 2003). Approaches have included targeting SOS-mediated nucleotide exchange activity (Maurer et al., 2012; Sun et al., 2012), targeting intracellular RAS transport mechanisms that are mediated by PDEδ (Zimmermann et al., 2013), and targeting binding pockets on RAS (Lim et al., 2014; Welsch et al., 2017; Xiong et al., 2017) (Figure S1). Previously we reported development of covalent GDP mimetics designed to selectively target the oncogenic KRAS G12C mutant based on the presence of the nucleophilic cysteine residue at codon 12 (Xiong et al.,

2017). While our originally reported tool compounds were promising in terms of potency and selectivity they were not suitable for optimization because they included a highly polar diphosphate pharmacophore that prevents cellular penetration. Attempts to chemically shield or introduce bisphosphate isosteres resulted in either compound instability or dramatic losses in potency (Lim et al., 2014; Xiong et al., 2017). At the same time, others discovered a novel allosteric regulatory site beneath the switch II pocket (SIIP) that was successfully utilized to covalently target KRAS G12C (Ostrem et al., 2013; Lito et al., 2016; Patricelli et al., 2016). We hypothesized that it might be possible to overcome the limits of current GDP mimetic compounds by designing compounds that incorporate elements of both SIIP and the guanosine pharmacophores, or by developing bivalent compounds that could recruit ligases to affect the ubiquitin-mediated degradation of RAS (Toure and Crews, 2016; Winter et al., 2015) (Figure S1). As a first step in that direction, here we characterize and elaborate a series of quinazoline SIIP binders whose chemical structures were first reported in the patent literature (Ren et al., 2014). Using X-ray crystallography and novel SIIP-directed biochemical assays we identified design principles that contribute to the potency of this class of inhibitor and inform the development of bivalent inhibitors. Notably we find that introduction of an amino amide substituent to the quinazoline scaffold allows further interactions with KRAS G12C, and remarkably increases the labeling efficiency and rates, potency, and selectivity of KRAS G12C inhibitors. In addition, we demonstrate that these compounds are capable of selectively inhibiting KRAS G12C-dependent signaling and cancer cell proliferation at sub-micromolar concentrations.

RESULTS

A Novel Readout for the Labeling Efficiency of KRAS Inhibitors

To explore the possibility of designing compounds that occupy both the SIIP and guanine binding site, we considered previously reported SIIP compounds, including the well-characterized chloro hydroxy aniline compounds (ARS-853) (Lito et al., 2016; Patricelli et al., 2016; Westover et al., 2016), and a class of relatively uncharacterized quinazoline-containing compounds that appeared in the patent literature (Ren et al., 2014). The quinazoline compounds offered significant advantages to present chemical diversity to sub-regions of the SIIP. To better understand the potential properties of the quinazoline compounds, we evaluated the ability of these compounds to inhibit the function of KRAS G12C.

We prepared several examples of quinazoline reported by Araxes Pharma to effectively label G12C KRAS by mass spectrometry, including compound **1** decorated with fluorophenyl and piperazinyl substituents and an electrophilic acrylamide warhead attached to the piperazine (Figure 1A) (Ren et al., 2014) (Araxes patent WO2015054572). As an initial test of cellular efficacy, we utilized the cancer cell line H358, a KRAS-addicted non-small-cell lung cancer cell line harboring the KRAS G12C allele (Singh et al., 2009). Interestingly, when protein extracts from H358 cells exposed to **1** were subjected to western blot analysis, we noted an upward shift in the KRAS G12C band in a time-dependent manner (Figure 1B). A similar phenomenon was also observed in 293T cells transiently transfected with Flag-tagged KRAS G12C (Figure S3B). We verified that this shift is a consequence of covalent attachment of compounds to KRAS G12C by incubating the inhibitors with purified recombinant KRAS G12C and observing a similar electrophoretic mobility shift, and by observing the expected mass gain using mass spectrometry (Figures 1C and 1D). This electrophoretic mobility shift provided us with a convenient and direct means of assessing target engagement of KRAS for subsequent iterations of compounds in this series.

Attaching an Amide Substituent to KRAS G12C Inhibitor Enhances its Labeling Efficiency and Potency

We profiled a set of analogs of **1** in order to explore the structure-activity relationship. We initially fixed the quinazoline 4- and 7-positions with piperazinyl-acrylamide and 2-fluorophenyl substituents, and introduced a variety of amine substituents at the C2-position (Figure 2A). To evaluate their relative potency, we treated H358 cells and assessed the electrophoretic mobility of KRAS G12C and the impact on downstream MAPK signaling by monitoring the phosphorylation status of ERK by immunoblotting. Of the compounds prepared, **1_AM,** with an amino amide substituent, showed the most complete labeling of KRAS at 10 μM. FRF-01-167, the only example with a tertiary amine at the quinazoline 2-position, showed no labeling of KRAS, while other examples showed labeling to varying extents (Figure 2B). As expected, the degree of KRAS G12C mobility shift tightly correlated with the inhibition of ERK phosphorylation (Figures 2B and S2). Furthermore, we found that **1_AM** induced the electrophoretic mobility shift of KRAS G12C at a faster rate than compound **1** (Figure 2C), indicating improved labeling kinetics. We also compared **1_AM** to **1** for the ability to decrease active KRAS G12C levels. Consistent with prior observations on ARS-853 series compounds, which show a propensity for binding to GDP-bound KRAS preferentially (Lito et al., 2016; Patricelli et al., 2016), treating H358 cells with **1_AM** decreased levels of GTP-bound KRAS by ~80% compared with **1** (Figure 2D), with corresponding decrease in phosphorylation of ERK.

As an additional measurement of how substitutions at the 2-position alter interactions between KRAS G12C and the compounds, we performed differential scanning fluorimetry (DSF), which measures ligand-induced changes in protein thermal stability (Niesen et al., 2007). Compound **1_AM** demonstrated a small enhancement in the thermal stability relative to **1** of fully labeled KRAS G12C when compared with unlabeled GDP-bound protein, with a small but reproducible change in the melting temperature (ΔTm) of 9°C versus 8.5°C for **1_AM** and **1**, respectively (Figure 2E). This increase suggests that an N-linked amide substituent at the 2-position may increase labeling efficiency with KRAS G12C relative to compounds lacking such moieties.

Development of Potent KRAS-G12C Inhibitors with the Amide Substituent

With the new finding that the amide substituent confers potency advantages, we next evaluated a series of quinazoline matched pairs, with and without the 2-amino amide substituent (Figure 3A). Addition of a fluorine at position 8 (pairs **2** and **4**) modestly improved the potency of compounds relative to those without, while addition of a hydroxynaphthyl at the 7-position

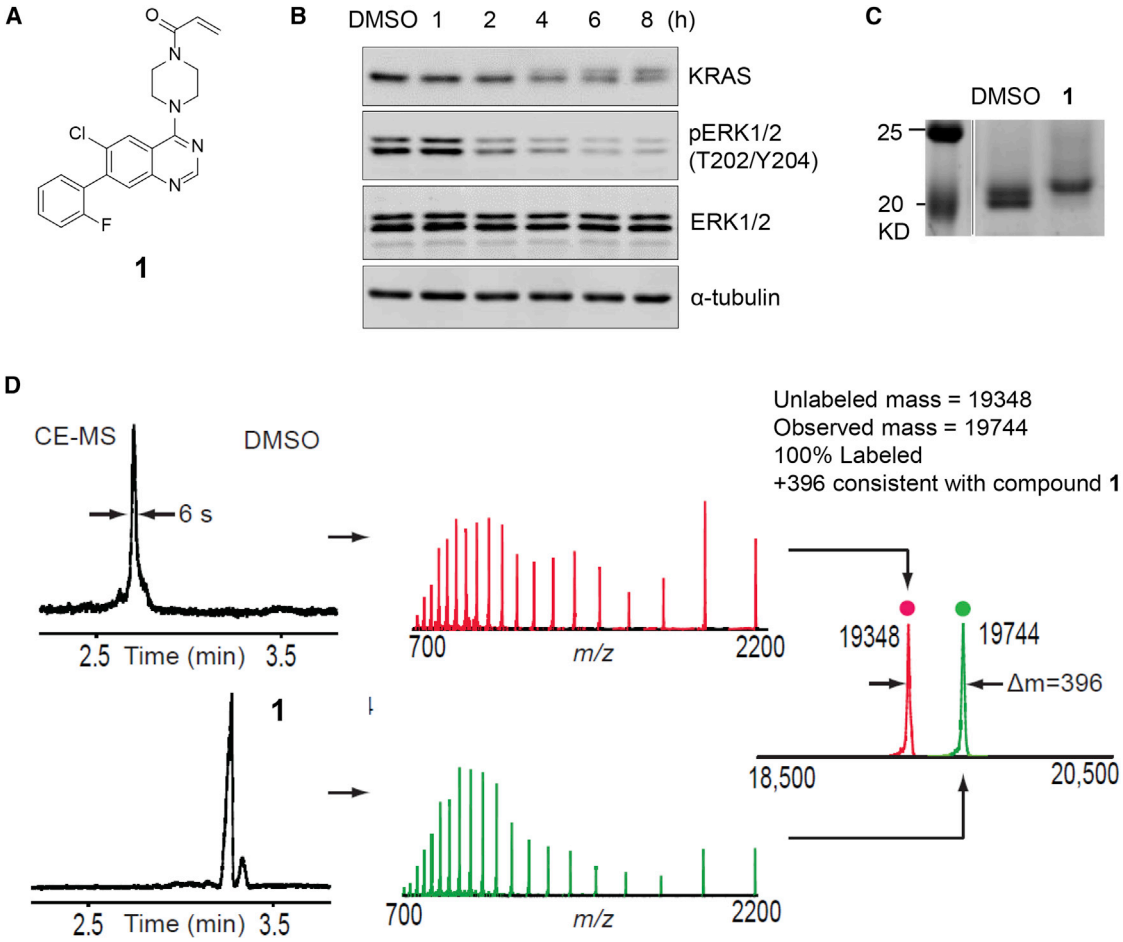

Figure 1. Electrophoretic Mobility of KRAS as a Readout for the Labeling Efficiency of KRAS Inhibitors

(A) Chemical structure of **1** (Araxes patent WO2015054572).

(B) KRAS-G12C mutant cells (H358) were treated with compound **1** in a time-dependent manner at 10 μM. Electrophoretic mobility of KRAS-G12C and MAPK phosphorylation were determined by immunoblotting with the indicated antibodies.

(C) Purified recombinant KRAS-G12C protein was incubated with **1** for 2 hr at 10 μM, and the protein-**1** mixture was resolved on a 12% SDS-PAGE.

(D) Capillary electrophoresis-mass spectrometry (CE-MS analysis) confirms covalent labeling of KRAS-G12C. After incubation of protein with DMSO or compound **1,** as in Figure 1C, reactions were resolved by CE and introduced to the mass spectrometer by electrospray ionization directly from the chip. Zero-charge mass spectra reveal a shift in protein mass corresponding to **1**.

(pairs **3** and **4**) substantially further enhanced potency as measured by inhibition of ERK phosphorylation and DSF (Figures 3B and 3C). In all pairs the presence of amide improved the potency of compounds for engagement of KRAS and inhibition of ERK phosphorylation, when tested in H358 (KRAS G12C) cells (Figure 3B). Similar findings were readily apparent in five additional KRAS G12C cancer cell lines (H23, H1792, Calu-1, H2122, and Mia PaCa-2) (Figures S3A), as well as in 293T cells with ectopic expression of KRAS G12C (Figure S3B).

We further evaluated these compounds for changes in levels of GTP-bound KRAS, and for shifts in thermal stability by DSF. Consistent with its effect on KRAS G12C mobility shift and on ERK phosphorylation, adding the amide substituent to **2**, **3,** and **4** decreased GTP-bound KRAS (Figure 3D), and increased the thermal stability of KRAS G12C (Tm: 14.0°C versus 12.0°C for pair **2**; 18.5°C versus 15.5°C for pair **3**; 20°C versus 15°C for pair **4**) (Figure 3C). Interestingly, larger shifts in Tm are seen when comparing compound pairs with and without the hydroxynaphthyl group (9°C versus 18.5°C for **1_AM** versus **3_AM**). Both compound **4** and **4_AM** labeled and inhibited KRAS G12C at sub-micromolar concentrations (Figure 3B).

Measuring Target Labeling via a Novel SIIP Alpha Assay

As one of the primary challenges to the development of new SIIP compounds, all screening assays have relied upon covalent interactions between the protein and compounds that have been monitored using either mass spectrometry (Ostrem et al., 2013; Patricelli et al., 2016) or the electrophoretic gel shift assay described earlier. We reasoned that it might be possible to develop a competition binding assay using a probe based on **4_AM** to detect binding. We previously developed a competition binding assay to evaluate for small-molecule binding in the guanosine nucleotide pocket using a covalent GTP-biotin probe, tagged KRAS, and AlphaScreen beads (Xiong et al., 2017). We developed a similar binding assay for the SIIP using a biotinylated version of **4_AM** with the biotin extending from the

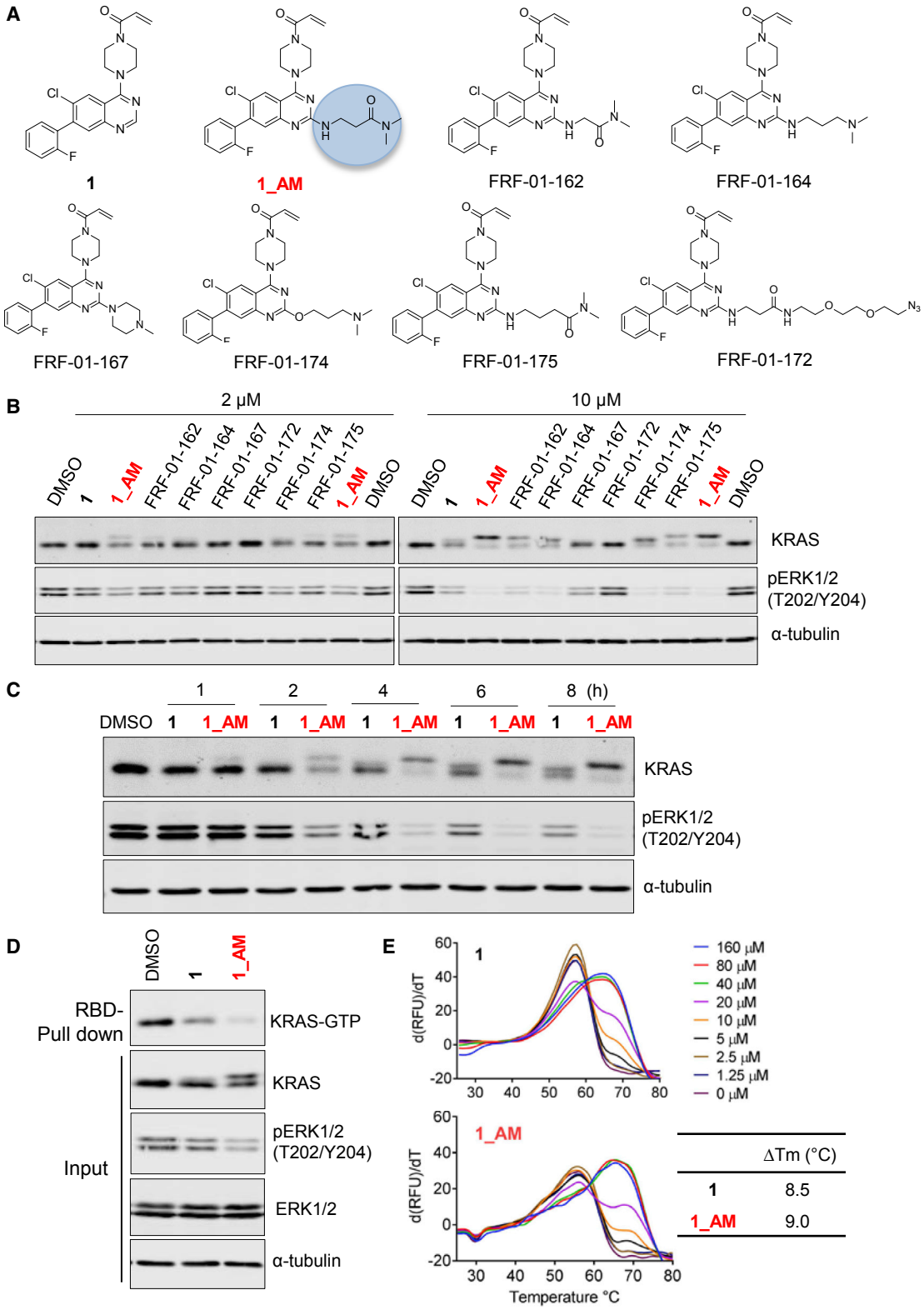

Figure 2. Amide Substituent Enhances the Covalent Labeling Efficiency and the Potency of KRAS-G12C Inhibitors

(A) Chemical structures of the synthetic molecules for studying the structure-activity relationship of the amino amide substituent (the amino amide substituent in **1_AM** is highlighted in the gray circle).

(legend continued on next page)

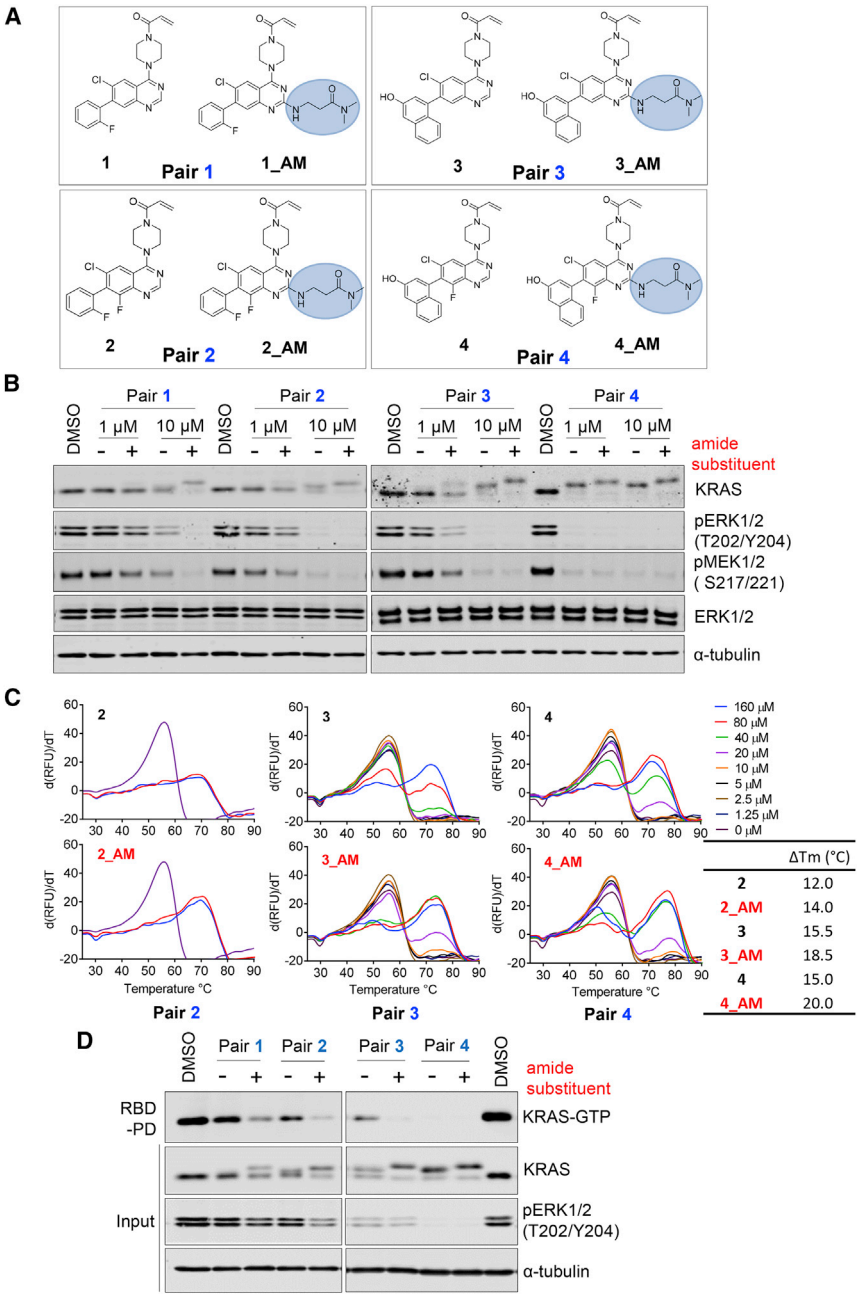

Figure 3. Development of Potent KRAS-G12C Inhibitors with the Amide Substituent

(A) Chemical structures of the four pairs of SIIP binders, organized by presence or absence of the amino amide substituent (light blue highlights).

(B) Pairwise comparison of compound set in H358 cells by immunoblot for electrophoretic mobility of KRAS-G12C, and MAPK and MEK phosphorylation show a comparative improvement in compound potency by adding the amino amide substituent. Pairs **3** and **4**, which include the hydroxynaphthyl, are substantially more potent than **1** and **2** that lack this group.

(C) Differential scanning fluorimetry (DSF) comparison of compound pairs **2, 3,** and **4**. DSF shows increases in thermal stability for compounds containing the amino amide substituent in a dose-dependent manner. First derivatives of temperature-dependent signals are shown.

(D) Immunoblot analysis after RBD pull-down of GTP-KRAS from H358 cells exposed to compound pairs shows decreases in recovery of GTP-KRAS for compounds including the amino amide substituent and for pairs including the hydroxynaphthyl (**1** and **2** versus **3** and **4**).

See also Figure S3.

amide linker, **5** (Figures S3C and S3D). The assay was performed in competition fashion by co-incubating with test compounds in escalating doses, with fixed concentrations of Flag-tagged KRAS G12C and **5**, then developing the assay using AlphaScreen beads. Optimization for a 384 well format resulted in a sufficient Alpha signal to produce an assay window that could be used for robust dose-response measurements (Figure S3E). Dose-response experiments showed good discrimination between covalent quinazoline compounds in a pattern similar to that observed previously using DSF and the western blot assays. Specifically, when comparing substitutions at the quinazoline 2-positions, both compounds **1_AM** and **3_AM** showed 3-fold increases in potency compared with their counterparts **1** and **3**. Also, substitutions of 2-fluorophenyl (pair **1**) for 3-hydroxynaphthyl (pair **3**) showed a 10-fold improvement in half maximal inhibitory concentration (IC_{50}). Finally, addition of a fluorine at position 8 (compare pair **4** with pair **3** and pair **2** with pair **1**) substantially improves potency (Figure S3E). Of note, consistent with their cellular activities, both **4** and **4_AM** exhibit lower IC_{50} compared with pairs **1**, **2**, and **3**, and no significant difference was observed between **4** and **4_AM** (Figure S3E). It should be noted that, because this assay is not performed under equilibrium conditions and relies on a covalent probe, the

(B) H358 cells were exposed to compounds as indicated. Immunoblot analysis shows an electrophoretic mobility shift for KRAS G12C, and a correlated change in MAPK phosphorylation.

(C) H358 cells were treated with **1** or **1_AM** as indicated. **1_AM** labels with faster kinetics.

(D) Pull-down of active/GTP-bound KRAS by Raf-RBD after exposure to **1** or **1_AM** shows a comparative decrease in GTP-KRAS for **1_AM** compared with **1**.

(E) Differential scanning fluorimetry (DSF) shows a substantial increase in thermal stability of KRAS-G12C-labeled pair 1 compounds in a dose-dependent manner. First derivatives of temperature-dependent signals are shown.

See also Figure S2.

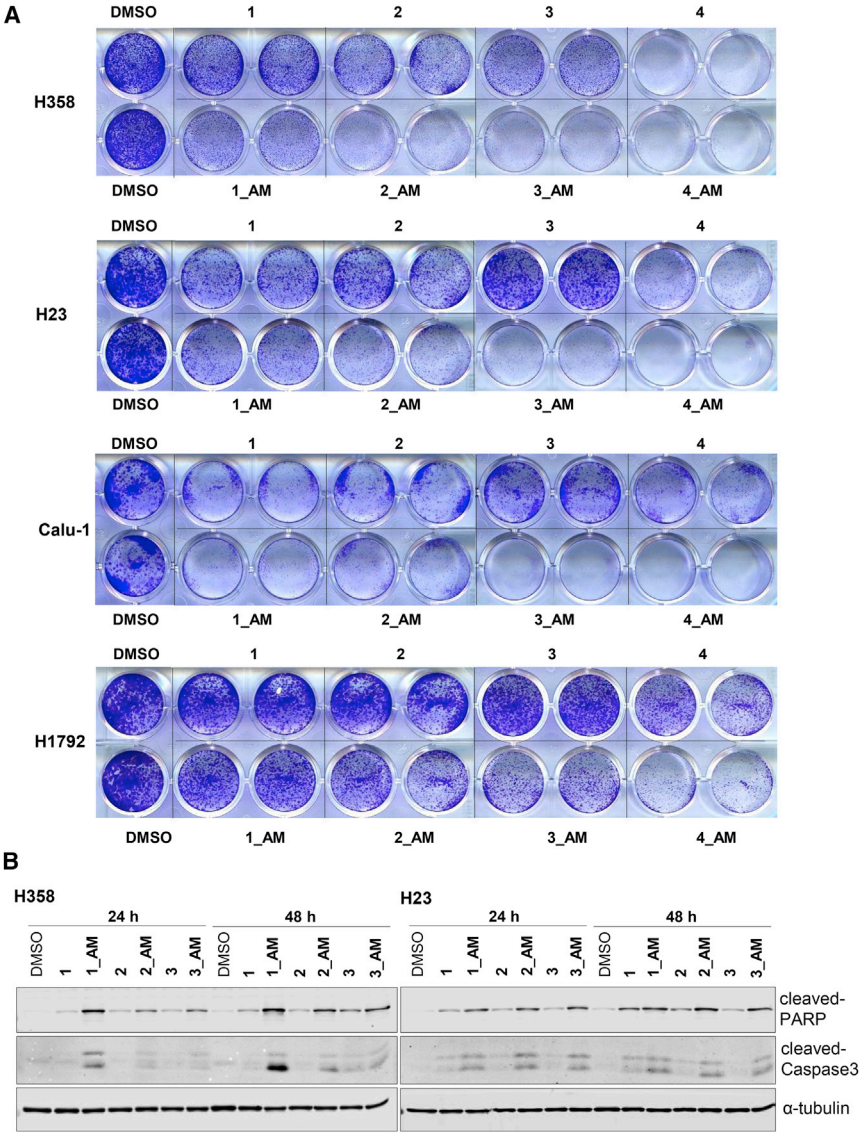

Figure 4. Enhanced Anti-proliferative Potency and Induction of Apoptotic Cell Death by Attachment of the Amide Substituent

(A) Exposure of KRAS-G12C lung cancer cell lines, H358, H23, Calu-1, and H1792, to four pairs of compounds at 5 μM for 5 days shows consistent improvements in anti-proliferative properties of compounds including the amino amide substituent (each compound treatment in duplicate wells).

(B) Appearance of apoptosis markers, cleaved PARP, and cleaved Caspase-3, in two KRAS-G12C lung cancer cell lines, H358 and H23, is enhanced in compounds including the amide substituent.

resulting IC_{50} values are batch-dependent and are not accurate estimates of compound K_d values. Nevertheless when calibrated on a per-batch basis to a control (**4_AM** IC_{50}), the results are highly reproducible between assay runs for rank-ordering compounds.

Enhanced Anti-proliferative Potency and Induction of Apoptotic Cell Death by Attachment of the Amide Substituent

Given that compounds with the amide substituent increased labeling efficiency to KRAS G12C, as well as potency in inhibiting ERK phosphorylation, we proceeded to investigate if these characteristics would translate into an impact on KRAS G12C-dependent cell proliferation. To this end, we treated KRAS-G12C cancer cells lines for 5 days with all the four pairs of compounds at the final concentration of 5 μM. Compared with their parental analogs, compounds with the amide substituent demonstrated enhanced cell growth inhibition (Figure 4A). To understand if an induction of cell death may be responsible for cell growth inhibition upon KRAS G12C inhibitor treatment, we used the cleaved form of PARP and Caspase-3 as the readout of apoptotic cell death, and found that attachment of the amide substituent significantly increased apoptosis (Figure 4B). Therefore, we concluded that the amide substituent enhances the anti-proliferative and cell-killing potency of KRAS G12C inhibitors.

X-Ray Crystallography Reveals Two Configurations of SWII for Quinazoline SIIP Compounds

To understand the structural basis of the structure-activity relationship findings, we solved X-ray crystal structures of KRAS G12C bound to **1_AM** and **3_AM**. Additional electron density within the SIIP confirmed **1_AM** or **3_AM** bound between helix α2 and helix α3, similar to previously reported SIIP binders such as compounds 12 and ARS-853 (Ostrem et al., 2013; Patricelli et al., 2016) (Figure S5). The structures were notable for substantial differences in the position of SWII with **1_AM,** showing an extended conformation compared with **3_AM** (Figure 5). In the **1_AM** complex, protein residue Met72 is rotated away from helix α3 to accommodate **1_AM**'s phenyl ring, resulting in the outward rotation of helix α2 (Figure 5B). The piperazine ring of **1_AM** also displaces loop 4 (part of SWII) away from the binding pocket. As a result, the entirety of SWII is shifted away from the protein main body. This conformation is similar to the conformation seen previously with **1** (Figure 5A, PDB: 5V71). The main exception is that the amide substituent of **1_AM** interacts with His95 through π-π stacking, while in **1** a hydrogen bond is observed (Figures 5D–5F).

In contrast to **1** and **1_AM**, SWII is considerably altered by **3_AM** binding (Figure 5C). As in **1_AM**, Met72 moves to accommodate the naphthalene ring of **3_AM**. However, the hydrogen bond between Asp69 and the hydroxynaphthyl group of **3_AM** causes Met72 to shift toward helix α3, thereby pinning the SWII helix against the binding pocket. This conformation is

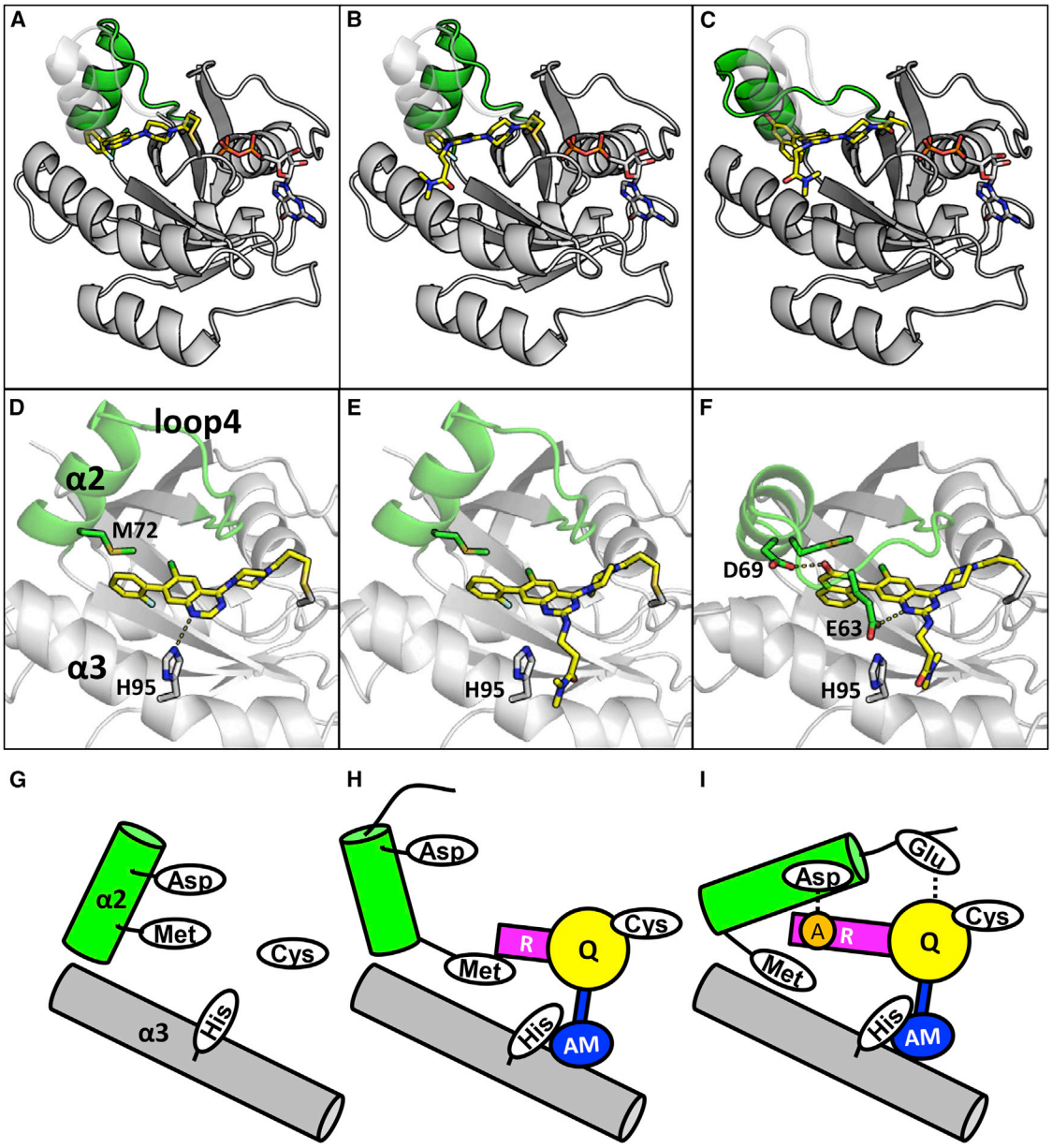

Figure 5. Ligand-Dependent Conformational Changes of SIIP

(A–C) Crystal structures of KRAS mutant G12C in bound to compound **1** (A), **1_AM** (B), and **3_AM** (C) show new alterations in conformation of SWII (green) relative to that seen in for "apo" GDP-KRAS (transparent gray). Inhibitors and GDP in sticks and colored by an element with carbon yellow (inhibitor) or white (GDP).

(D–F) Detailed view of interactions in SIIP corresponding to (A–C). Dashed lines represent hydrogen bond interactions.

(G–I) Schematic diagram of interactions and structural changes in SWII for "apo" GDP-KRAS (G), **1/1_AM** (H), and **3_AM** (I). Dashed lines represent hydrogen bond interactions. Blue circle (AM), amide substituent; yellow circle (Q), quinazoline core; cyan stick (R), steric ring; and orange circle (A), H-bond acceptor. See also Figure S5 and Table S1.

reinforced by hydrogen bonds between Glu63 and **3_AM**. The sum of these interactions gives a closed SWII conformation (Figures 5C and 5F). The addition of these new interactions seen with the compounds bearing hydroxynaphthyl and/or the amide substituent are consistent with enhancements in thermal stability seen for DSF, improved rankings seen in the Alpha assay, and enhancement of potencies of compounds tested for electrophoretic mobility shift or pERK activity.

The Amide Substituent Increased the Selectivity of KRAS G12C Inhibitors

All data to this point suggest that the covalent portion of SIIP compounds contributes significantly to the potency of SIIP compounds. We therefore expected our current panel of compounds to have activity only against cells bearing the KRAS G12C mutation. As expected, MAPK signaling was not affected in multiple RAS cancer cell lines bearing non-G12C mutations.

In A549 (G12S), H441 (G12V), and HCT116 (G13D) cells, inhibitors failed to suppress ERK phosphorylation (Figure 6A). In addition, these inhibitors showed no cell growth inhibition in non-G12C cell lines, A549 and H441. To further evaluate the specificity of our compounds toward the KRAS G12C isoform, we developed an isogenic *Ras-less* MEFs model system expressing different human KRAS mutants. In this system endogenous HRas/NRas/KRas were knocked out resulting in a non-proliferative phenotype. Re-introduction of the human KRAS mutant and wild-type isoforms restored proliferation in this system (Drosten et al., 2010). We found that compounds **1**, **2**, **3**, and **4**, as well as their derivatives with amide substituents, showed increased anti-proliferative potency in $KRAS^{G12C}$ *Ras-less* cells relative to $KRAS^{G12V}$ *Ras-less* cells (Figure S6). All these data suggest that the compounds selectively target G12C, not the other mutated forms of KRAS.

Interestingly, for cell lines harboring wild-type KRAS (HCC827, PC9), ERK phosphorylation was suppressed when cells were exposed to compounds **1**, **2**, **3**, and **4** at 10 μM (Figure 6B, dashed black arrow). Notably, the amide side chain containing compounds dramatically reversed this effect (Figure 6B, bold black arrow), suggesting that the amide substituent appears sufficient to improve the selectivity profile of the quinazoline compounds. However, perhaps more importantly, these results also suggest that the reversible component of quinazoline compounds have the capacity to bind to a SIIP in wild-type KRAS. To explore this possibility further, we performed Active RAS pull-down experiments to determine the level of GTP-bound KRAS in cells exposed to our panel of SIIP binders. Remarkably, we observed decreased levels of KRAS-GTP for cells exposed to compounds lacking the amide substituent compared with those where it was maintained (Figure 6C). These results support the hypothesis that compounds lacking the amide substituent are able to bind to wild-type KRAS-GDP, enriching the cellular pools of GDP-KRAS, and thereby depleting the ratio of GTP-KRAS to GDP-KRAS. These results also demonstrate that the amide substituent functions to improve the selectivity of covalent G12C-targeted quinazoline compounds.

Sub-micromolar Inhibition of KRAS G12C Cell Lines

Prior SIIP compounds such as ARS-853 showed anti-proliferative activity in the high-micromolar range in cell-proliferation assays (Lito et al., 2016; Patricelli et al., 2016). As a direct comparison between ARS-853 and our panel of compounds we measured cell proliferation and MAPK phosphorylation in the KRAS G12C cancer cell lines, Calu-1 and H358. ARS-853 showed a 50% decrease in pERK at ~5 μM, while **1_AM**, **3_AM**, and **4_AM** all showed enhanced pERK inhibition, with **4_AM** showing ~50% inhibition at 100 nM (Figure 7A). Similarly, **1_AM** and **4_AM** showed substantial improvements in IC_{50} values for anti-proliferative activity in both H358 and Calu-1 cells (Figure 7B).

We further compared the amide substituent-modified compounds, **1_AM**, **3_AM**, and **4_AM** with ARS-853 in terms of the kinetics of target labeling. To this end, we treated cells with inhibitors for different time points and harvested cell lysates for assaying the electrophoretic mobility of KRAS G12C. Consistent with the improved anti-pERK and anti-proliferative potency, all compounds with the amide substituent caused a faster alteration of electrophoretic mobility of KRAS G12C, with alterations observed as early as 1 hr post treatment (Figure 7C). These data suggest that addition of the amide substituent improved the labeling rate of KRAS G12C inhibitors.

DISCUSSION

The high affinity of GTP for the most common oncogenic RAS variants has impeded the development of cell-permeable orthosteric RAS inhibitors. Recent studies reported the discovery of compounds using a tethering approach exemplified by ARS-853 that covalently modify cysteine 12 of KRAS G12C and induce formation of a pocket adjacent to the GTP/GDP binding site which has been termed the SIIP (Lito et al., 2016; Ostrem et al., 2013; Patricelli et al., 2016). These compounds bind preferentially to GDP-KRAS and trap KRAS G12C in a conformation incompatible with effector binding, thereby interrupting RAS-dependent signaling and proliferation. Because these compounds function as allosteric covalent inhibitors, a key question is whether molecular-recognition features exist to allow development of compounds with sufficient potency and selectivity to enable their advancement into murine G12C tumor models, and ultimately into clinical development. For example, ARS-853 inhibits KRAS G12C lung cancer cell lines at IC_{50} values in the high-micromolar range, which is approximately 100-fold less potent than what is achieved with a typical inhibitor of oncogenic kinase such as ALK or EGFR.

We sought to explore whether new SIIP binders could be developed that would allow potential extension into portions of the nucleotide or other binding pockets, or as potential starting points for bivalent molecules capable of inducing RAS degradation through ligase recruitment (Toure and Crews, 2016; Winter et al., 2015). We focused on developing the appropriate biochemical and cellular assays that would allow characterization of a series of trisubstituted quinazoline acrylamides recently reported in the patent literature (Ren et al., 2014). We first demonstrated that a gel mobility shift assay is able to detect covalent modification of cellular KRAS G12C, providing a tool for rapid identification of optimal substituents. We also developed a competitive AlphaScreen assay and DSF assay that give results in good agreement with the electrophoretic mobility shift of KRAS G12C and the inhibition of ERK phosphorylation, and allowed rank-ordering of compounds. Together these assays provide an efficient means to characterize these and potential new SIIP binders. Optimal compounds include **4** and **4_AM,** which inhibit cell proliferation at ~500 nM concentrations and represent substantial improvements over ARS-853 (Figures 7A and S3E).

To rationalize the structure-activity relationships we solved co-structures of compounds **1**, **1_AM**, and **3_AM** with KRAS G12C, which revealed a number of important features of quinazoline scaffold SIIP binding compounds: (1) the appropriate trajectory for the electrophilic acrylamide to approach cysteine 12; (2) the need for a steric substituent to displace Met72, creating space within the SIIP; (3) the potential for hydrogen-bonding interactions with residue Asp69, which secures a closed conformation of SWII and enhances the stability of the RAS-inhibitor complex; and (4) the potential for interactions between His95 and amide substituents arising from the quinazoline 2-position (Figures 5G–5I). Full engagement of all of these elements results in large ligand-induced differences in the ultimate

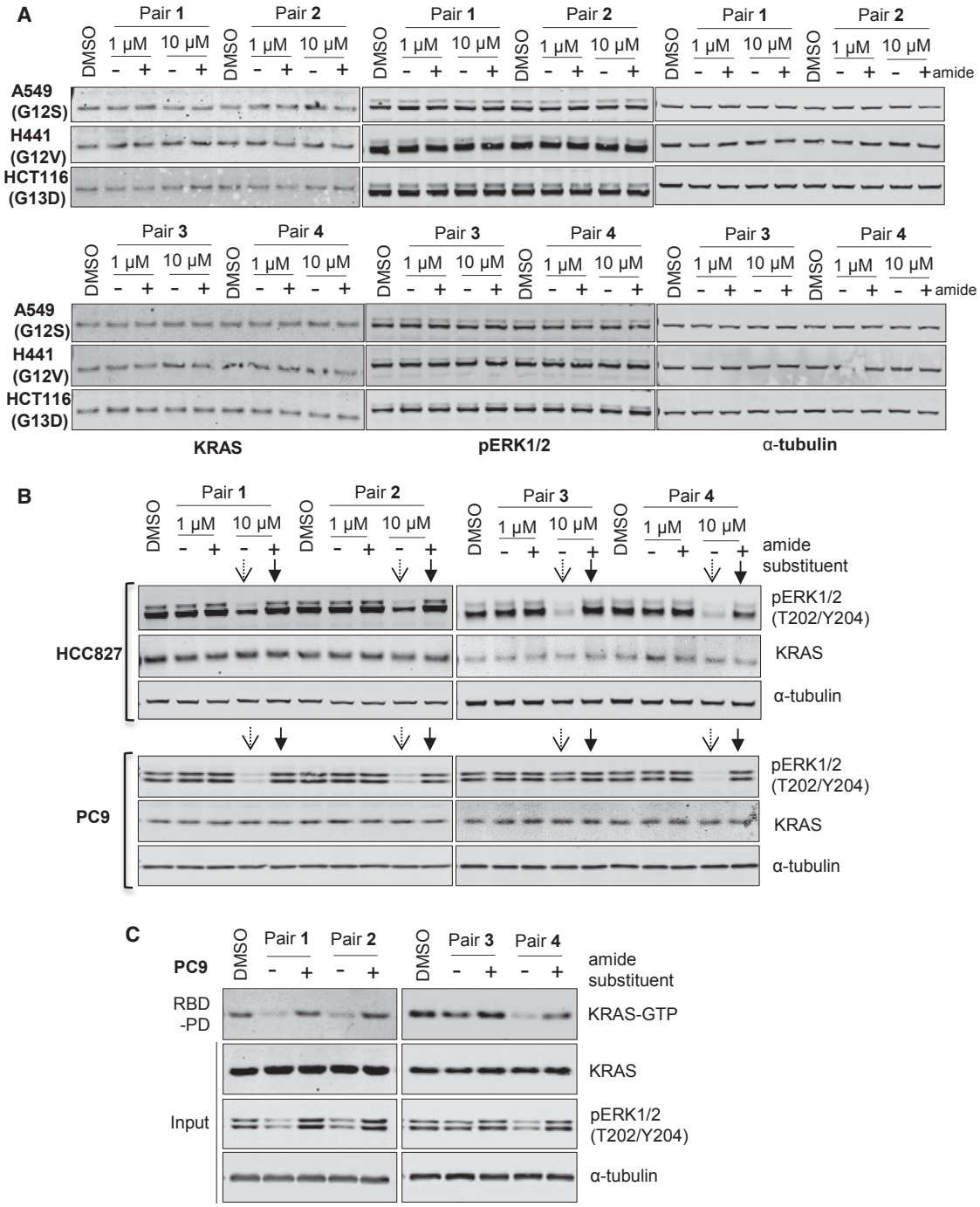

Figure 6. Amide Substituent Improves the Selectivity of KRAS-G12C Inhibitors

(A) Exposure of non-G12C KRAS cell lines, A549 (G12S), H441 (G12V), and HCT116 (G13D) treated to compounds for 6 hr at 1 and 10 μM shows no effect on KRAS protein and pERK levels as determined by immunoblotting.

(B) Exposure of KRAS wild-type/EGFR mutant cell lines, HCC827, and PC9 cells, show inhibition of pERK for selected compounds lacking amino amide substituent (dashed black arrow), but show restored pERK level for compounds including the amino amide substituent (bold black arrow).

(C) PC9 cells were treated with the indicated compounds for 6 hr at 10 μM. The effect on the level of active/GTP-bound KRAS was determined by a RAS-binding domain pull-down assay and immunoblotting with KRAS-specific antibody.

See also Figure S4 and Table S2.

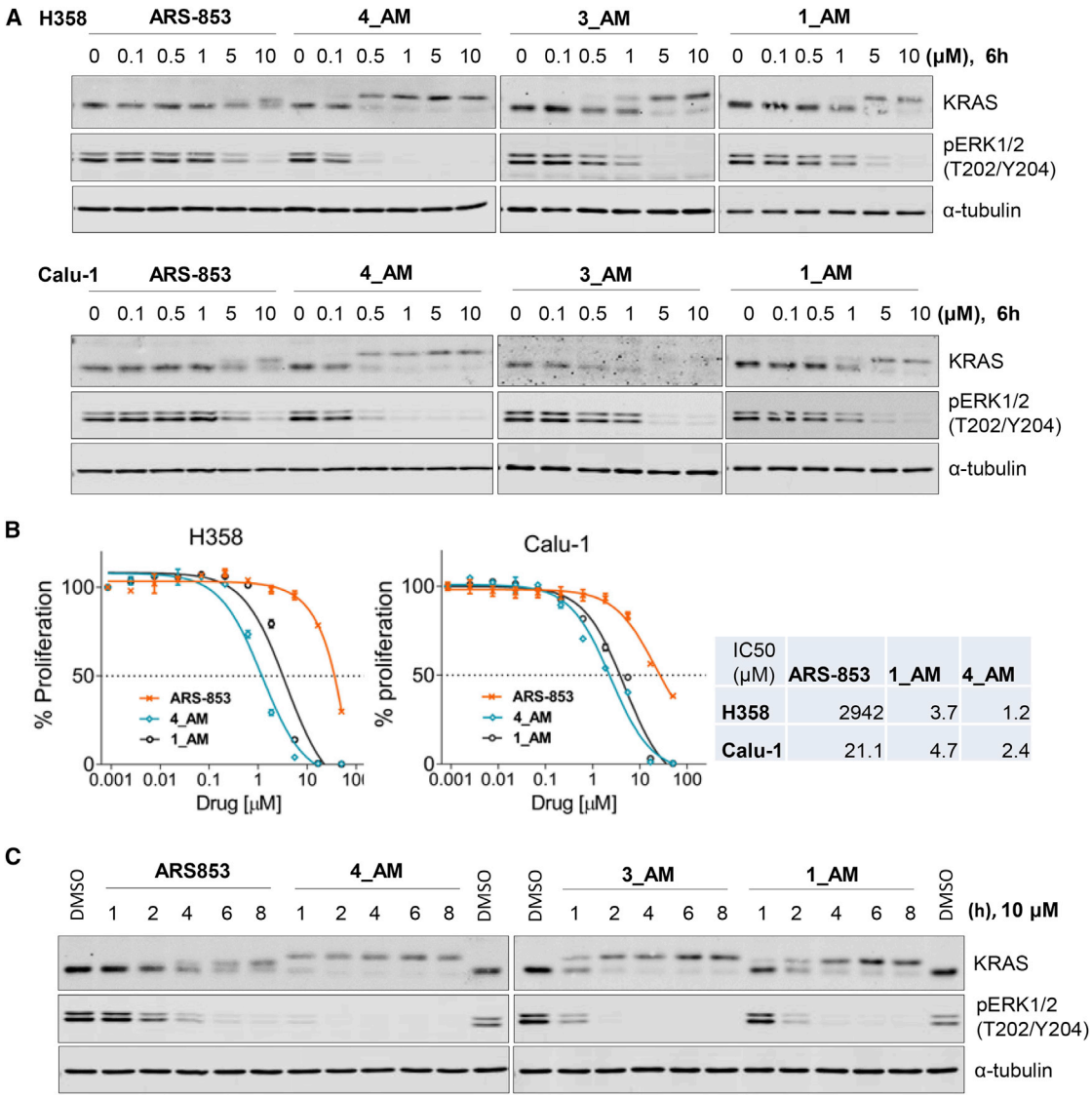

IC50 (μM)	ARS-853	1_AM	4_AM
H358	2942	3.7	1.2
Calu-1	21.1	4.7	2.4

Figure 7. SIIP Inhibitors for KRAS-G12C with Sub-micromolar Potency

(A) Dose response of KRAS and pERK levels in KRAS-G12C cell lines, H358 and Calu-1, after 6 hr exposure of **1_AM**, **3_AM**, **4_AM**, and ARS-853.

(B) Dose response of cell viability for H358 and Calu-1 cells treated for 5 days with indicated inhibitors. Data are represented as mean ± SD (n = 3).

(C) Time courses of KRAS and pERK levels in H358 cells treated with **1_AM**, **3_AM**, **4_AM**, and ARS-853 at 10 μM show enhanced labeling kinetics for **4_AM**.

positioning of the SWII helix underscoring the "induced-fit" nature of binding to this pocket. These co-structures will enable further refinement of these compounds using computer-aided ligand discovery and optimization efforts.

Our results demonstrate that optimized quinazoline compounds with a 2-aminoamide substituent are not only potent, but also selective for G12C in complementary cellular systems. First we assessed their ability to inhibit KRAS-dependent signaling in established cancer cell lines harboring various activated alleles of KRAS including G12C cells (H358, Calu-1, H23, H1792, and MiaPaca-2) and non-G12C cells (A549, H441, and HCT116). We observed that these compounds selectively inhibit KRAS-dependent signaling in G12C cells and show no activity in non-G12C mutant KRAS cells. Second, we utilized the RAS-less MEF system to enable assessment of cellular inhibition in an isogenic system. The new series of compound show, on average, 5- to 10- fold selectivity for $KRAS^{G12C}$ over $KRAS^{G12V}$. The best compounds exhibit ~500 nM IC_{50} in G12C and an ~20-fold window in $KRAS^{G12V}$ RAS-less cells.

Interestingly a number of compounds lacking a substituent at the quinazoline 2-position exhibited anti-proliferative activity in EGFR-driven cell lines that contain wild-type KRAS. This observation is important, not only because it demonstrates the need for inclusion of substituents in the 2-position to maintain selectivity for G12C, but it also demonstrates for the first time that SIIP compounds may reversibly interact with the SIIP in non-G12C KRAS proteins, raising the possibility of developing selective SIIP inhibitors against non-KRAS RAS isoforms and/or other

common non-G12C mutations that line the SIIP. Since SIIP compounds show a preference for binding to GDP-bound KRAS (Ostrem et al., 2013), one potential explanation for the off-targeting effects seen in KRAS wild-type cells may relate to higher levels of intracellular RAS-GDP complexes in KRAS WT cells relative to that seen in non-G12C KRAS mutants. Previously, we noted that KRAS G12V, G12D, G12A, G12R, and G13D have lower intrinsic GTPase activities relative to wild-type or G12C. Since many of these mutants have been shown to be insensitive to GAP-stimulated hydrolysis, this suggests that intrinsic rates of GTP hydrolysis will dictate the availability of GDP-KRAS complexes for interaction with SIIP compounds. Given that wild-type and KRAS G12C cells have faster intrinsic GTP hydrolysis rates, we expect that GDP-KRAS will be proportionately higher in cell lines with wild-type or G12C genotypes compared with many other oncogenic mutations (Lu et al., 2015). Another possible explanation is that EGFR mutations make the cells more dependent on KRAS signaling, and therefore more sensitive to direct KRAS inhibitors. If the availability of GDP-RAS is the limiting feature for certain RAS mutations, this would present an inherent challenge to targeting the SIIP in RAS mutants with slow intrinsic GTPase/GTP exchange activities, such as Q61 mutants (Hunter et al., 2015).

Collectively our findings provide optimized lead compounds (**4_AM**) and a screening road-map that will allow further development of SIIP binders. In particular, we believe our results suggest that there is the potential for sufficient potency and selectivity to be achieved in the SIIP without relying on covalent ligation to cysteine 12, which would potentially enable the development of inhibitors of other activating KRAS mutants including KRAS G12V and G12D, and perhaps other isoforms of RAS, such as HRAS or NRAS, Q61R, Q61L, and Q61K.

SIGNIFICANCE

Oncogenic KRAS mutations, some of the most common genetic abnormalities found in lung cancer, induce persistent RAS signaling and are an essential feature for tumor initiation and maintenance. RAS had long been considered "undruggable" but recent strategies targeting the mutated cysteine in KRAS G12C have raised hopes of directly inhibiting aberrant KRAS G12C function. Among the various covalent approaches, allosteric inhibitors that access an inducible pocket formed by movement of switch II, a dynamic structural element in KRAS, have shown promise, although early tool compounds have been limited from advancement into animal studies by compound potency. In this study, we demonstrate that covalent, quinazoline-based switch II pocket (SIIP) compounds effectively suppress GTP loading of KRAS G12C, MAPK phosphorylation, and the growth of cancer cells harboring G12C. Notably we find that adding an amide substituent to the quinazoline scaffold allows additional interactions with KRAS G12C, and remarkably increases the labeling efficiency and rates, potency, and selectivity of KRAS G12C inhibitors. Structural studies reveal a new configuration of the SIIP and elucidate additional key interactions made by substituents located at the quinazoline 2-, 4-, and 7-positions, explaining the increased potency of this class of inhibitors. Optimized lead compounds in the quinazoline series selectively inhibit KRAS G12C-dependent signaling and cancer cell growth at submicromolar concentrations.

STAR★METHODS

Detailed methods are provided in the online version of this paper and include the following:

- KEY RESOURCES TABLE
- CONTACT FOR REAGENT AND RESOURCE SHARING
- EXPERIMENTAL MODEL AND SUBJECT DETAILS
  - Cell Lines
- METHOD DETAILS
  - Protein Preparation and Crystallization
  - Crystal Structure Determination
  - Capillary Electrophoresis-Mass spectrometry Analysis (CE-MS)
  - Immunoblotting
  - Differential Scanning Fluorimetry
  - Active RAS Determination by RBD Pulldown Assay
  - Cell Proliferation Assays
  - Competition Binding Assay
  - Chemical Synthesis
- QUANTIFICATION AND STATISTICAL ANALYSIS
- DATA AND SOFTWARE AVAILABILITY

SUPPLEMENTAL INFORMATION

Supplemental Information includes six figures, two tables, chemical synthesis with six schemes, and two pdb files and can be found with this article online at http://dx.doi.org/10.1016/j.chembiol.2017.06.017.

AUTHOR CONTRIBUTIONS

M.Z., K.D.W., and N.S.G. designed the study, interpreted the data, and wrote the manuscript. M.Z., J.L., L.L., F.F., C.Q., S.B.F., T.W.G., C.A., R.P., M.C., and J.S. performed the experiment. D.A.S., Y.X., E.S.F., K.W., J.A.M., and P.A.J. provided critical reading. All the authors have given approval to the final version of the manuscript.

ACKNOWLEDGMENTS

We acknowledge the funding from Astellas Pharma (to K.D.W., P.A.J., and N.S.G.), DOD W81XWH-16-1-0106 (to K.D.W.), and Jimmy V Foundation (to K.D.W.). We thank the staff of the UT Southwestern Medical Center structural biology laboratory and beamline 19ID of Advanced Photon Source for assistance with X-ray data collection and processing. Results shown in this report are derived from work performed at Argonne National Laboratory, Structural Biology Center at the Advanced Photon Source. Argonne is operated by UChicago Argonne, LLC, for the US Department of Energy, Office of Biological and Environmental Research under contract DE-AC02-06CH11357.

Received: May 5, 2017
Revised: June 14, 2017
Accepted: June 30, 2017
Published: August 3, 2017

REFERENCES

Adams, P.D., Afonine, P.V., Bunkoczi, G., Chen, V.B., Davis, I.W., Echols, N., Headd, J.J., Hung, L.W., Kapral, G.J., Grosse-Kunstleve, R.W., et al. (2010). PHENIX: a comprehensive Python-based system for macromolecular structure solution. Acta Crystallogr. D Biol. Crystallogr. *66*, 213–221.

Adjei, A.A., Mauer, A., Bruzek, L., Marks, R.S., Hillman, S., Geyer, S., Hanson, L.J., Wright, J.J., Erlichman, C., and Kaufmann, S.H. (2003). Phase II study of the farnesyl transferase inhibitor R115777 in patients with advanced non-small-cell lung cancer. J. Clin. Oncol. *21*, 1760–1766.

Ambrogio, C., Gomez-Lopez, G., Falcone, M., Vidal, A., Nadal, E., Crosetto, N., Blasco, R.B., Fernandez-Marcos, P.J., Sanchez-Cespedes, M., Ren, X., et al. (2016). Combined inhibition of DDR1 and Notch signaling is a therapeutic strategy for KRAS-driven lung adenocarcinoma. Nat. Med. *22*, 270–277.

Bardeesy, N., and DePinho, R.A. (2002). Pancreatic cancer biology and genetics. Nat. Rev. Cancer *2*, 897–909.

Campbell, P.M., and Der, C.J. (2004). Oncogenic Ras and its role in tumor cell invasion and metastasis. Semin. Cancer Biol. *14*, 105–114.

Cox, A.D., and Der, C.J. (2010). Ras history: the saga continues. Small GTPases *1*, 2–27.

Downward, J. (2003). Targeting RAS signalling pathways in cancer therapy. Nat. Rev. Cancer *3*, 11–22.

Drosten, M., Dhawahir, A., Sum, E.Y., Urosevic, J., Lechuga, C.G., Esteban, L.M., Castellano, E., Guerra, C., Santos, E., and Barbacid, M. (2010). Genetic analysis of Ras signalling pathways in cell proliferation, migration and survival. EMBO J. *29*, 1091–1104.

Emsley, P., Lohkamp, B., Scott, W.G., and Cowtan, K. (2010). Features and development of coot. Acta Crystallogr. D Biol. Crystallogr. *66*, 486–501.

Fisher, G.H., Wellen, S.L., Klimstra, D., Lenczowski, J.M., Tichelaar, J.W., Lizak, M.J., Whitsett, J.A., Koretsky, A., and Varmus, H.E. (2001). Induction and apoptotic regression of lung adenocarcinomas by regulation of a K-Ras transgene in the presence and absence of tumor suppressor genes. Genes Dev. *15*, 3249–3262.

Hall, B.E., Bar-Sagi, D., and Nassar, N. (2002). The structural basis for the transition from Ras-GTP to Ras-GDP. Proc. Natl. Acad. Sci. USA *99*, 12138–12142.

Hunter, J.C., Manandhar, A., Carrasco, M.A., Gurbani, D., Gondi, S., and Westover, K.D. (2015). Biochemical and structural analysis of common cancer-associated KRAS mutations. Mol. Cancer Res. *13*, 1325–1335.

Karnoub, A.E., and Weinberg, R.A. (2008). Ras oncogenes: split personalities. Nat. Rev. Mol. Cell Biol. *9*, 517–531.

Lim, S.M., Westover, K.D., Ficarro, S.B., Harrison, R.A., Choi, H.G., Pacold, M.E., Carrasco, M., Hunter, J., Kim, N.D., Xie, T., et al. (2014). Therapeutic targeting of oncogenic K-Ras by a covalent catalytic site inhibitor. Angew. Chem. Int. Ed. *53*, 199–204.

Lito, P., Solomon, M., Li, L.S., Hansen, R., and Rosen, N. (2016). Allele-specific inhibitors inactivate mutant KRAS G12C by a trapping mechanism. Science *351*, 604–608.

Lu, J., Hunter, J., Manandhar, A., Gurbani, D., and Westover, K.D. (2015). Structural dataset for the fast-exchanging KRAS G13D. Data Brief *5*, 572–578.

Maurer, T., Garrenton, L.S., Oh, A., Pitts, K., Anderson, D.J., Skelton, N.J., Fauber, B.P., Pan, B., Malek, S., Stokoe, D., et al. (2012). Small-molecule ligands bind to a distinct pocket in Ras and inhibit SOS-mediated nucleotide exchange activity. Proc. Natl. Acad. Sci. USA *109*, 5299–5304.

Niesen, F.H., Berglund, H., and Vedadi, M. (2007). The use of differential scanning fluorimetry to detect ligand interactions that promote protein stability. Nat. Protoc. *2*, 2212–2221.

Ostrem, J.M., Peters, U., Sos, M.L., Wells, J.A., and Shokat, K.M. (2013). K-Ras(G12C) inhibitors allosterically control GTP affinity and effector interactions. Nature *503*, 548–551.

Otwinowski, Z., and Minor, W. (1997). [20] Processing of X-ray diffraction data collected in oscillation mode. Methods Enzymol. *276*, 307–326.

Patricelli, M.P., Janes, M.R., Li, L.S., Hansen, R., Peters, U., Kessler, L.V., Chen, Y., Kucharski, J.M., Feng, J., Ely, T., et al. (2016). Selective inhibition of oncogenic KRAS output with small molecules targeting the inactive state. Cancer Discov. *6*, 316–329.

Pylayeva-Gupta, Y., Grabocka, E., and Bar-Sagi, D. (2011). RAS oncogenes: weaving a tumorigenic web. Nat. Rev. Cancer *11*, 761–774.

Ren, P., Liu, Y., Li, L., and Feng, J.. (2014). Irreversible covalent inhibitors of the GTPase K-Ras G12C. Patent WO2014143659 A1, filed March 14, 2014, and published September 18, 2014.

Singh, A., Greninger, P., Rhodes, D., Koopman, L., Violette, S., Bardeesy, N., and Settleman, J. (2009). A gene expression signature associated with "K-Ras addiction" reveals regulators of EMT and tumor cell survival. Cancer Cell *15*, 489–500.

Sun, Q., Burke, J.P., Phan, J., Burns, M.C., Olejniczak, E.T., Waterson, A.G., Lee, T., Rossanese, O.W., and Fesik, S.W. (2012). Discovery of small molecules that bind to K-Ras and inhibit Sos-mediated activation. Angew. Chem. Int. Ed. *51*, 6140–6143.

Toure, M., and Crews, C.M. (2016). Small-molecule PROTACS: new approaches to protein degradation. Angew. Chem. Int. Ed. *55*, 1966–1973.

Welsch, M.E., Kaplan, A., Chambers, J.M., Stokes, M.E., Bos, P.H., Zask, A., Zhang, Y., Sanchez-Martin, M., Badgley, M.A., Huang, C.S., et al. (2017). Multivalent small-molecule pan-RAS inhibitors. Cell *168*, 878–889.e29.

Westover, K.D., Janne, P.A., and Gray, N.S. (2016). Progress on covalent inhibition of KRAS(G12C). Cancer Discov. *6*, 233–234.

Winter, G.E., Buckley, D.L., Paulk, J., Roberts, J.M., Souza, A., Dhe-Paganon, S., and Bradner, J.E. (2015). Phthalimide conjugation as a strategy for in vivo target protein degradation. Science *348*, 1376–1381.

Xiong, Y., Lu, J., Hunter, J., Li, L., Scott, D., Choi, H.G., Lim, S.M., Manandhar, A., Gondi, S., Sim, T., et al. (2017). Covalent guanosine mimetic inhibitors of G12C KRAS. ACS Med. Chem. Lett. *8*, 61–66.

Ying, H., Kimmelman, A.C., Lyssiotis, C.A., Hua, S., Chu, G.C., Fletcher-Sananikone, E., Locasale, J.W., Son, J., Zhang, H., and Coloff, J.L. (2012). Oncogenic Kras maintains pancreatic tumors through regulation of anabolic glucose metabolism. Cell *149*, 656–670.

Zhang, Z., and Marshall, A.G. (1998). A universal algorithm for fast and automated charge state deconvolution of electrospray mass-to-charge ratio spectra. J. Am. Soc. Mass Spectrom. *9*, 225–233.

Zimmermann, G., Papke, B., Ismail, S., Vartak, N., Chandra, A., Hoffmann, M., Hahn, S.A., Triola, G., Wittinghofer, A., and Bastiaens, P.I. (2013). Small molecule inhibition of the KRAS-PDE [delta] interaction impairs oncogenic KRAS signalling. Nature *497*, 638.

STAR★METHODS

KEY RESOURCES TABLE

REAGENT or RESOURCE	SOURCE	IDENTIFIER
Antibodies		
Mouse monoclonal anti-KRAS	Sigma-Aldrich	Cat# SAB1404011; RRID: AB_10736949
Rabbit monoclonal anti-phospho-ERK	Cell Signaling Technology	Cat# 4370S; RRID: AB_2315112
Rabbit monoclonal anti-ERK	Cell Signaling Technology	Cat# 4695S; RRID; AB_390779
Rabbit monoclonal anti-phospho-MEK1/2	Cell Signaling Technology	Cat# 9154P; RRID: AB_2138017
Mouse monoclonal anti-alpha-Tubulin	Cell Signaling Technology	Cat# 3873S; RRID: AB_1904178
Chemicals, Peptides, and Recombinant Proteins		
KRAS G12C	Ken D. Westover's lab	2.F.4-KRASG12C
SYPRO® Orange	Sigma-Aldrich	S5692
Critical Commercial Assays		
CellTiter-Glo Luminescent Cell Viability Assay	Promega	Cat# G7573
Active Ras Pull-down and Detection Kit	ThermoFisher Scientific	Cat# 16117
AlphaScreen	PerkinElmer	6760613R
Deposited Data		
KRAS G12C/1_AM structure	Protein databank	PDB: 5V9L
KRAS G12C/3_AM structure	Protein databank	PDB: 5V9O
Experimental Models: Cell Lines		
Human: H358	Pasi A. Janne's laboratory	N/A
Human: H23	Pasi A. Janne's laboratory	N/A
Human: H1792	Pasi A. Janne's laboratory	N/A
Human: Mia PaCa-2	ATCC	ATCC-CCL-1420
Human: Calu-1	Pasi A. Janne's laboratory	N/A
Human: H441	Pasi A. Janne's laboratory	N/A
Human: HCT116	ATCC	ATCC-CCL-247
Human: 293T	Jean Zhao's laboratory	N/A
Human: HCC827	Pasi A. Janne's laboratory	N/A
Human: PC9	Pasi A. Janne's laboratory	N/A
Recombinant DNA		
Plasmid: pCDH_FLAG_KRAS WT	This paper	N/A
Plasmid: pCDH_FLAG_KRAS G12C	This paper	N/A
Software and Algorithms		
GraphPad Prism	Graphpad Software Inc	https://www.graphpad.com/scientific-software/prism/
ImageJ	National Institutes of Health	https://imagej.nih.gov/ij/

CONTACT FOR REAGENT AND RESOURCE SHARING

Further information and requests for resources and reagents should be directed to and will be fulfilled by the Lead Contact Nathanael Gray (Nathanael_Gray@dfci.harvard.edu).

EXPERIMENTAL MODEL AND SUBJECT DETAILS

Cell Lines

Sources of Cell Lines

Human lung cancer cell lines, including KRAS G12C cell lines (H358, H23, Calu-1, H1792, H2122), A549 (KRAS G12S), H441 (KRAS G13V), and KRAS WT (PC9, HCC827) were authenticated.and obtained from Pasi A. Janne's laboratory. HEK293T cells were

obtained from Jean Zhao's laboratory and were not further authenticated. MiaPaca-2 and HCT116 cell lines were obtained from ATCC and were not further authenticated. All cells were grown in RPMI1640 or DMEM medium (Life Technologies), supplemented with 10% fetal bovine serum (Gibco), 50 units/mL penicillin, 50 units/mL streptomycin, and maintained in humidified 37°C/5%CO_2 incubator.

Generation of RAS-less Mouse Embryo Fibroblasts Expressing Human $KRAS^{G1C}$ and $KRAS^{G12V}$

$KRAS^{G1C}$ and $KRAS^{G12V}$ retroviral plasmids were created by point mutagenesis from pBABE $KRAS^{WT}$ plasmid (Addgene, Plasmid #75282). Retroviruses were generated by co-transfection of pBABE plasmids together with pAmpho plasmid into 293T cells using FuGENE® HD Transfection Reagent (Promega). The retroviruses were transduced into $Hras^{-/-}$; $Nras^{-/-}$; $Kras^{lox/lox}$ MEFs (a kind gift from Mariano Barbacid) followed by 2 weeks of puromycin selection (1 ug/mL). To obtain $KRAS^{G1C}$ and $KRAS^{G12V}$ Ras-less MEFs, cells were then cultured in the presence of 4-hydroxytamoxifen (4OHT) (Sigma, 600 nM) for another 2 weeks to remove the endogenous KRAS. Cell growth assays were performed with the colorimetric MTS assay as described before (Ambrogio et al., 2016). All experimental points were a result of three to six replicates, and all experiments were repeated at least three times. The data was graphically displayed using GraphPad Prism 5 for Windows (GraphPad Software). Each point (mean ± standard deviation) represents growth of treated cells compared to untreated cells. The curves were fitted using a non-linear regression model with a sigmoidal dose response.

METHOD DETAILS

Protein Preparation and Crystallization

Protein was expressed and purified as described previously (Lim et al., 2014). Point mutations were generated using the GeneArt® site-directed mutagenesis system (Life Technologies). Compound **1_AM** and **3_AM** were dissolved in 100% DMSO and incubated with KRas G12C at molar ratio (3:1) at 20°C for two hours and then 4°C for overnight. The mixture was analyzed by electrospray MS to confirm complete labeling, and further purified by Superdex75 in buffer: 20 mM Hepes pH 8.0, 150 mM NaCl, 5 mM $MgCl_2$ and 0.5 mM DTT. Crystals grew from hanging vapor diffusion drops with following condition: 1.6M sodium phosphate monobasic monohydrate, potassium phosphate dibasic pH7.1 for **1_AM** and 0.1M Tris pH9.0, ammonium sulfate 1.6M for **3_AM**. Crystals were cryoprotected in mother liquid with 20% glycerol for **1_AM** and 3M ammonium sulfate for **3_AM**, and flash frozen in liquid nitrogen.

Crystal Structure Determination

Diffraction images were collected at the advanced photon source beamline 19-ID. Data was integrated and scaled using HKL2000/3000 packages (Otwinowski and Minor, 1997). Molecular replacement was performed with 4OBE as the search model using Phaser software. Manual and automated model building and refinement were performed using Phenix package and coot software (Adams et al., 2010; Emsley et al., 2010). Figures were prepared using Pymol (The PyMOL Molecular Graphics System, Version 1.5.0.4 Schrödinger, LLC). Final model and scaled reflection data was deposited at the protein databank (5V9L, 5V9O). Final collection and refinement statistics are presented in Table S1.

Capillary Electrophoresis-Mass spectrometry Analysis (CE-MS)

RAS G12C was treated with DMSO or a 10-fold molar excess of compound 1 for 2 hours at room temperature. Reactions were directly analyzed by CE-MS using a ZipChip CE system and autosampler (908 Devices, Boston, MA) interfaced to a QExactiv HF mass spectrometer (ThermoFisher Scientific, San Jose, CA). Solutions were loaded for 5 seconds and separation performed at 500 V/cm on an HR chip (22 cm separation channel) for 5 minutes with a background electrolyte consisting of 50% acetonitrile/1% formic acid. Pressure assist was utilized and started at 30 seconds. The mass spectrometer acquired full scan mass spectra in profile mode from *m/z* 300-4000 (15k resolution, 1E6 target, 50 ms max fill time, lock mass enabled). Mass spectra were deconvoluted using MagTran version 1.03 b2 (Zhang and Marshall, 1998).

Immunoblotting

Cells were washed once with 1x phosphate buffered saline (PBS) and then lysed in RIPA buffer (50 mM Tris, pH 7.5, 150 mM NaCl, 1% NP-40, 0.5% sodium deoxycholate, and 0.1% SDS) supplemented with protease and phosphatase inhibitors (Roche). Protein concentrations were determined by using the Pierce BCA protein assay kit (Life Technologies). Equal amount of protein was resolved on SDS-PAGE, and was subsequently transferred onto nitrocellulose membrane (Bio-Rad). The membrane was blocked with 5% non-fat milk in TBS-0.1%Tween-20 and was then incubated with primary antibodies overnight at 4°C with gentle rotating. After washing, the membrane was incubated with fluorophore-conjugated secondary antibodies for 1 hr at room temperature. The membrane was then washed and scanned with an Odyssey Infrared scanner (Li-Cor Biosciences). Primary antibodies include anti-KRAS (Sigma #SAB1404011), anti-phospho-p44/42 MAPK (Erk1/2) (Cell Signaling Technology # 9101S), anti- p44/42 MAPK (Erk1/2) (Cell Signaling Technology # 6509), anti-phospho-MEK1/2 (Ser217/221) (Cell Signaling Technology # 9154P), anti-MEK1/2 (Cell Signaling Technology # 9126S), and anti-alpha-Tubulin (Cell Signaling Technology # 3873S). Secondary antibodies used were IRDye700-conjugated anti-mouse IgG and IRDye800-conjugated anti-rabbit IgG (Rockland, Gilbertsville, PA).

Differential Scanning Fluorimetry

KRAS G12C protein was diluted to 10μM in analysis buffer consisting of 20mM HEPES pH 7.5, 100mM NaCl, 5% glycerol and subjected to a range of test compound concentrations at 25°C for 1 hour (diluted from 10mM DMSO stock). SYPRO® Orange (Sigma-Aldrich, Cat. S5692) was added in DSF buffer and samples analyzed in a CFX Connect™ RT-PCR Detection System (Bio-Rad). Samples were heated from 25°C to 100°C at a rate of 1.5°C/minute, taking a fluorescence reading every 0.5°C using a SYBR_FAM channel matching the excitation and emission wavelengths of SYPRO orange (λex 470 nm; λem 570 nm). Melting points for samples were determined by taking the first derivative of fluorescence readings and inspecting for peaks in the derivative signal using Bio-Rad CFX Manager and Prism GraphPad 7.01.

Active RAS Determination by RBD Pulldown Assay

Cells (5×10^6) pre-attached to a 10 cm dish were treated with 10 μM of compound for 6 hours. RAS activity was determined by the Active Ras Pull-Down and Detection Kit from Thermo Scientific according to the manufacturer's instructions. In brief, cells were lysed with 0.5mL of lysis buffer and scraped off, and lysate was centrifuged at 16,000 g for 15 min at 4°C. Pre-cleared lysates were subsequently added to 80 μg of GST-tagged RBD and prewashed glutathione agarose beads for 1 hour at 4°C under constant rocking. The beads were subsequently pelleted and washed 3 times and eluted for Western blotting with 50 μL of 2X reducing sample buffer.

Cell Proliferation Assays

Cells were seeded in 24-well plates (2×10^3-5×10^3) in 1 ml medium. On the next day, cells were treated with the compounds at 5 μM. 6 days after the initial treatment, cells were fixed with 1% formaldehyde, and stained with crystal violet (0.05%, wt/vol), a chromatin-binding cytochemical stain. The plates were washed extensively, and imaged with a scanner.

Competition Binding Assay

KRAS-G12C was purified as described before (Xiong et al., 2017). KRAS-G12C was diluted to 50nM in reaction buffer consisting of 20mM HEPES pH 7.5, 100mM NaCl, 5% glycerol, 0.1% BSA and placed in 384 well plate. With the Echo® 555 liquid hander (Labcyte Inc.), proteins were subjected to a range of test compound concentrations from 2nM to 64μM, and then the probe (Cpd **5**) was added at 50nM finally. Plates were sealed and shaken, incubated for 2 hours at 25°C. Anti-FLAG AlphaScreen acceptor beads and Streptavidin donor beads (PerkinElmer, catalog number 6760613R) were diluted in reaction buffer, then added to the reaction at 10μg/ml. Following a 2 hour incubation at 25°C, alpha signal was measured using a Synergy Neo plate reader (BioTek) with the recommended AlphaScreen settings. GraphPad Prism software (version 7.01) was used to analyze data. Raw alpha signal was converted to percent alpha signal (relative to DMSO). The IC50 values were determined by nonlinear regression of plots of log [inhibitor] vs. percentage of alpha signal

Chemical Synthesis

The method details are 13 pages and provided as Supplementary Materials.

QUANTIFICATION AND STATISTICAL ANALYSIS

All statistical analyses and viability curves were produced using Prism 6 (GraphPad Software).

DATA AND SOFTWARE AVAILABILITY

Structure files and coordinates have been deposited to PDB under these accession numbers: 5V9L for KRAS G12C/**1_AM** and 5V9O for KRAS G12C/**3_AM**.

Short Article

Structure

KRAS G12C Drug Development: Discrimination between Switch II Pocket Configurations Using Hydrogen/Deuterium-Exchange Mass Spectrometry

Graphical Abstract

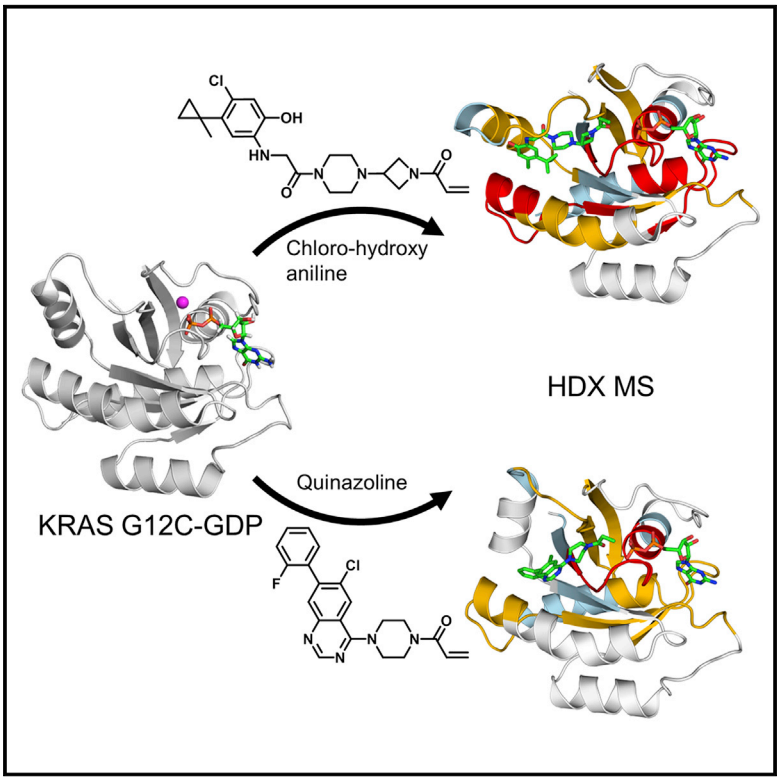

Authors

Jia Lu, Rane A. Harrison, Lianbo Li, ..., Nathanael S. Gray, John R. Engen, Kenneth D. Westover

Correspondence

j.engen@neu.edu (J.R.E.), kenneth.westover@utsouthwestern.edu (K.D.W.)

In Brief

Covalent inhibitors are promising for addressing cancers driven by KRAS G12C, the most common KRAS mutation in lung cancer. Lu et al. characterize a quinazoline switch II pocket (SIIP) inhibitor and demonstrate the utility of HDX MS for characterizing SIIP compounds.

Highlights

- HDX mass spectrometry detects differences between classes of RAS SIIP inhibitors
- X-ray crystal structures show conformational dynamics upon SIIP inhibitor binding
- Quinazoline SIIP inhibitor has similar activity to chloro hydroxy aniline inhibitor

Lu et al., 2017, Structure *25*, 1–7
September 5, 2017 © 2017 Elsevier Ltd.
http://dx.doi.org/10.1016/j.str.2017.07.003

Please cite this article in press as: Lu et al., KRAS G12C Drug Development: Discrimination between Switch II Pocket Configurations Using Hydrogen/Deuterium-Exchange Mass Spectrometry, Structure (2017), http://dx.doi.org/10.1016/j.str.2017.07.003

Structure
Short Article

KRAS G12C Drug Development: Discrimination between Switch II Pocket Configurations Using Hydrogen/Deuterium-Exchange Mass Spectrometry

Jia Lu,[1,5] Rane A. Harrison,[2,5] Lianbo Li,[1] Mei Zeng,[3,4] Sudershan Gondi,[1] David Scott,[3,4] Nathanael S. Gray,[3,4] John R. Engen,[2,*] and Kenneth D. Westover[1,6,*]
[1]Departments of Biochemistry and Radiation Oncology, The University of Texas Southwestern Medical Center at Dallas, Dallas, TX 75390, USA
[2]Department of Chemistry and Chemical Biology, Northeastern University, Boston, MA 02115, USA
[3]Department of Cancer Biology, Dana-Farber Cancer Institute, Boston, MA 02115, USA
[4]Department of Biological Chemistry and Molecular Pharmacology, Harvard Medical School, Boston, MA 02115, USA
[5]These authors contributed equally
[6]Lead Contact
*Correspondence: j.engen@neu.edu (J.R.E.), kenneth.westover@utsouthwestern.edu (K.D.W.)
http://dx.doi.org/10.1016/j.str.2017.07.003

SUMMARY

KRAS G12C, the most common RAS mutation found in non-small-cell lung cancer, has been the subject of multiple recent covalent small-molecule inhibitor campaigns including efforts directed at the guanine nucleotide pocket and separate work focused on an inducible pocket adjacent to the switch motifs. Multiple conformations of switch II have been observed, suggesting that switch II pocket (SIIP) binders may be capable of engaging a range of KRAS conformations. Here we report the use of hydrogen/deuterium-exchange mass spectrometry (HDX MS) to discriminate between conformations of switch II induced by two chemical classes of SIIP binders. We investigated the structural basis for differences in HDX MS using X-ray crystallography and discovered a new SIIP configuration in response to binding of a quinazoline chemotype. These results have implications for structure-guided drug design targeting the RAS SIIP.

INTRODUCTION

RAS mutations were some of the first identified acquired genetic causes of cancer and are common in many forms of malignancy, particularly gastrointestinal, skin, and lung cancers (Prior et al., 2012). Oncogenic RAS mutations result in a dysregulated excess of cellular GTP-bound RAS, the activated form for RAS, which transduces signals resulting in processes necessary for cancer such as cell growth and proliferation (Pylayeva-Gupta et al., 2011), invasiveness (Campbell and Der, 2004; Lundy et al., 1986), and evasion of immune surveillance (Seliger et al., 1998; Weijzen et al., 1999). RAS transduces signals by direct protein-protein interactions raising the possibility that specific mutations may impact RAS function within the context of cancer in unique ways. This hypothesis is supported not only by biochemical (Hunter et al., 2015) and laboratory models (Fasano et al., 1984; Feig and Cooper, 1988; Kim et al., 2016), but also by a stratification in the clinical behavior of tumors bearing certain RAS mutations (Montalvo et al., 2016). Accordingly, RAS mutation-specific strategies are under development.

The interface for most RAS-RAS effector interactions centers around two dynamic structural elements in RAS called switch I and switch II. Consistent with the role of guanosine nucleotides in controlling the signaling state of RAS, the switches also form a large portion of the guanosine nucleotide binding pocket. Accordingly, the conformations of switches I and II are responsive to the identity of the bound nucleotide, with the GTP-bound form being more compact by virtue of interactions between switch II and the terminal gamma phosphate of GTP that draw switch II toward the protein center (Figure 1A). In the absence of that interaction, switch II is less constrained and has been observed in multiple conformations in X-ray crystal and nuclear magnetic resonance structures. This mobility in switch II has enabled unanticipated strategies to target KRAS G12C directly.

KRAS G12C is the most common KRAS mutation found in non-small-cell lung cancer and presents a fortuitous opportunity to selectively target this oncogenic KRAS mutation directly using covalent inhibitors, given that cysteine 12 extends a nucleophilic thiol side chain susceptible to electrophilic attack. The established use of cysteine as a target for rationally designed covalent warheads in small-molecule inhibitors (Liu et al., 2013) prompted several groups, including ours, to explore the KRAS G12C mutation as a handle for direct KRAS targeting in a G12C, tumor-selective manner. We demonstrated that the guanine nucleotide binding site immediately adjacent to the G12C mutation is targetable by using a covalent guanosine diphosphate (GDP)-mimetic compound, SML 8-73-1 (Lim et al., 2014). SML 8-73-1 competed efficiently with more than three times physiologic concentrations of GDP and guanosine triphosphate (GTP) to irreversibly inactivate KRAS G12C and is highly selective for KRAS G12C over other GTP-binding proteins (Hunter et al., 2014). Simultaneously, the group led by Shokat and Wells showed that a binding site on the opposite side of

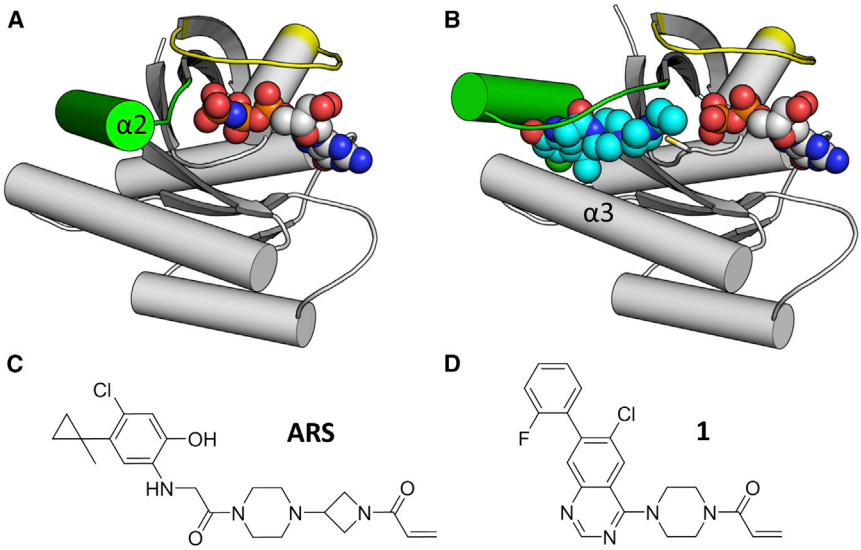

Figure 1. Switch II Configuration Changes in Response to SIIP Inhibitors

(A) GTP-bound HRAS (PDB: 4L9W) shows that the helical portion of switch II (α2) engages the gamma phosphate of GTP, resulting in a closed conformation. Switch II in green, switch I in yellow, GTP in spheres.

(B) ARS-853-bound KRAS G12C (PDB: 5F2E) shows an open switch II conformation. In addition to α2, ARS-853 (cyan spheres) also interacts with α3.

(C and D) Chemical structures of ARS-853 and **1**.

Cys12, beneath switch II, could also be utilized to target Cys12 (Ostrem et al., 2013). This class of compounds, termed switch II pocket (SIIP) binders, requires a substantial rearrangement of switch II to accommodate binding (Figure 1B). This class of compounds has been evolved to improve both potency and selectivity to yield lead compounds with potencies in the low micromolar range (Patricelli et al., 2016).

Multiple chemical scaffolds have been reported as SIIP binders, but structural information is available for one major class consisting of a chloro hydroxy aniline core with a reactive acrylamide warhead (Figure 1C) (Patricelli et al., 2016). However, quinazoline-containing compounds have also been reported (Figure 1D; Table S1) (Li et al., 2015), although characterized in a limited fashion. The flexibility and conformational dynamics of switch II complicates structure-guided drug design work on quinazoline scaffolds because the conformation of switch II is uncertain. Here we demonstrate that hydrogen/deuterium-exchange mass spectrometry (HDX MS), a method capable of detecting differences in switch II dynamics for native RAS family proteins (Harrison et al., 2016), can detect differences in the conformational state of switch II induced by the quinazoline versus chloro hydroxy aniline scaffolds. Further, we use X-ray crystallography to explain the differences in HDX MS signatures seen after treatment with quinazoline-containing compounds. This analysis reveals a new configuration of the SIIP and has implications for subsequent iterations of compound optimization or design.

RESULTS

Differential Effects of Classes of SIIP Binders

When the original series of chloro hydroxy aniline compounds was reported, we also noted that a series of 4-piperazino quinazoline compounds were also included in patent claims but characterization was limited (Li et al., 2015). We hypothesized that these compounds, with their divergent chemical scaffolds, had the potential to engage KRAS G12C SIIP in different ways leading to rearrangement of switch II and the binding pocket. As high level tests for differences in how these two classes of compounds interact, we analyzed these compounds in biochemical and cellular assays.

To assess the relative impact of the two different compounds on the thermodynamic stability of these two protein-ligand complexes, we conducted differential scanning fluorimetry (DSF) on compound-labeled KRAS G12C protein samples. DSF is a convenient method for measuring thermal stability that relies on a dye that becomes fluorescent when in contact with hydrophobic residues as proteins unfold upon heating, and has been used previously to characterize ARS-853 (Lito et al., 2016). KRAS G12C was overexpressed and purified as previously reported, then exposed to either ARS-632, a chloro hydroxy aniline compound similar to ARS-853 (Table S1), and **1**, a chemotype based on a 4-piperazino quinazoline compound, until covalent labeling was complete as measured by mass spectrometry (MS) (Figure S1). The melting temperatures (T_m) of KRAS G12C labeled with either **1** or ARS-632 demonstrated a substantial increase in T_m of 10.5 or 13.5, respectively, compared with GDP-bound protein (Figures 2A and 2B).

As an additional measure of compound reactivity, we performed a kinetic chemosensor assay that detects the availability of free thiol in compound-exposed KRAS G12C over time using a cysteine-reactive compound, 7-diethylamino-3-(4-maleimidophenyl)-4-methylcoumarin. Of note, we have previously used a similar assay setup to evaluate binding of covalent GDP-competitive compounds (Hunter et al., 2014). In this assay, all three compounds were statistically similar in their labeling rates, with half-lives of 10–15 min (Figure S2).

To assess the relative effects of **1** versus ARS-632 on KRAS signaling in cells, we subjected the KRAS G12C mutant cell line H358 to escalating concentrations of compounds and measured the phosphorylation of ERK, a prominent downstream member of the MAPK signaling pathway. Compounds showed roughly equivalent potencies such that 10 μM concentrations were required to reduce pERK by roughly 50% (Figure 2C). Of note, no reduction was seen in cancer cell lines containing other non-G12C mutations (A549, H441, and HCT116), indicating the selectivity of compound **1** for KRAS G12C (Figure S3). Interestingly, with escalating compound concentrations we also noted a decrease in the RAS band and simultaneous appearance of a new higher-molecular-weight band. We demonstrated that this phenomenon is due to a shift in the protein mobility after

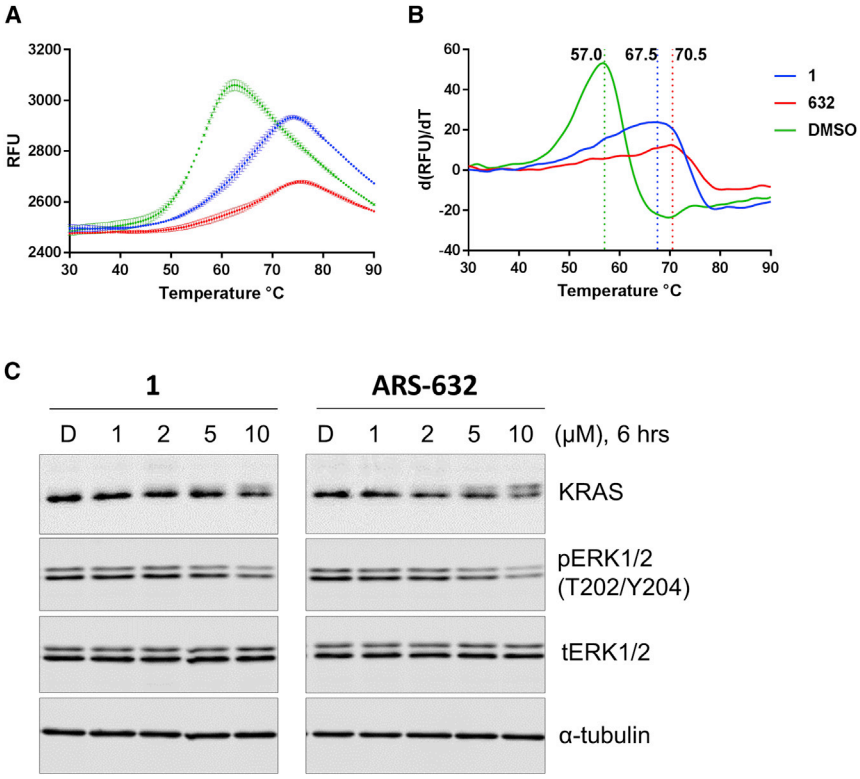

Figure 2. KRAS G12C-1 and KRAS G12C-ARS-632 Both Show Enhanced Thermal Stability and Similar in Potency for Inhibition of KRAS G12C-Depenent MAPK Signaling in H358 Cells

(A) Raw DSF measurements for KRAS G12C fully labeled with either ARS-632 or **1**.

(B) First derivative of (A) shows the shifts in T_m (dashed vertical lines) associated with protein labeling.

(C) Impact of compound exposure on MAPK signaling. Levels of pERK were evaluated in the KRAS-G12C-containing cancer cell line H358 as a surrogate for RAS signaling through the MAPK pathway. Cells were treated with compound **1** or ARS-632 as indicated for 6 hr. Phosphorylation of ERK1/2 was determined by immunoblotting.

compound labeling by performing SDS-PAGE on compound-labeled recombinant KRAS G12C (Figure S4). Of note, this phenomenon is further characterized and confirmed in a separate manuscript reporting analogs of **1** (Zeng et al., 2017). Together, these results suggest that the currently available quinazoline class compounds are similar in potency to previously reported chloro hydroxy anilines. We further characterized **1** to understand if further optimization is possible for the quinazoline class of compounds.

HDE MS

HDX MS has been used to compare the conformations of protein states, such as native versus non-native, wild-type versus mutant, and apo- versus protein- or ligand-bound (Engen, 2003; Pirrone et al., 2015). We previously used HDX MS to differentiate between guanosine monophosphate-purine nucleoside phosphorylase- and GDP-bound KRAS G12C, and showed that the protein dynamics of KRAS G12C covalently bound to GDP-mimetic SML-8-73-1 are similar to the inactive, GDP-bound protein (Lim et al., 2014). In another study, we used HDX MS to elucidate differences in switch II behavior that distinguish members of the Ras subfamily from the Rho subfamily (Harrison et al., 2016). Given the ability of HDX MS to detect changes in switch II dynamics, we hypothesized that HDX MS would be able to detect different conformations of switch II induced by the two major classes of SIIP binders, if such differences exist.

Samples containing KRAS G12C alone and covalently bound to the compounds were independently exposed to deuterium, the exchange reaction quenched, the protein digested into peptides using pepsin, and the relative deuterium level of each peptide measured using MS. To determine the effects of each compound on KRAS G12C dynamics, the relative deuterium level of protein alone was subtracted from the relative deuterium level of compound-bound protein at each labeling time point for each peptide (Figure 3A). Covalent attachment to either SIIP inhibitor significantly altered the protein dynamics of KRAS G12C, as demonstrated by the reduction of deuteration throughout many regions of KRAS G12C upon binding either ARS-632 or **1**. The greatest difference in HDX of KRAS G12C when bound to these compounds occurred in switch II (Figures 3B and 3C). In switch II, the difference in deuteration was >1.0 Da at every single time point (see also Figure S5). While binding either compound impacted identical regions of KRAS G12C, the effects of ARS-632 were always larger than those of **1**. The C-terminal portion of switch II incorporated 2.0–2.5 Da less deuterium between 1 and 10 min when bound to ARS than when bound to **1**. The effects of ARS-632 were more than those of **1** in other regions as well, including in the region containing the DxxG motif and the region immediately N-terminal to the N/TKxD motif (containing a portion of an α helix that is proximal to the SIIP). Other parts of KRAS (the P loop (GxxGxGKS/T), switch I, the N/TKxD motif, and near the C terminus), were only subtly affected by compound binding and the differences between the HDX signatures was very small. The HDX results reveal that these compounds clearly affected the structures to different degrees and in different places.

Crystal Structure of 1-KRAS G12C

To understand the structural basis for the HDX MS findings, we solved an X-ray crystal structure of KRAS G12C bound to **1**. Hexagon-shaped protein crystals were readily obtained from 1.8 M sodium phosphate monobasic monohydrate, potassium phosphate dibasic, pH 6.9, and diffracted to 2.2 Å when subjected to synchrotron radiation. Analysis revealed a P3 space group with a unit cell a = 84.9, b = 84.9, and c = 130.8 Å. The structure was solved using molecular

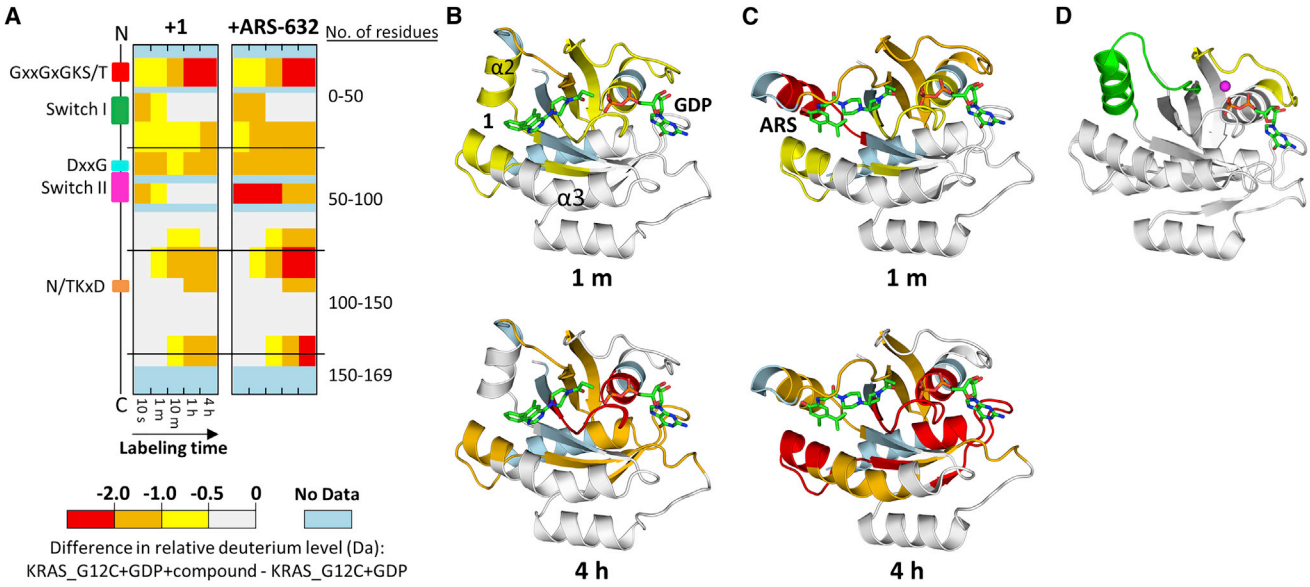

Figure 3. HDX MS Detects Changes in Switch II dynamics Induced by SIIP Binders

(A) Differences in HDX are represented by relative deuterium levels of inactive protein covalently bound to compound minus that of inactive GDP-bound protein alone, scale shown at top. Two-dimensional representations of KRAS G12C are given in linear fashion from N terminus (top) to C terminus (bottom), and the locations of key structural elements are shown on the left. All deuterium-labeling time points are shown, increasing from left to right.

(B and C) Crystal structures of **1** (B) or ARS-853 (C) bound to KRAS G12C with HDX MS differences at labeling time point 1 min (upper panel) and 4 hr (lower panel) annotated using the color scheme from subpanel (A).

(D) KRAS G12C bound to GDP alone (PDB: 4LDJ) provided for comparison. In (D), switch I is shown in yellow and switch II in green; magnesium is represented as a magenta sphere.

replacement with GDP-bound KRAS (PDB ID: 4OBE) as a search model (Table 1).

Additional electron density within the SIIP confirmed that **1** binds between helix α2 and helix α3 in the presence of GDP, similar to previously reported SIIP binders, such as compounds 12 and ARS-853, ARS-853 being identical to ARS-632 with the exception of a methyl substituent. However, different from prior co-crystal structures, a new configuration of switch II was observed with the helix α2 (part of switch II) extended away from the main body of the protein compared with ARS- or GDP-only-bound protein (Figures 3B–3D). The extended configuration of switch II is consistent with the HDX MS findings showing rapid deuterium exchange for switch II in the sample treated with **1,** based on the greater degree of switch II solvent exposure (Figures 3B and 3D). It is also consistent with the relatively more rapid exchange in helix α3 in **1**-bound protein attributable to fewer interactions between helix α3, helix α2, and inhibitor, as seen in the ARS-bound structures.

The open switch II is partially driven by conformational changes to avoid a steric clash that would occur between the quinazoline ring and Glu62 if Glu62 remained in the same position as seen with ARS-853. As a result, interactions between the compound and Tyr64 and Arg68 are lost, leaving switch II less unconstrained. Met72 is rotated away from helix α3 to accommodate **1**'s phenyl ring, also contributing to an outward rotation of helix α2. The piperazine ring of **1** also displaces loop 4 (part of switch II) away from the binding pocket. As a result, the entirety of switch II is shifted away from the protein main body. Otherwise, **1** binding is stabilized by hydrogen bonds to His95 and Lys16 in addition to multiple hydrophobic interactions with Tyr96, Gln99, Thr58, and Met72. In contrast, when bound to ARS-853, Met72 points toward helix α3 because the phenolic hydroxyl group and carbonyl of ARS-853 form hydrogen bonds with Asp69 and Arg68 on helix α2, respectively. A diagrammatic representation is shown in Figure 4.

DISCUSSION

Here we describe the structure of a previously unreported SIIP inhibitor-induced configuration of KRAS G12C resulting from binding to a quinazoline scaffold wherein the switch II position is dramatically altered, presenting a reconfigured SIIP that is applicable to RAS-directed drug design. These conformational changes in KRAS were readily demonstrated by HDX MS such that binding to ARS-632 resulted in a reduction in deuterium exchange in the SIIP relative to unbound protein, while exchange in the SIIP of KRAS G12C bound to **1** was accelerated relative to ARS-632 because of fewer interactions between **1** and switch II, leading to a solvent exposed switch II. All other portions of the compound-bound proteins exchanged deuterium similarly whether bound to ARS-632 or **1**, consistent with our X-ray crystal structure. Both prototypical chemotypes showed similar thermal stability and efficacy for inhibition of MAPK signaling in KRAS G12C-dependent cells.

These results have implications for future efforts to rationally design new iterations of SIIP-targeted RAS therapies. Key principles related to how ligands engage the dominant protein-ligand

Table 1. X-Ray Diffraction and Refinement Statistics

Data Collection	G12C-1
Space group	P3
Cell dimensions	
a, *b*, *c* (Å)	84.93, 84.93, 130.79
α, β, γ (°)	90.00, 90.00, 120.00
Resolution (Å)	50.00–2.23 (2.27–2.23)
R_{sym} or R_{merge}	0.183 (1.536)
I/sI	17.00 (1.33)
Completeness (%)	87.7 (48.0)
Redundancy	7.8 (5.0)
Refinement	
Resolution (Å)	40.39–2.23
No. of reflections	45,197
R_{work}/R_{free}	0.189/0.230
No. of atoms	
Protein	8,082
Ligand/ion	342
Water	375
B factors	
Protein	42.10
Ligand/ion	32.09
Water	37.19
RMSD	
Bond lengths (Å)	0.002
Bond angles (°)	0.596

RMSD, root-mean-square deviation.

interfaces within the SIIP and how these interactions in turn dictate the state of switch II can be discerned from these results. The binding pocket is composed of three main interfaces: negatively charged residues Glu62 and Glu63 on loop 4, the charged residues Arg68 and Asp69 on helix α2, and the hydrophobic residues His95 and Tyr96 on helix α3. The nature of interactions with these groups dictates the overall switch II conformation, particularly Arg68. ARS-632 primarily engages two interfaces on switch II while **1** primarily interacts with the hydrophobic residues on helix α3. Key among the ARS-632 interactions is hydrogen bonds between ARS-632 and Arg68 and Asp69, which constrain switch II in a closed conformation that is less solvent accessible (Figure S6). Interestingly, previous SIIP binders (Ostrem et al., 2013), such as compound **8** (Figure S7), which do not form hydrogen bonds with Arg68 but instead engage in long-range hydrophobic interactions with gamma and delta carbons in the Arg68 side chain, adopt an intermediate (half-way between that seen with ARS-632 versus **1**) switch II conformation (Figure S7). Of note, a comparison of temperature factors for helix α2 between PDB: 5F2E (ARS-853) and PDB: 5V71 (current structure) show averages of 12.6 versus 11.9 for helix α2 versus total protein in PDB: 5F2E (1.4 Å structure) and 56.2 versus 42.1 for PDB: 5V71, suggesting relatively more flexibility for helix α2 in PDB: 5V71. If this flexibility enables formation of additional interactions between helix α3 and derivatives of **1**, this would be predicted to improve the potency of this class of compounds. Harnessing these structural principles will likely be important for KRAS G12C-directed targeting strategies, where compound potency remains an issue given the micromolar potency of ARS-632 and **1** for inhibition of MAPK signaling (Patricelli et al., 2016). Our new structure will not only aid further exploration of the quinazoline chemotype, it also reveals a new conformation for the KRAS SIIP that may be targetable by other entirely different chemotypes discoverable through structure-guided design principles.

The SIIP may have utility beyond covalent inhibitors that can only be applied to the KRAS G12C mutation. The SIIP was discovered in, and to date has primarily been considered in the context of, KRAS G12C, which presents an accessible cancer-specific cysteine as a handle for covalent binding of small molecules containing an electrophilic warhead. However, in addition to covalent inhibitors, the SIIP may also be applicable to selective reversible inhibition of other oncogenic mutants or other cancer-associated RAS superfamily members. We believe that mutation-specific selectivity is plausible because the locations of oncogenic mutation hotspots in KRAS, codons 12, 13, and 61, either form part of the SIIP or are immediately adjacent to it, raising the possibility of engineering specificity by creating interactions between specific cancer-associated KRAS mutations and substituents of SIIP-binding compounds. Indeed, it is encouraging that recent attempts to develop reversible inhibitors of KRAS G12D based on interactions with switch I and switch II

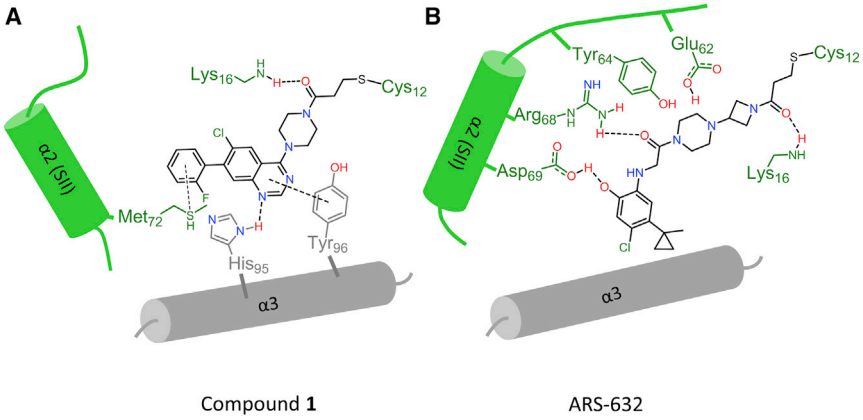

Figure 4. Schematic Representation of Key Interactions between Switch II Compounds and Adjacent α Helices

(A and B) Different interaction patterns are observed for **1** versus ARS-853 in the switch II binding pocket: (A) **1** is stabilized by pi-pi interaction with helix α3 residues His95 and Tyr96. (B) Arg68 and Asp69 in helix α2 (switch II) make hydrogen bonds to stabilize ARS-853.

have gained traction (Welsch et al., 2017). However, it should be noted that these new inhibitors do not utilize the SIIP, which may hold advantages both for potency and selectivity. Nevertheless, the key barrier to generating reversible SIIP-binding compounds will be achieving sufficient binding affinity, a property that has not been measured.

It bears mentioning that the most commonly used biochemical assay techniques for screening and evaluating the relative potencies of SIIP binders have been MS-based measures of irreversible compound binding, and these techniques cannot be used to measure affinities of reversible candidate SIIP compounds. So far, development of assays that can measure non-covalent interactions within the SIIP has been challenging. Indeed, as part of this study we attempted to measure the affinity between a non-covalent analog of compound **1** and KRAS G12C using isothermal calorimetry but could not detect binding. This could be due to limitations inherent to the assay technique or due to lack of binding activity for the experimental compound, but distinguishing between the two is difficult in the absence of a reversible SIIP-binding positive control. Lack of effective assays that accurately assess the state of switch II and the SIIP limits progress in searching for reversible SIIP-binding compounds. As shown here, HDX MS can be used to effectively compare the effects of various compounds, although HDX MS would likely not be attractive as a primary screening assay due to practical limits to throughput. Indeed, development of efficient screening methods focused on the SIIP would be greatly facilitated by the availability of intermediate- to high-potency reversible probes that could be conjugated to fluorophores or other easily detectable compounds; however, such probes are currently unavailable. Additional assay techniques will be required to develop such probes. This work, together with our prior published work, implicate HDX MS as a promising technique for identifying the next generation of SIIP-binding inhibitors given its ability to detect changes in switch II dynamics.

STAR★METHODS

Detailed methods are provided in the online version of this paper and include the following:

- KEY RESOURCES TABLE
- CONTACT FOR REAGENT AND RESOURCE SHARING
- EXPERIMENTAL MODEL AND SUBJECT DETAILS
  - Cell Lines
- METHOD DETAILS
  - HDX MS
  - Protein Preparation and Crystallization
  - Crystal Structure Determination
  - Differential Scanning Fluorimetry
  - Chemosensor Assay
  - Western Blots
- QUANTIFICATION AND STATISTICAL ANALYSIS
- DATA AND SOFTWARE AVAILABILITY

SUPPLEMENTAL INFORMATION

Supplemental Information includes seven figures and one table and can be found with this article online at http://dx.doi.org/10.1016/j.str.2017.07.003.

AUTHOR CONTRIBUTIONS

The manuscript was written through contributions of all authors. All authors have given approval to the final version of the manuscript.

ACKNOWLEDGMENTS

Department of Defence W81XWH-16-1-0106 (K.D.W.), Jimmy V Foundation (K.D.W.), Astellas (K.D.W. and N.S.G.), NIH (R01-GM101135) (J.R.E.), and a research collaboration with the Waters Corporation (J.R.E.). X-ray crystallography was performed at Argonne National Laboratory, Structural Biology Center at the Advanced Photon Source. Argonne is operated by UChicago Argonne, LLC, for the US Department of Energy, Office of Biological and Environmental Research under contract DE-AC02-06CH11357.

Received: March 28, 2017
Revised: May 26, 2017
Accepted: July 6, 2017
Published: August 3, 2017

REFERENCES

Adams, P.D., Afonine, P.V., Bunkoczi, G., Chen, V.B., Davis, I.W., Echols, N., Headd, J.J., Hung, L.W., Kapral, G.J., Grosse-Kunstleve, R.W., et al. (2010). PHENIX: a comprehensive Python-based system for macromolecular structure solution. Acta Crystallogr. D Biol. Crystallogr. *66*, 213–221.

Campbell, P.M., and Der, C.J. (2004). Oncogenic Ras and its role in tumor cell invasion and metastasis. Semin. Cancer Biol. *14*, 105–114.

Emsley, P., Lohkamp, B., Scott, W.G., and Cowtan, K. (2010). Features and development of coot. Acta Crystallogr. D Biol. Crystallogr. *66*, 486–501.

Engen, J.R. (2003). Analysis of protein complexes with hydrogen exchange and mass spectrometry. Analyst *128*, 623–628.

Fasano, O., Aldrich, T., Tamanoi, F., Taparowsky, E., Furth, M., and Wigler, M. (1984). Analysis of the transforming potential of the human H-ras gene by random mutagenesis. Proc. Natl. Acad. Sci. USA *81*, 4008–4012.

Feig, L.A., and Cooper, G.M. (1988). Relationship among guanine nucleotide exchange, GTP hydrolysis, and transforming potential of mutated ras proteins. Mol. Cell. Biol. *8*, 2472–2478.

Harrison, R.A., Lu, J., Carrasco, M., Hunter, J., Manandhar, A., Gondi, S., Westover, K.D., and Engen, J.R. (2016). Structural dynamics in ras and related proteins upon nucleotide switching. J. Mol. Biol. *428*, 4723–4735.

Hunter, J.C., Gurbani, D., Ficarro, S.B., Carrasco, M.A., Lim, S.M., Choi, H.G., Xie, T., Marto, J.A., Chen, Z., Gray, N.S., et al. (2014). In situ selectivity profiling and crystal structure of SML-8-73-1, an active site inhibitor of oncogenic K-Ras G12C. Proc. Natl. Acad. Sci. USA *111*, 8895–8900.

Hunter, J.C., Manandhar, A., Carrasco, M.A., Gurbani, D., Gondi, S., and Westover, K.D. (2015). Biochemical and structural analysis of common cancer-associated KRAS mutations. Mol. Cancer Res. *13*, 1325–1335.

Kim, E., Ilic, N., Shrestha, Y., Zou, L., Kamburov, A., Zhu, C., Yang, X., Lubonja, R., Tran, N., and Nguyen, C. (2016). Systematic functional interrogation of rare cancer variants identifies oncogenic alleles. Cancer Discov. *6*, 714–726.

Li, L., Feng, J., Wu, T., Ren, P., Liu, Y., Liu, Y., and Long, Y.O.. (2015). Inhibitors of kras g12c. (Google Patents).

Lim, S.M., Westover, K.D., Ficarro, S.B., Harrison, R.A., Choi, H.G., Pacold, M.E., Carrasco, M., Hunter, J., Kim, N.D., Xie, T., et al. (2014). Therapeutic targeting of oncogenic K-Ras by a covalent catalytic site inhibitor. Angew. Chem. Int. Ed. *53*, 199–204.

Lito, P., Solomon, M., Li, L.-S., Hansen, R., and Rosen, N. (2016). Allele-specific inhibitors inactivate mutant KRAS G12C by a trapping mechanism. Science *351*, 604–608.

Liu, Q., Sabnis, Y., Zhao, Z., Zhang, T., Buhrlage, S.J., Jones, L.H., and Gray, N.S. (2013). Developing irreversible inhibitors of the protein kinase cysteinome. Chem. Biol. *20*, 146–159.

Lundy, J., Grimson, R., Mishriki, Y., Chao, S., Oravez, S., Fromowitz, F., and Viola, M. (1986). Elevated ras oncogene expression correlates with lymph node metastases in breast cancer patients. J. Clin. Oncol. *4*, 1321–1325.

Montalvo, S.K., Li, L., and Westover, K.D. (2016). Rationale for RAS mutation-tailored therapies. Future Oncol. *13*, 263–271.

Ostrem, J.M., Peters, U., Sos, M.L., Wells, J.A., and Shokat, K.M. (2013). K-Ras (G12C) inhibitors allosterically control GTP affinity and effector interactions. Nature *503*, 548–551.

Otwinowski, Z., and Minor, W. (1997). Processing of X-ray diffraction data collected in oscillation mode. Methods Enzymol. *276*, 307–326.

Patricelli, M.P., Janes, M.R., Li, L.-S., Hansen, R., Peters, U., Kessler, L.V., Chen, Y., Kucharski, J.M., Feng, J., and Ely, T. (2016). Selective inhibition of oncogenic KRAS output with small molecules targeting the inactive state. Cancer Discov. *6*, 316–329.

Pirrone, G.F., Iacob, R.E., and Engen, J.R. (2015). Applications of hydrogen/deuterium exchange MS from 2012 to 2014. Anal. Chem. *87*, 99–118.

Prior, I.A., Lewis, P.D., and Mattos, C. (2012). A comprehensive survey of Ras mutations in cancer. Cancer Res. *72*, 2457–2467.

Pylayeva-Gupta, Y., Grabocka, E., and Bar-Sagi, D. (2011). RAS oncogenes: weaving a tumorigenic web. Nat. Rev. Cancer *11*, 761–774.

Seliger, B., Harders, C., Lohmann, S., Momburg, F., Urlinger, S., Tampe, R., and Huber, C. (1998). Down-regulation of the MHC class I antigen-processing machinery after oncogenic transformation of murine fibroblasts. Eur. J. Immunol. *28*, 122–133.

Wales, T.E., and Engen, J.R. (2006). Hydrogen exchange mass spectrometry for the analysis of protein dynamics. Mass Spectrom. Rev. *25*, 158–170.

Weijzen, S., Velders, M., and Kast, W. (1999). Modulation of the immune response and tumor growth by activated Ras. Leukemia *13*, 502–513.

Welsch, M.E., Kaplan, A., Chambers, J.M., Stokes, M.E., Bos, P.H., Zask, A., Zhang, Y., Sanchez-Martin, M., Badgley, M.A., and Huang, C.S. (2017). Multivalent small-molecule Pan-RAS inhibitors. Cell *168*, 878–889.e29.

Zeng, M., Lu, J., Li, L., Feru, F., Quan, C., Gero, T., Ficarro, S., Xiong, Y., Ambrogio, C., Paranal, R., et al. (2017). Potent and selective covalent quinazoline inhibitors of KRAS G12C. Cell Chem Biol. http://dx.doi.org/10.1016/j.chembiol.2017.06.017.

STAR★METHODS

KEY RESOURCES TABLE

REAGENT or RESOURCE	SOURCE	IDENTIFIER
Antibodies		
Mouse monoclonal anti-KRAS	Sigma-Aldrich	Cat# SAB1404011
Rabbit monoclonal anti-phospho-ERK	Cell Signaling Technology	Cat# 4370S
Rabbit monoclonal anti-ERK	Cell Signaling Technology	Cat# 4695S
Mouse monoclonal anti-alpha-Tubulin	Cell Signaling Technology	Cat# 3873S
Chemicals, Peptides, and Recombinant Proteins		
GeneArt® site-directed mutagenesis system for Human KRAS G12C	Life Technologies	Cat# A13282
KRAS G12C and WT	Westover lab	N/A
Deposited Data		
KRAS G12C/ compound **1** structure	Protein databank	PDB: 5V71
Experimental Models: Cell Lines		
Human: H358 (Male)	Pasi Janne Lab	ATCC-CRL-5807
Human: A549 (Male)	Pasi Janne Lab	ATCC-CCL-185
Human: H441 (Male)	Pasi Janne Lab	ATCC-HTB-174
Human: HCT116 (Male)	Pasi Janne Lab	ATCC-CCL-247
Recombinant DNA		
Plasmid pcDNA2.0_KRAS_WT	Westover lab	N/A
Plasmid pcDNA2.0_KRAS_G12C	Westover lab	N/A
Software and Algorithms		
GraphPad Prism	Graphpad Software Inc	https://www.graphpad.com/scientific-software/prism/
DynamX 3.0	Waters	http://www.waters.com/waters/
HKL2000/3000	HKL Research, Inc.	http://www.hkl-xray.com/hkl-3000
Phenix		https://www.phenix-online.org/
Coot		https://www2.mrc-lmb.cam.ac.uk/personal/pemsley/coot/
Pymol	The PyMOL Molecular Graphics System, Version 1.5.0.4	Schrödinger, LLC
ChemDraw Professional 15.0	PerkinElmer	http://www.cambridgesoft.com/

CONTACT FOR REAGENT AND RESOURCE SHARING

Further information and requests for resources and reagents should be directed to and will be fulfilled by the Lead Contact Kenneth Westover (Kenneth.Westover@UTSouthwestern.edu).

EXPERIMENTAL MODEL AND SUBJECT DETAILS

Cell Lines

Sources of Cell Lines

Human lung cancer cell lines, including cell lines H358 (KRAS G12C), A549 (KRAS G12S), and H441 (KRAS G13V) were authenticated and obtained from Pasi A. Janne's laboratory. Cell line HCT116 (KRAS G13D) was obtained from ATCC and was not further authenticated. All cells were grown in RPMI1640 or DMEM medium (Life Technologies), supplemented with 10% fetal bovine serum (Gibco), 50 units/mL penicillin, 50 units/mL streptomycin, and maintained in humidified 37°C/5% CO2 incubator.

Sources of Bacterial Strains

Escherichia coli BL21(DE3)

METHOD DETAILS

HDX MS

Each compound (**1** and ARS, 10 mM in DMSO) was slowly diluted into sample buffer (10 mM HEPES, 25 mM NaCl, pH 8.0) until a final concentration of 1000 μM was achieved. This solution was then combined with an equal volume (10:1 molar excess, compound:protein) of KRAS G12C (100 μM in 20 mM HEPES, 25 mM NaCl, pH 8.0) and allowed to incubate for approximately 18 hours at room temperature. A compound-free protein sample was also prepared by combining KRAS G12C alone with an equal volume of 90:10 sample buffer:DMSO, and this solution was also allowed to incubate in an identical manner. Intact mass analyses were performed to confirm that nearly all KRAS G12C was labeled with compound (Figure S1), and that all protein samples would remain stable for the duration of analyses. It was also confirmed that the 5% DMSO in all protein samples used for labeling did not significantly impact HDX MS results (data not shown).

HDX MS experiments were performed in a similar manner to those described previously (Harrison et al., 2016; Lim et al., 2014). Samples containing KRAS G12C alone and bound to each compound (**1** and ARS) were independently labeled with deuterium in triplicate, using identical experimental conditions so that each compound-bound form could be compared to KRAS G12C alone. HDX was initiated by diluting 4.0 μL of protein sample (50 μM in 15 mM HEPES, 25 mM NaCl, pH 8.0) 15-fold in labeling buffer (10 mM HEPES, 25 mM NaCl, pD 8.0) containing 99% deuterium oxide at room temperature. The labeling reaction was quenched at five predetermined time points (10 s, 1 m, 10 m, 1 h, 4 h) through the addition of 64.0 μL quench buffer (2.0 M guanidinium chloride, 0.8% formic acid, pH 2.1) at 0°C. Quenched samples were immediately flash frozen using dry ice and were stored at -80°C for less than one week prior to analysis. Deuterium measurement with mass spectrometry was performed as previously described (Harrison et al., 2016; Lim et al., 2014). Deuterium incorporation graphs (Figure S5) were generated using DynamX 3.0 software (Waters) by subtracting the centroid of the isotopic distribution at each labeling time point from the centroid of the isotopic distribution of the undeuterated reference species. Since the data were not corrected for back-exchange, each data point represents the relative deuterium level at each time point for each peptide (Wales and Engen, 2006). The average error of triplicate measurements at a single data point was ±0.08 Da, therefore any differences in relative deuterium level >0.50 Da between compound-bound and compound-free KRAS G12C were considered to be meaningful.

Protein Preparation and Crystallization

Protein was expressed and purified as described previously (Hunter et al., 2014; Lim et al., 2014). Point mutations were generated using the GeneArt® site-directed mutagenesis system (Life Technologies). A construct encoding codon-optimized N-terminal His-tobacco etch virus (TEV)-G12C V-Ki-ras2 Kirsten rat sarcoma viral oncogene homolog (K-Ras) in the pJExpress vector (DNA2.0) was synthesized and used to transform BL21(DE3) cells. Cells were grown in Luria broth (LB) to OD 600 0.7 and induced with 250 mM isopropyl β-D-1-thiogalactopyranoside (IPTG) for 16 h at 16°C. Cells were pelleted and resuspended in lysis buffer [20 mM sodium phosphate (pH 8.0), 500 mM NaCl, 10 mM imidazole, 1 mM 2-mercaptoethanol (BME), 5% (vol/vol) glycerol] containing PMSF, benzamidine, and 1 mg/mL lysozyme. Lysates were flash-frozen and stored at −80°C until use. Protein was purified over an IMAC cartridge (BioRad) following standard Ni-affinity protocols and desalted into crys-tallization buffer [20 mM Hepes (pH 8.0), 150 mM NaCl, 5 mM $MgCl_2$, 0.5 mM DTT]. The N-terminal His tag was cleaved by overnight digestion with a 1:5 ratio of TEV protease at 4°C, and the TEV and Tag were removed by reverse purification over an IMAC cartridge. Protein was concentrated to 30–40 mg/mL in a 10-kDa cutoff Amicon filter (Millipore), aliquoted, and then flash-frozen and stored under liquid nitrogen.

1 was dissolved in 100% DMSO and incubated with KRAS G12C at a 3:1 molar ratio at 20°C for two hours and then 4°C for overnight. The mixture was analyzed by mass spectrometry to confirm 100% labeling, and was further purified by Superdex75 in buffer: 20 mM Hepes pH 8.0, 150 mM NaCl, 5 mM $MgCl_2$ and 0.5 mM DTT. Crystals grew from sitting vapor diffusion drops with the following condition: 1.8M sodium phosphate monobasic monohydrate, potassium phosphate dibasic pH6.9. Crystals were cryoprotected in mother liquor with 20% glycerol and flash frozen in liquid nitrogen.

Crystal Structure Determination

Diffraction images were collected at the advanced photon source beamline 19-ID. Data were integrated and scaled using HKL2000/3000 packages (Otwinowski and Minor, 1997). Molecular replacement was performed with 4OBE as the search model using Phaser software. Manual and automated model building and refinement were performed using Phenix package and coot software (Adams et al., 2010; Emsley et al., 2010). Figure images were prepared using Pymol (The PyMOL Molecular Graphics System, Version 1.5.0.4 Schrödinger, LLC) and ChemDraw Professional 15.0. Final model and scaled reflection data were deposited at the protein databank (5V71). Final collection and refinement statistics are presented in Table 1.

Differential Scanning Fluorimetry

KRAS G12C protein was diluted to 10 μM in analysis buffer consisting of 20mM HEPES pH 7.5, 100mM NaCl, 5% glycerol and subjected to a range of test compound concentrations at 25°C for 1 hour (diluted from 10mM DMSO stock). SYPRO® Orange (Sigma-Aldrich, Cat. S5692) was added in DSF buffer and samples analyzed in a CFX Connect™ RT-PCR Detection System (Bio-Rad). Samples were heated from 25°C to 100°C at a rate of 1.5°C/minute, taking a fluorescence reading every 0.5°C using a SYBR_FAM channel matching the excitation and emission wavelengths of SYPRO orange (λex 470 nm; λem 570 nm). Melting points

for samples were determined by taking the first derivative of fluorescence readings and inspecting for peaks in the derivative signal using Bio-Rad CFX Manager and Prism GraphPad 7.01. (GraphPad Software, Inc., La Jolla, CA).

Chemosensor Assay

The chemosensor assay was performed as previously described (Hunter et al., 2014). Briefly, G12C or WT KRAS were incubated with DMSO or compounds at ambient temperature for the indicated durations. At each time point, protein sample was mixed with CPM in a black 384-well plate and fluorescence was read at 384/470 nm. Normalization was as follows: background was subtracted from each time point using the signal from WT KRAS and percent CPM was calculated using the signal derived from KRAS G12C protein alone at each time point as the maximal possible signal (100% labeling). Other readings are normalized accordingly. Prism GraphPad 7.01. was used to run the data analysis.

Western Blots

Human non-small cell lung cancer KRAS G12C mutant cell line H358 were grown in RPMI1640 medium (Gibco) supplemented with 10% heat-inactivated FBS (Lonza) and incubated in humidified 37°C/5% CO2 incubator. Cells were washed once with 1x phosphate buffered saline (PBS) and then lysed in RIPA buffer (50 mM Tris, pH 7.5, 150 mM NaCl, 1% NP-40, 0.5% sodium deoxycholate, and 0.1% SDS) supplemented with protease and phosphatase inhibitors (Roche). Protein concentrations were determined by using the Pierce BCA protein assay kit (Life Technologies). Equal amount of protein was resolved on SDS-PAGE, and was subsequently transferred onto the nitrocellulose membrane (Bio-Rad). The membrane was blocked with 5% non-fat milk in TBS-0.1%Tween-20 and was then incubated with primary antibodies overnight at 4°C with gentle rotating. After washing, the membrane was incubated with fluorophore-conjugated secondary antibodies for 1 hour at room temperature. The membrane was then washed and scanned with an Odyssey Infrared scanner (Li-Cor Biosciences). Primary antibodies included anti-KRAS (Sigma #SAB1404011), anti-Phospho-p44/42 MAPK (Erk1/2) (Cell Signaling Technology # 9101S), and anti-alpha-Tubulin (Cell Signaling Technology # 3873S). Secondary antibodies used were IRDye700-conjugated anti-mouse IgG and IRDye800-conjugated anti-rabbit IgG (Rockland, Gilbertsville, PA).

QUANTIFICATION AND STATISTICAL ANALYSIS

All statistical analyses were produced using Prism 6 (GraphPad Software).

DATA AND SOFTWARE AVAILABILITY

The crystal structure of ***1***-KRAS G12C has been deposited in the RCSB Protein Data Bank under code: 5V71.

Deuterium incorporation graphs were generated using DynamX 3.0 software (Waters). Diffraction data were integrated and scaled using HKL2000/3000 packages (Otwinowski and Minor, 1997). Molecular replacement was performed with 4OBE as the search model using Phaser software. Manual and automated model building and refinement were performed using Phenix package and coot software (Adams et al., 2010; Emsley et al., 2010).

Figure images were prepared using Pymol (The PyMOL Molecular Graphics System, Version 1.5.0.4 Schrödinger, LLC) and ChemDraw Professional 15.0.

The Supplemental_final.pdf file was provided as Supplemental Material.